THE EFFECT OF INCREASED AXLE LOADING ON SATURATED AND UNSATURATED RAILWAY FOUNDATION MATERIALS

GODISANG DAVID MPYE

A thesis presented in partial fulfilment of the requirement for the degree of
PHILOSOPHIAE DOCTOR (CIVIL ENGINEERING)
in the
FACULTY OF ENGINEERING, BUILT ENVIRONMENT AND INFORMATION TECHNOLOGY

UNIVERSITY OF PRETORIA

December 2020

To my Mother, Mrs E M Mpye,
and my late Father, Mr A M Mpye

THESIS SUMMARY

THE EFFECT OF INCREASED AXLE LOADING ON SATURATED AND UNSATURATED RAILWAY FOUNDATION MATERIALS

GD MPYE

Supervisor: Professor PJ Gräbe

Department: Civil Engineering

University: University of Pretoria

Degree: Philosophiae Doctor (Civil Engineering)

The aim of the research is to investigate the effect of increased axle loading on saturated and unsaturated railway foundation materials for heavy haul applications. The research methodology comprises of a literature review to identify the lacuna in the scientific knowledge, finite element modelling for characterisation of railway cyclic loading, development of a cyclic triaxial apparatus for laboratory testing and experimental work, followed by analysis, interpretation and discussion of results and lastly the formulation of conclusions and recommendations.

The axle loading of interest start with a base load of 20 tonnes per axle for general freight followed by increased axle loading of 26, 30, 32.5 and 40 tonnes per axle for heavy haul. The test materials used in the experimental work are representative of the subballast and subgrade layers in a railway substructure. As a reproduction of the climatic conditions in the field and the loading from passing trains, experimental testing was carried out on saturated samples under undrained conditions and unsaturated samples under constant water content. Unsaturated samples were prepared to matric suctions of 50, 100 and 225 kPa via axis translation. Monotonic and cyclic tests were conducted to investigate the behaviour of railway foundation materials. Critical state theory for saturated and unsaturated soils is used as a method of analysis in establishing the failure criterion and the failure envelope. Various parameters,

such as stress states, strains, resilient modulus, pore water pressure and matric suction are also utilised in investigating trends and behaviours.

Based on the monotonic test results, the shear strength of unsaturated samples was found to be greater than that of saturated samples, attributed mainly to strain hardening caused by the unsaturated soil conditions, with the presence of a peak deviator stress when plotted on the stress-strain graph. However, unsaturated samples were also found to be prone to load-collapse during monotonic shear, even when the water content and confining stress remained constant, which resulted in brittle behaviour with the sudden rupture and formation of multiple bifurcation shear bands and slip planes.

Based on the cyclic tests on saturated materials, it was discovered that increased axle loading can result in phase-transition in soil behaviour, based on the stress states in the soil relative to the critical state line plotted in the effective stress space. Stress states below the critical state line resulted in a no-phase transition with dilation behaviour. Stress states on the critical state line resulted in a single-phase transition from dilation to contraction. Stress states above the critical state line resulted in a double-phase transition from dilation to contraction behaviour and then strain-softening. It is therefore concluded that increased axle loading can only be sustained by materials which presented dilation and no phase-transition in soil behaviour, which occurred at axle loading of 20 and 26 tonnes per axle for the subballast and subgrade materials.

Based on the cyclic tests on unsaturated materials, it was established that increased axle loading did not cause material failure for all load axle cases and materials. The stress states of all tests plotted well below the failure envelope in the net stress space, which is indicative of resilient and elastic behaviour. Increased axle loading instead resulted in decreased permanent strain, until the critical level of repeated deviator stress of 32.5 tonnes per axle was found, where the permanent strain increased. It is therefore concluded that, as a result of the increased shear strength from the strain hardening property of unsaturated materials, an increased axle loading of 32.5 tonnes per axle can be safely sustained by the tested materials provided the matric suction in the soil is greater than 50 kPa.

DECLARATION

I, the undersigned hereby declare that:

- I understand what plagiarism is and I am aware of the University's policy in this regard;
- The work contained in this thesis is my own original work;
- I did not refer to work of current or previous students, lecture notes, handbooks or any other study material without proper referencing;
- Where other people's work has been used this has been properly acknowledged and referenced;
- I have not allowed anyone to copy any part of my thesis;
- I have not previously in its entirety or in part submitted this thesis at any university for a degree.

DISCLAIMER:

The work presented in this report is that of the student alone. Students were encouraged to take ownership of their projects and to develop and execute their experiments with limited guidance and assistance. The content of the research does not necessarily represent the views of the supervisor or any staff member of the University of Pretoria, Department of Civil Engineering. The supervisor did not read or edit the final report and is not responsible for any technical inaccuracies, statements or errors. The conclusions and recommendations given in the report are also not necessarily that of the supervisor, sponsors or companies involved in the research.

Signature of student:	
Name of student:	**Godisang David Mpye**
Student number:	**27018858**
Date:	**2020-11-30**

ACKNOWLEDGMENTS

I wish to express my appreciation to the following organisations and persons who made this thesis possible:

a) This Thesis is based on a research project of University of Pretoria. Permission to use the material is gratefully acknowledged. The opinions expressed are those of the author and do not necessarily represent the policy of Transnet Freight Rail and University of Pretoria.

b) The University of Pretoria, Transnet Freight Rail, Durham University (United Kingdom), Department of Higher Education and National Research Foundation for financial support, the provision of training and the use of laboratory facilities during the course of the study.

c) The following persons are gratefully acknowledged for their assistance during the course of the study:

   i) Professors D Toll and A Osman (Durham University, United Kingdom) for the exposure and teachings in unsaturated soils mechanics and the development of the proposal.

   ii) Professor G Heymann (University of Pretoria, South Africa) for the ad-hoc consultation and advice.

d) Professor PJ (Hannes) Gräbe (University of Pretoria, South Africa), my supervisor for the picture-perfect supervision, guidance and support.

e) My mother, for the constant and relentless encouragement and support.

f) My dear friend, Dr Nceba Ndzwayiba, for the good and supportive company.

g) My lovely cousin, Tebogo, and her partner, Carsten, for the fun travels and destressing times.

h) My sisters, Obakeng and Regomoditswe, and brother-in-law, Molefe, for the support and encouragement.

TABLE OF CONTENTS

LIST OF TABLES

LIST OF FIGURES

LIST OF SYMBOLS

a	empirical soil parameter for power model
b	empirical soil parameter for power model
e	void ratio
f	frequency
m	empirical soil constant for power model
n	wheel loads per load cycle
n_l	number of the layer of soil sample being considered
n_t	total number of layers of soil sample,
p'	mean effective stress (or effective mean stress)
$\bar{p}$	net mean stress (or mean net stress)
p	mean total stress (or total mean stress)
q	deviator stress (or deviatoric stress)
t	time
u_a	pore air pressure
u_w	pore water pressure
v	specific volume
A_c	corrected area of sample
A_0	original (or initial) area of sample
B	B-value (pore pressure coefficient)
E	Young's modulus of elasticity
G	shear modulus.
H	height of sample
H_n	height of the n-th layer of sample
H_0	original (or initial) height of sample
L	influence length
M	slope of critical state line (or failure envelope) of saturated soils
M(s)	slope of critical state line (failure envelope) of unsaturated soils
M_r	resilient modulus
N_a	number of load cycles per million gross tonnage
N	number of load cycles (or number of repeated load application)

P_s	static wheel load
R	radius of sample
R_0	original (or initial) radius of sample
s	matric suction
s_i	initial matric suction
T_s	surface tension
U_n	undercompaction percentage of n-th layer
U_{ni}	undercompaction percentage of the initial layer
U_{nt}	undercompaction percentage of the last layer
V	speed
V_a	volume of air
V_c	volume of contractile skin
V_w	volume of water
V_s	volume of solids
V_t	total volume
V_v	volume of voids

γ	self weight
$\Delta\sigma_d$	cyclic deviator stress (or cyclic amplitude)
ε_a	axial strain
ε_p	cumulative plastic strain
ε_r	resilient strain
ε_R	radial strain
ε_v	volumetric strain
$\mu(s)$	intercept term of unsaturated soils as a function of matric suction
ν	Poisson's ratio
σ	total normal stress
σ'	effective normal stress
$\bar{\sigma}$	net normal stress
σ'_m	maximum effective normal stress
σ_1	total major principal stress
σ_3	total minor principal stress

σ'_1	effective major principal stress
σ'_3	effective minor principal stress
σ_a	axial stress
σ_d	deviator stress (or deviatoric stress)
σ_{di}	initial deviator stress
σ_r	radial (or confining) stress
σ_s	compressive strength
σ_{max}	maximum vertical pressure
σ_{min}	minimum vertical pressure
σ_x	normal stress in x-direction
σ_y	normal stress in y-direction
σ_z	normal stress in z-direction
τ_{xy}	shear stress in xy-plane,
τ_{xz}	shear stress in xz-plane,
τ_{yz}	shear stress in yz-plane.
ϕ'	effective angle of shearing resistance
ψ_m	matric suction
ψ_o	osmotic suction
ψ_t	total suction

LIST OF ABBREVIATIONS

DYNTTS	Dynamic Triaxial Testing
GDS	Global Digital Systems
IHHA	International Heavy Haul Association
LVDT	Linear Variable Displacement Transformer
OCR	Over Consolidation Ratio
ORE	Office de Recherches et d'Essais
PPC	Pore Pressure Controller
PPT	Pore Pressure Transducers
STDDPC	Standard Digital Pressure Controller
SWCC	Soil Water Characteristic Curve
SWRC	Soil Water Retention Curve

CHAPTER 1
INTRODUCTION

1.1 BACKGROUND

The transportation of bulk freight by rail is more feasible as compared to other modes of transportation from a sustainability and economics point of view. On sustainability, the Department of Transport (2017) stated in its Draft National Rail Policy that new railway investments gravitate towards efficiency by increasing the axle loads, raising the train speed and (or) extending the train length. On the economic side, Harries (1977) and Havenga (2012) showed that the cost per tonne per kilometer of transporting freight by rail is inversely proportional to the distance. The transportation of heavy and bulk freight over a long distance becomes more financially feasible by rail. Custodians of various transport systems agree that the advantages and benefits of transporting freight by rail outweigh the disadvantages, such that road-to-rail strategies are being initiated. The endeavour and demand for the long distance transportation of bulk freight by rail is increasing in developed and developing countries including Australia, Brazil, China, South Africa, Sweden and the United States of America. However, this demand inevitably results in increased axle loading being imposed on current and new track infrastructures. It therefore remains crucially important that the performance of each track component and system at increased axle loading across all engineering disciplines (i.e., civil, electrical, mechanical and signalling) be well-understood; if not, advanced research should be deployed.

This study is concerned with the civil engineering aspects of increased axle loading and track geotechnics with a focus on the behaviour of unsaturated railway foundation materials, which are related to the permanent way and earthworks of the railway track structure. Gräbe (2002) stated that permanent way and earthworks construction costs of railway track comprise about 82 % of total track construction expenditure. It therefore emphasises the need to properly understand the behaviour of railway foundation materials, so as to produce sustainable, cost effective designs for a maintenance-free track substructure. Since the 1940s, as pioneered by Terzaghi (1946) and Taylor (1948), saturated soil conditions have become popular in contemporary geotechnical analysis and design, with the rationale of being the worst-case scenario. It is therefore for this reason that saturated soil conditions form part of this study. However, the inclusion of unsaturated soil conditions in railway foundations brings about the complexity and uniqueness of this study as recommended by Gräbe (2002) and motivated by the various researchers including Fredlund and Rahardjo (1993), Lu and Lukos (2004), Murray and Sivakumar (2010) and Blight (2013) who collectively agree that shallow foundation structures are situated within the vadose zone with the prevalence of unsaturated soil conditions. In the vadose or

unsaturated zone, the degree of saturation is between 0 and 100 %, where the presence of pore air in the soil matrix is responsible for the development of negative pore water pressure (Fredlund, 2018).

The first justification of the study is the growing demand for increased axle loading in the railway fraternity. The second justification of the study is that the cost of earthworks in a railway project is substantial and the railway substructure needs to be designed to be maintenance-free during its entire life cycle. The third and last justification is that soil conditions in a shallow foundation, such as a railway foundation in an arid to semiarid environment, are mostly unsaturated.

1.2 OBJECTIVES OF THE RESEARCH

The study consists of three research objectives, which are as follows:

1. Investigation of the effect of unsaturated soil conditions on the soil behaviour, in comparison with saturated soil conditions,

2. Investigation of the effect of increased axle loading on saturated railway foundation materials,

3. Investigation of the effect of increased axle loading on unsaturated railway foundation materials.

1.3 SCOPE OF THE RESEARCH

The scope of the research is confined to the substructure materials of a railway foundation, namely the subballast and the subgrade materials. The ballast material is not included in the research as its physical properties and design life are different to that of the subballast and subgrade materials, i.e., the ballast layer can be maintained by means of tamping, screening or replacing, whereas the subballast and subgrade materials are supposed to be maintenance-free throughout the design life of the track. Five axle loadings are considered, starting from 20 tonnes per axle as the base load case to establish initial conditions, with increased axle loading of 26, 30, 32.5 and 40 tonnes per axle. Two soil conditions are considered for each material and axle load case, namely saturated conditions where the matric suction is 0 kPa and then unsaturated conditions with matric suction of 50, 100 and 225 kPa.

The calculations of the cyclic loading on the subballast and subgrade layers are determined by means of finite element modelling using ABAQUS. The track structure is developed as a multi-layer system

with representative properties for each track component in a conventional railway track, including rails, sleepers, ballast, subballast and subgrade. An elastic analysis is carried out mainly because the aim of the model is to determine the stresses and not the strains or deformations. The stresses for each axle load case, i.e., 20, 26, 30, 32.5 and 40 tonnes per axle, are calculated at a depth of 0 m for the subballast material and 200 mm for the subgrade material, relative to the formation level. The stresses from the finite element analysis are thereafter used as input parameters for the experimental work.

Laboratory equipment and apparatus were acquired and developed for the experimental work. The apparatus included a Wesley triaxial cell equipped with a high air entry disk for unsaturated soil conditions, an actuator unit capable of monotonic and cyclic loading, hydraulic pressure controllers, pneumatic pressure controller, pressure transducers and local instrumentation devices in the form of miniature Linear Variable Differential Transformers (LVDT).

Laboratory tests were carried out on two reconstituted materials which were representative of the subballast and subgrade materials, with a maximum particle size of 2 mm. Soil samples are prepared to be identical to each other and representative of the field conditions after construction. Monotonic and cyclic triaxial tests are carried out on materials under saturated and unsaturated soil conditions. All samples are saturated to a B-value greater than 0.95 under the application of back-pressure and cell pressure. Saturated samples are sheared under undrained conditions to replicate the development of pore pressures during loading. Samples for unsaturated tests are unsaturated by introducing pore air into the sample and allowing the pore pressure to equilibrate to the specific matric suction of 50, 100 or 225 kPa.

Critical state soil mechanics for saturated and unsaturated soils is used as the model of analysis to determine the failure criterion, failure envelope and shear strength. The effect of unsaturated soil conditions on soil behaviour is investigated based on the monotonic test results. Cyclic loading is limited to 2000 load cycles and a frequency of 1 Hz. Comparative analyses are carried out to determine the effect of increased axle loading on the behaviour of saturated and unsaturated railway foundation materials, based on the stress states, resilient modulus, resilient strains, plastic strains and pore pressure response.

1.4 METHODOLOGY

The objectives of the research are achieved by implementing the following methodology:

- A detailed literature review delving on the railway track structure, track loading and increased axle loading, fundamental principles of saturated and unsaturated soils and the triaxial testing thereof,

- Finite element modelling and analysis for the characterisation of cyclic railway loading under field conditions to triaxial stress space for laboratory testing, in order to simulate the same effect of a passing train,

- Development of laboratory testing apparatus, capable of performing monotonic and cyclic loading under saturated and unsaturated soil conditions,

- Preparation of soil samples using two test materials representative of track foundation materials in the subballast and subgrade layers of a railway foundation,

- Data collection in the laboratory by means of conducting comparative triaxial tests including monotonic and cyclic loading test for the respective axle load cases. Representative field loading conditions for saturated materials were in the form undrained conditions and for unsaturated materials it was in the form of constant water content,

- Analysis and interpretation of the results to investigate and quantify the effect of increased axle loading on the behaviour of saturated and unsaturated railway foundation materials by investigating various soil parameters.

1.5 ORGANISATION OF THE THESIS

Chapter 1 forms part of the introduction to the thesis, which commences by discussing the global trend and demand for long distance transportation of bulk commodities by rail, which inevitably leads to increased axle loading on railway foundation materials and therefore forms part of the rationale or motivation for this research. The chapter also contains the objectives, methodology and the scope of the research.

Chapter 2 contains the literature review of the thesis. It begins with a brief description of the railway network in South Africa, followed by a discussion of the superstructure which delves into increased

axle loading and substructure, focusing on railway foundation materials. Thereafter, the chapter covers the science and fundamental principles of saturated and unsaturated soils in railway foundations. The chapter closes off with a discussion which argues and presents the lacuna in knowledge related to increased axle loading and railway foundation materials.

Chapter 3 contains the finite element modelling and analyses carried out to characterise the cyclic loading on the subballast and subgrade materials as a result of increased axle loading from a base load of 20 tonnes per axle to increased loads of 26, 30, 32.5 and 40 tonnes per axle, which are representative of heavy haul standards.

Chapter 4 contains a description of and discussion on the laboratory equipment in the form of a cyclic triaxial apparatus for saturated and unsaturated soil conditions and the related instrumentation developed for the experimental work of the research.

Chapter 5 contains the experimental work of the research, which commences with an outline of the methodology carried out for data collection, followed by a brief discussion of each stage of the test procedure and the presentation of the related preliminary results.

Chapter 6 contains the results from the analysis and interpretation thereof with discussions, specific to the effect of increased axle loading on various parameters related to saturated and unsaturated soils, including stress states, excess pore water pressure, matric suction, resilient and permanent strains amongst others.

Chapter 7 contains the conclusions of the research and closes off with recommendations related to further studies on cyclic loading and on unsaturated soils.

CHAPTER 2
LITERATURE REVIEW

2.1 HEAVY HAUL AND RAILWAY NETWORK IN SOUTH AFRICA

The transportation of freight by rail plays an important role in the daily economic activities and development of a country. As a result, the advantages associated with the freight transportation by rail are well known. Advantages include reduced energy consumption, maximised payload per km, minimised costs per km and per tonnes, less land occupation and reduced air pollution compared to road transport. These advantages are further optimised on heavy haul railway lines. In June of 1998, the Action Board of the International Heavy Haul Association (IHHA) approved the criteria under Clause 4.9.1 of the by-laws for a railway line to be classified as a heavy haul line (IHHA, 1998). The criteria are as follows and a railroad must meet at least two of them inclusive of regular operations or contemplation thereof:

- Regular operations of a combined train of at least 5000 tonnes gross mass,
- Haulage of revenue freight of at least 20 million gross tonnes per annum over a given line haul segment of at least 150 km in length and
- Operation of equipment with axle loadings of 25 tonnes or more.

The freight railway network in South Africa is depicted in Figure 2-1. In South Africa, the Coal Export Line between Ermelo and Richard Bay and the Iron Ore Export Line between Sishen and Saldanha meet all the requirements for a heavy haul line set by the IHHA. The characteristics of the heavy haul lines are presented in Table 2-1 as reported the by the national freight rail operator.

Table 2-1: Characteristics of the Coal and Iron-ore export lines (Transnet Freight Rail, 2019)

Property	Units	Coal Export Line	Iron-Ore Export Line
Gross tonnage per train	tonnes	22 000	41 000
Gross tonnage per year*	million tonnes	72.0	58.4
Gross tonnage per axle	tonnes	26	30
Length per train	km	2.2	4.0
Length of railway lines	km	580	861
Payload per wagon	tonnes	84	100

*actual gross tonnage in 2018/19 fiscal year

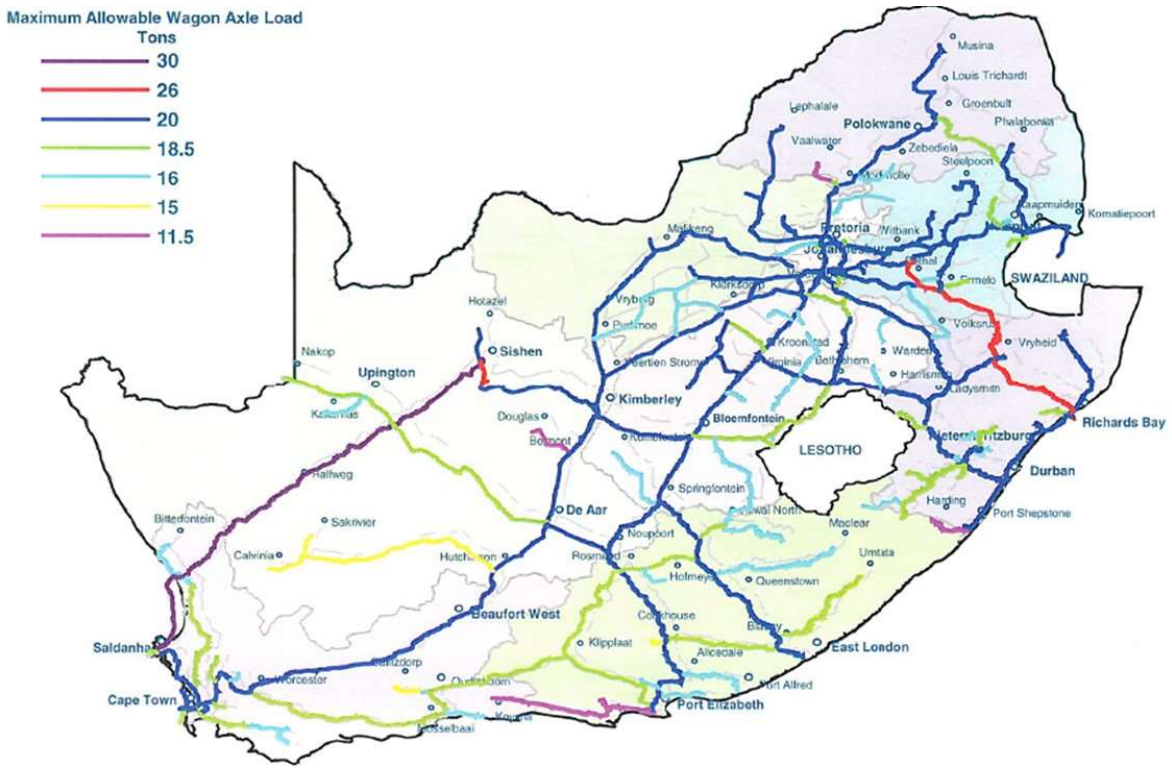

Figure 2-1: Freight railway infrastructure in South Africa (Courtesy of Transnet Freight Rail)

The current railway track structure on the South African network is the conventional track structure, also known as ballasted track which is shown in Figure 2-2. It consists mainly of the superstructure and substructure. The superstructure consists of rails, fastening systems and sleepers, while the substructure consists of the ballast, subballast, placed soil and natural in-situ subgrade. Track geotechnology and foundation design methods are predominantly concerned with the components situated in the substructure below the foundation level. However, the superstructure cannot be disregarded because it is the point of origin of the train loads, which are to be distributed into the underlying weaker layers.

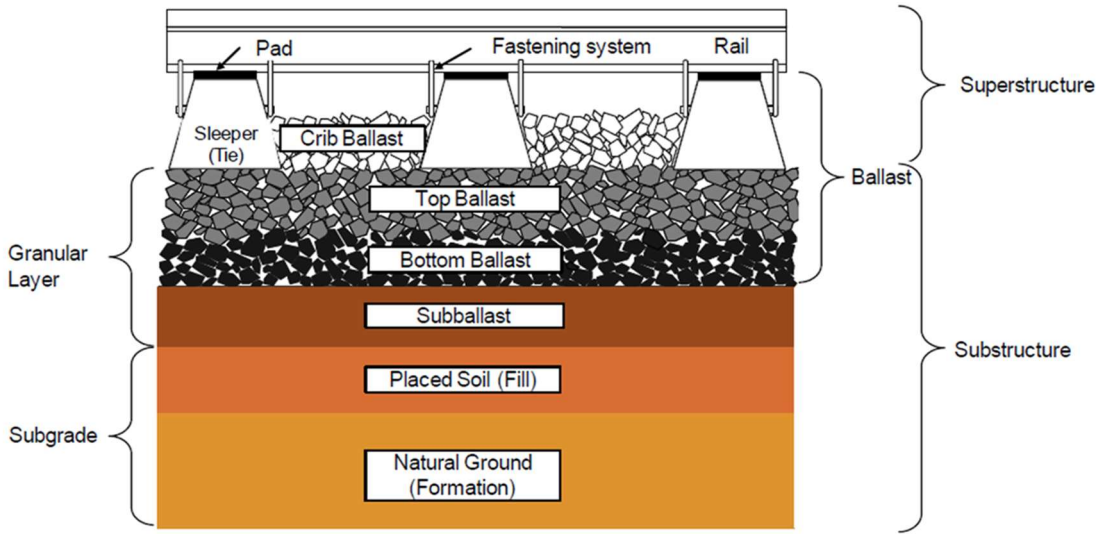

Figure 2-2: Conventional railway track structure (adapted from Selig and Waters, 1994)

2.2 SUPERSTRUCTURE - INCREASED AXLE LOADING

The superstructure is the component in the track structure which bears the highest stresses imposed by the train loading. Esveld (2001) emphasised that the loading on railway track comprises three components, namely: longitudinal, vertical and lateral. According to ORE D 161 (1987), the vertical load component which is measured in metric tonnes per axle is important for the design and maintenance of the railway track foundation. The axle loads of the railway network in South Africa is shown in Figure 2-1. It ranges from 11.5 to 30 tonnes per axle. The heaviest axle load is on the Iron-Ore Export Line at 30 tonnes, followed by the Coal Export Line at 26 tonnes and the general freight lines at 20 tonnes. Lighter axle loads are for branch and pickup lines. Researchers have recognised that track loads are characterised by complex stresses as a result of the moving wheel loads, which are cyclic in nature. O'Reilly and Brown (1991) defined a cyclic load as a non-static repetitive load. Li et al. (2016) went further and stated that a cyclic load is characterised by shape, duration, magnitude of loading pulse, time interval between consecutive pulses and the total number of loading pulses. Gräbe (2002) highlighted that the complexity is compounded by reversal of shear stresses as a result of the rotations of principal stresses.

Internationally, governments both in developed and developing countries have in their sustainability policies on transportation a drive towards moving freight from road to rail. In recent years, railway operators have been under pressure to increase the overall throughput of commodities in response to global economic high demands. This has resulted in heavier and longer trains as evident in Table 2-2. In South Africa, the government of the day through its department of transport (DOT, 2017), drafted a white paper on National Rail Policy with a road-to-rail strategy, that will see the move of long-distance haulage of freight from the roads to railways. In relation to this study, the effect of increased axle loading on existing railway infrastructure needs to be critically evaluated from an engineering perspective. As depicted in Figure 2-1 and Figure 2-3, the axle load on the majority of the railway network is 20 tonnes per axle. In 2016, the freight railway operator in South Africa promulgated its long term planning framework, which will see an increased axle loading from 20 tonnes per axle to heavy haul standards as depicted in Figure 2-3 in addition to the existing two heavy hail railway lines.

Table 2-2: Axle loading and future trends in the world (after Li et al., 2016)

Country	Axle loads (tonnes)	Train length (Number of cars)	Future trend (train length or axle load)
United States and Canada	33	130 - 140	150 - 170 cars
Australia	35 - 40	200 - 240	333 cars
South Africa	26 - 30	200 - 216	332 cars
Brazil	27.5-32.5	330	37 tonnes
Sweden	30	68	-
China	25 - 27	210	30 tonnes

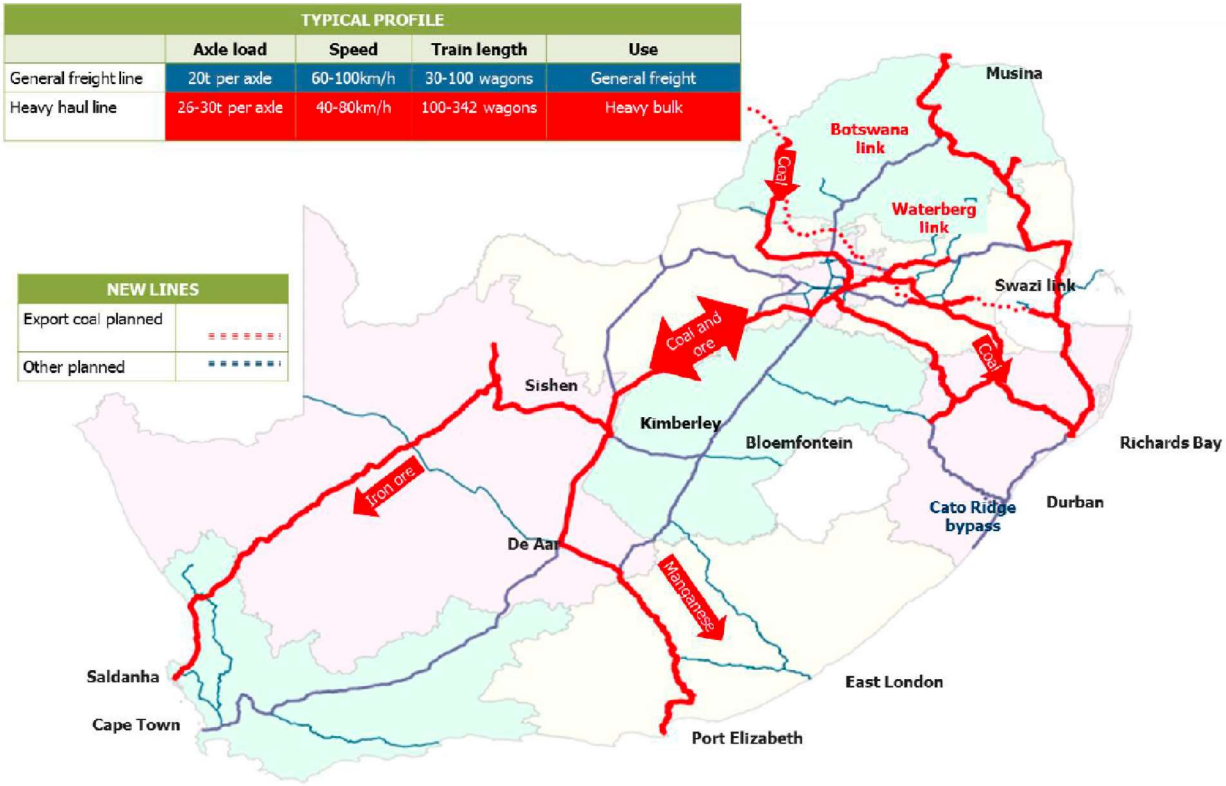

Figure 2-3: 30-year plan of axle load increase in South Africa (Transnet Freight Rail, 2016)

2.3 SUBSTRUCTURE - RAILWAY FOUNDATION

The substructure components which form part of the track foundation consists of the subballast and subgrade. The subballast is the layer(s) of material between the ballast and the subgrade. The particle size gradation of the subballast is generally finer than the top ballast and courser than that of the subgrade material. Selig and Waters (1994) stated that older railway tracks did not have a subballast layer. The inclusion of the subballast reduces the otherwise required greater thickness of the ballast material. The functions of the subballast are listed below:

- Reduce the traffic induced stresses at the bottom of the ballast layer to acceptable levels for the top of the subgrade,
- Prevent interpenetration of subgrade with the ballast,
- Prevent subgrade attrition by ballast,
- Prevent upwards migration of fine material from the subgrade,
- Permit drainage of water that might by flowing upwards from the subgrade and
- Extend the subgrade frost protection.

The subgrade is a combination of the placed soil and the natural in-situ ground. The main function of the subgrade is to provide a stable platform for the subballast, ballast and superstructure. The subgrade is regarded as a major component which supports the superstructure and provides resiliency and contributes significantly to the elastic and resilient deflection of the rail subjected to wheel loading. This leads to the realisation that a subgrade that is not sufficiently protected or improved will result in excessive maintenance cost. If enough care is not taken, delays in operation is inevitable and the ultimate result is a catastrophic train derailment due to foundation failure. Current railway foundation design methods have taken an ardent and keen interest in the behaviour of the subgrade when subjected to repetitive train loads. In fact, the main objective of these methods is to prevent premature failure of the foundation layers and the subgrade.

2.3.1 RESILIENT BEHAVIOUR

The resilient (or elastic) behaviour of a track foundation is the recoverable deformations due to loading, commonly quantified by means of the resilient modulus. The term resilient modulus was introduced at the University of California in Berkeley following pioneering work on pavement materials. Li and Selig (1994) presented Equation (2-1) as the general equation used to determine the resilient modulus.

$$M_r = \frac{\sigma_d}{\varepsilon_r} \tag{2-1}$$

Where:

M_r = resilient modulus,

ε_r = resilient strain (or recoverable strain),

σ_d = deviator stress.

Various authors such as Brown (1996) and Gräbe (2014) have highlighted that in a well designed pavement structure, most of the deflections will be recovered. Field measurements have indicated that the resilient deformations in a railway track foundation are much greater than the permanent deformations. In railway engineering, the structural performance of track foundation is measured against a set minimum criterion in terms of deformation and the resilient modulus is used to calculate the deflection and stresses at an arbitrary point within the foundation. Furthermore, the recently developed mechanistic methods adopt the use of the time variation of the resilient modulus to model and predict life cycle of a pavement (Shaw, 2006). Li and Selig (1994) stated that it has been found that the following factors have an influence on the resilient modulus of fine materials: (1) loading conditions and stress states inclusive of deviatoric stress, confining stress and number of loading cycles, their sequence and stress history; (2) soil type and its structure, in the form of compaction method and effort and (3) soil physical state, in terms of moisture content and dry density.

2.3.2 PLASTIC BEHAVIOUR

The permanent (or plastic) behaviour of a track foundation is the irrecoverable deformation due to loading, quantified by means of the cumulative plastic strain. Similar to the resilient behaviour, Li and Selig (1996) stated that the plastic strain is influenced by the following factors: (1) loading conditions and stress states, (2) soil type and its structure, and (3) soil physical state. Various models have been developed to calculate the cumulative plastic strains. Selig and Waters (1994) stated that the most commonly used model to predict the cumulative plastic strain under repeated loading is the power model, represented by Equation (2-2).

$$\varepsilon_p = aN^b \tag{2-2}$$

Where:

ε_p = cumulative plastic strain,

N = number of repeated load applications,

a, b = parameters dependant on soil type, soil properties and stress states.

A modification to Equation (2-2) was proposed by Li and Selig (1996) as presented as Equation (2-3) taking into account the effect of the three influencing factors, that is, deviatoric stress, soil type and physical state. However, Gräbe and Clayton (2009) concluded that the effect of principal stress rotation inherent in moving cyclic loading tends to significantly expedite the permanent deformations of railway foundations.

$$\varepsilon_p = a\left(\frac{\sigma_d}{\sigma_s}\right)^m N^b \tag{2-3}$$

Where:

σ_s = compressive strength,

m, b = soil parameters.

The majority of pavement design methods have largely been based on empirical procedures, probably because of the complex nature of the soil response to dynamic and cyclic loading and more complex under unsaturated soil conditions. The main cause of all track foundation failures is inherently related to loading exceeding the linear elastic limit, leading to plastic behaviour. Heyns (2004) comprehensively listed the following track foundation failure mechanisms:

- Progressive shear failure,
- Excessive permanent deformation,
- Massive shear failure,
- Attrition mud-pumping,
- Consolidation.

2.3.3 DESIGN METHODS

The state-of-the-art design methods which are scientific in nature and incorporate the fundamental principles of soil behaviour under cyclic loading are those by Li and Selig (1998) and Shahu et al. (2000). The two methods highlight the importance of stresses and strains as design parameters. The Li and Selig method utilises the allowable permanent strain in the foundation as a design criterion, while the Shahu et al. method utilises the allowable stress in the foundation as a design criterion.

Li and Selig method

Li and Selig (1998a) developed a track foundation method with a fundamental principle of preventing progressive shear failure and excessive plastic deformation based on saturated cyclic triaxial tests in accordance with Equation (2-4).

$$\rho = \int_0^t \varepsilon_p dt \tag{2-4}$$

Where:

ρ = total cumulative deformation,

t = thickness of the foundation.

The cumulative plastic strain is determined in accordance with Equation (2-4). The thickness of the foundation (t) is the unknown parameter to be determined. The design approach for preventing subgrade progressive shear failure is to limit the total cumulative plastic strain and total cumulative plastic deformation at the subgrade surface to below an allowable level for the design period, as represented by Equations (2-5) and (2-6) respectively.

$$\varepsilon_p \leq \varepsilon_{pa} \tag{2-5}$$

$$\rho_p \leq \rho_{pa} \tag{2-6}$$

Where:

ε_{pa} = allowable plastic strain at the subgrade surface,

ρ_a = allowable plastic deformation of the foundation layer.

Li and Selig (1998b) recommended maximum values of 2 % and 2.5 mm for the cumulative plastic strain and total cumulative plastic deformation respectively as design criteria for railway foundations. The main advantage of the Li and Selig method is that it is not solely empirical and involves fundamental scientific principles in the derivation of the strain development. The limitations of the method are that it does not consider the effect of the principal stress rotations and the compressibility of air by virtue of exclusion of unsaturated soil conditions.

Shahu et al. method

Shahu et al. (2000) developed a track foundation design method with a fundamental principle of limiting the maximum shear stresses on the subgrade surface to below the threshold of the subgrade soil in accordance with Equation (2-7).

$$R_{TS} = \frac{(\sigma_1 - \sigma_3)_{TS}}{(\sigma_1 - \sigma_3)_s} \quad (2\text{-}7)$$

Where:

R_{TS} = threshold stress ratio,

σ_1 = major principal stress,

σ_3 = minor principal stress,

$(\sigma_1 - \sigma_3)_{TS}$ = threshold deviatoric stress of the soil in terms of deviator stress,

$(\sigma_1 - \sigma_3)_s$ = applied deviatoric stress on the subgrade in terms of terms of deviator stress.

The design criterion is that the threshold stress ratio should be greater than unity. The method is based on an iterative process of stress analysis by varying the thickness of the foundation layer, until the threshold stress ratio is greater than unity. The threshold stress of the soil can be determined either analytically by means of numerical methods or experimentally in the laboratory using a triaxial apparatus.

2.4 SATURATED SOILS IN RAILWAY FOUNDATIONS

The theoretical study of saturated soils was formally published in a textbook format by Terzaghi (1943) after the discovery of pore pressures, then called neutral stress or pressure based on experiments conducted from the 1920s. The underlying condition associated with saturated soils is that the voids in the soil structure at the point of interest are filled with water such that the degree of saturation is 100 %. For a railway foundation, it would mean that the ground water table is located at the surface of the natural ground as depicted in Figure 2-4. It may well be argued whether saturated soil conditions are appropriate and applicable to railway foundations and other shallow foundations located in arid and semi-arid regions. However, well known constitutive models for unsaturated soils indicate that saturated conditions can be assumed to be the worst-case scenario if shear strength is to be taken as the design criteria.

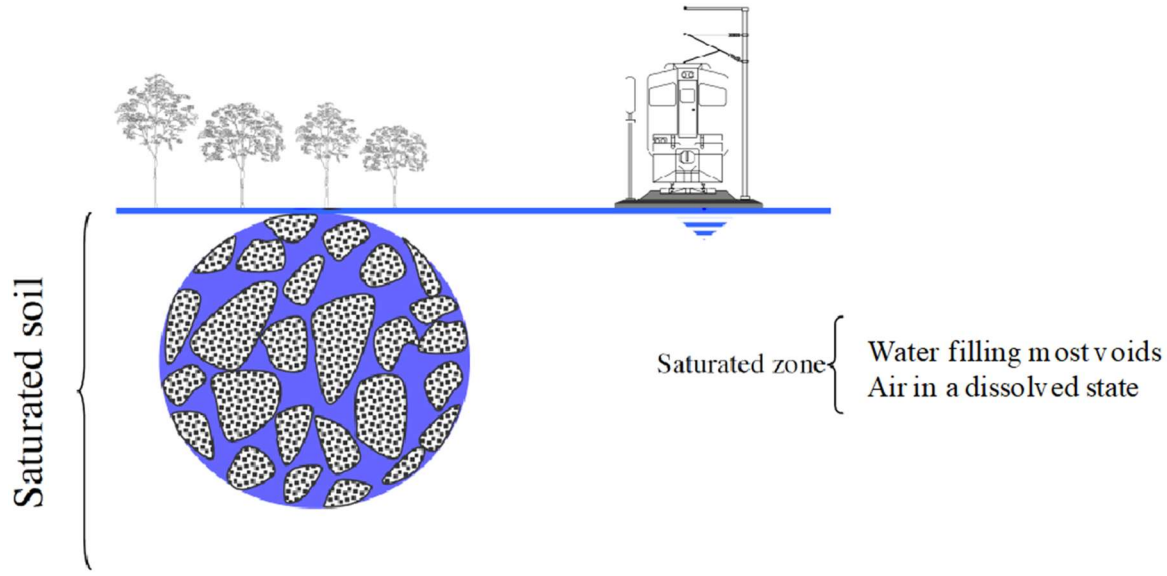

Figure 2-4: Saturated conditions in a railway foundation (Modified from Perez-Ruiz, 2009)

2.4.1 DEFORMATION STATE VARIABLES OF SATURATED SOILS

Deformation state variables are also nonmaterial variables required for the characterisation of deformation or deviation from an initial state (Fredlund and Rahardjo, 1993). In the development of the theory of consolidation, Terzaghi (1921, 1923) presented void ratio as a deformation state variable. As represented by Equation (2-8), void ratio is a volumetric parameter and it depends on the volume of voids and the volume of solids in a soil sample. The development of critical state soil mechanics theory introduced specific volume as a deformation state variable based on the void ratio as shown in Equation (2-9). The specific volume is the total volume of soil sample containing a unit volume of solid particles and it was introduced to simplify the mathematical expression and equations.

$$e = \frac{V_v}{V_s} \tag{2-8}$$

$$v = 1 + e \tag{2-9}$$

Where:

e = void ratio,

v = specific volume,

V_v = volume of voids,

V_s = volume of solids.

2.4.2 STRESS STATE VARIABLES OF SATURATED SOILS

Stress state variables are nonmaterial variables required for the characterisation of stress equilibrium conditions (Fredlund and Rahardjo, 1993). The use of effective stress as represented in Equation (2-10) was postulated by Terzaghi (1936) as the only stress state variable which controls the behaviour of

saturated soils. All effects associated with the change in stress, such as compression, distortion and shear resistance are exclusively due to changes in the effective stress. Up to date, the validity of effective stress as a stress state variable for saturated soils has been well accepted by the geotechnical engineering fraternity in general.

$$\sigma' = \sigma - u_w \tag{2-10}$$

Where:

σ' = effective normal stress,

σ = total normal stress,

u_w = pore water pressure.

2.4.3 CRITICAL STATE OF SATURATED SOILS

The critical state of saturated soils was originally verified experimentally and mathematically by Roscoe et al. (1958) whilst studying the critical void ratio of soils. The critical void ratio was defined as the state in the soil where continued shear distortion in drained tests will not result in a change in the void ratio (or specific volume) and continued shear distortion in undrained tests will not result in a change in the mean effective stress. Roscoe et al. (1958) recognised that the projection of the critical void ratio line from the $v : p'$ plane to the $q : p'$ plane formed a straight line which defines the maximum resistance to shearing under the application of axial load (or deviator stress), as originally depicted in Figure 2-5. This line was subsequently called the critical state line of saturated soils for shear stresses and defined by Equation (2-11).

$$q = Mp' \tag{2-11}$$

Where:

q = deviator stress,

p' = mean effective stress,

M = slope of the critical state line of saturated soils (or effective stress ratio at critical state).

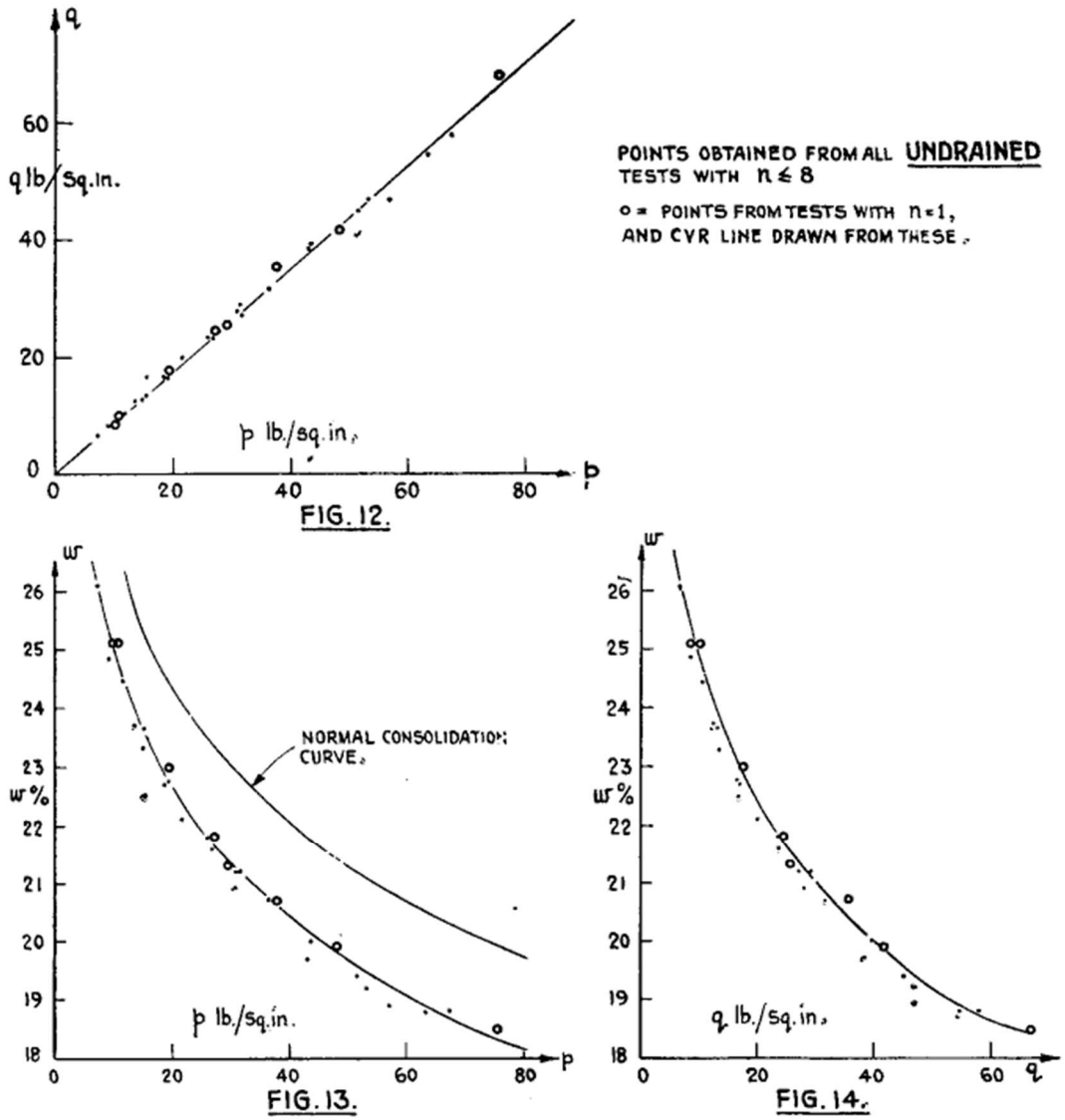

Figure 2-5: Projection of critical state line for saturated soils in $p{:}\,q$ plane from critical void ratio line in $p{:}\,w$ and $q{:}\,w$ plane (Rosoce et al., 1958) Note: w = void ratio

In triaxial space, the intermediate principal stress is equal to the minor principal stress and the mean effective stress and deviator stress are represented by Equations (2-12) and (2-13). With the use of Mohr circles developed by Mohr (1882) and Cambridge stress invariants as shown by Schofield and Wroth (1968) at critical state, the slope of the critical state line can be derived and determined using Equations (2-14) and (2-15).

$$p' = \frac{\sigma'_1 + 2\sigma'_3}{3} \tag{2-12}$$

$$q = \sigma'_1 - \sigma'_3 \tag{2-13}$$

$$M = \frac{6\sin\phi'}{3 - \sin\phi'} \tag{2-14}$$

$$\sin \phi' = \frac{\sigma'_1 - \sigma'_3}{\sigma'_1 + \sigma'_3} \quad (2\text{-}15)$$

Where:

σ'_1 = effective major principal stress,

σ'_3 = effective minor principal stress,

ϕ' = effective angle of shearing resistance of saturated soils at critical state.

Atkinson and Bransby (1978) maintained that the critical state line is the line where soil failure will occur, manifested as a state at which large shear distortion occur with no change in the applied stress or specific volume. Wood (1990) defined critical state as a condition of perfect plasticity. Up to date, the critical state line of a soil is considered a fundamental concept of soil behaviour such that it is often called the failure envelope and numerical models such as the CamClay by Schofield and Wroth (1968) postulate that stress states below the critical state line (or yield surface) will result in elastic behaviour and those slightly above (for dense sands) or on the critical state line will result in plastic behaviour. It is on these bases that the critical state of the soil is often considered as the ultimate shear strength.

2.5 UNSATURATED SOILS IN RAILWAY FOUNDATIONS

The study of unsaturated soils, also known as partially saturated soils, first appeared in the work conducted by Schofield (1935) whilst studying the concept of suction in the field of soil science. With a background of soil mechanics, Bishop (1961a) defined an unsaturated soil as a partially saturated soil containing air and water in the pore space, where the soil skeleton is in equilibrium with the surface tension of the air water interface around the pore space. Fredlund and Morgenstern (1977) extended the definition of an unsaturated soil as having three or more phases, namely solids, water, air and contractile skin. Lu and Likos (2004) simplified the definition by stating that an unsaturated soil is a soil with a degree of pore water saturation less than unity. The research work by Toll (2013) associated tropical conditions with unsaturated soils. Extensive research work by Blight (2013) associated arid and semi-arid regions with unsaturated soils. From these respective definitions, it clear that unsaturated soils are widespread across the globe and an important parameter that differentiates an unsaturated from a saturated soil is the presence of soil suction and a degree of saturation below unity. Pournaghiazar et al. (2013) stated that unsaturated soils are widely encountered in many geotechnical structures including fills, embankments and pavements for roads, railways and airfields.

As depicted generically in Figure 2-6, a railway track is founded mostly on unsaturated soils. That is, immediately below the ground surface, the soil is mainly under unsaturated soil conditions, whereby the voids are filled with air and water, whereas saturated conditions are encountered at much deeper

levels beyond the influence of the foundation. Weinert (1980) stated that in Southern Africa, the rate of evaporation is higher than the rate of precipitation giving rise to arid to semi-arid conditions which leads to unsaturated soil conditions. Blight (2013) went further and stated that the climate in Southern Africa is mainly semi-arid with severe dry winters giving rise to unsaturated soil conditions within the upper regions of the crust of the earth. It is therefore only realistic that conditions related to unsaturated soil conditions should be included in the geotechnical engineering models for analysis and design purposes.

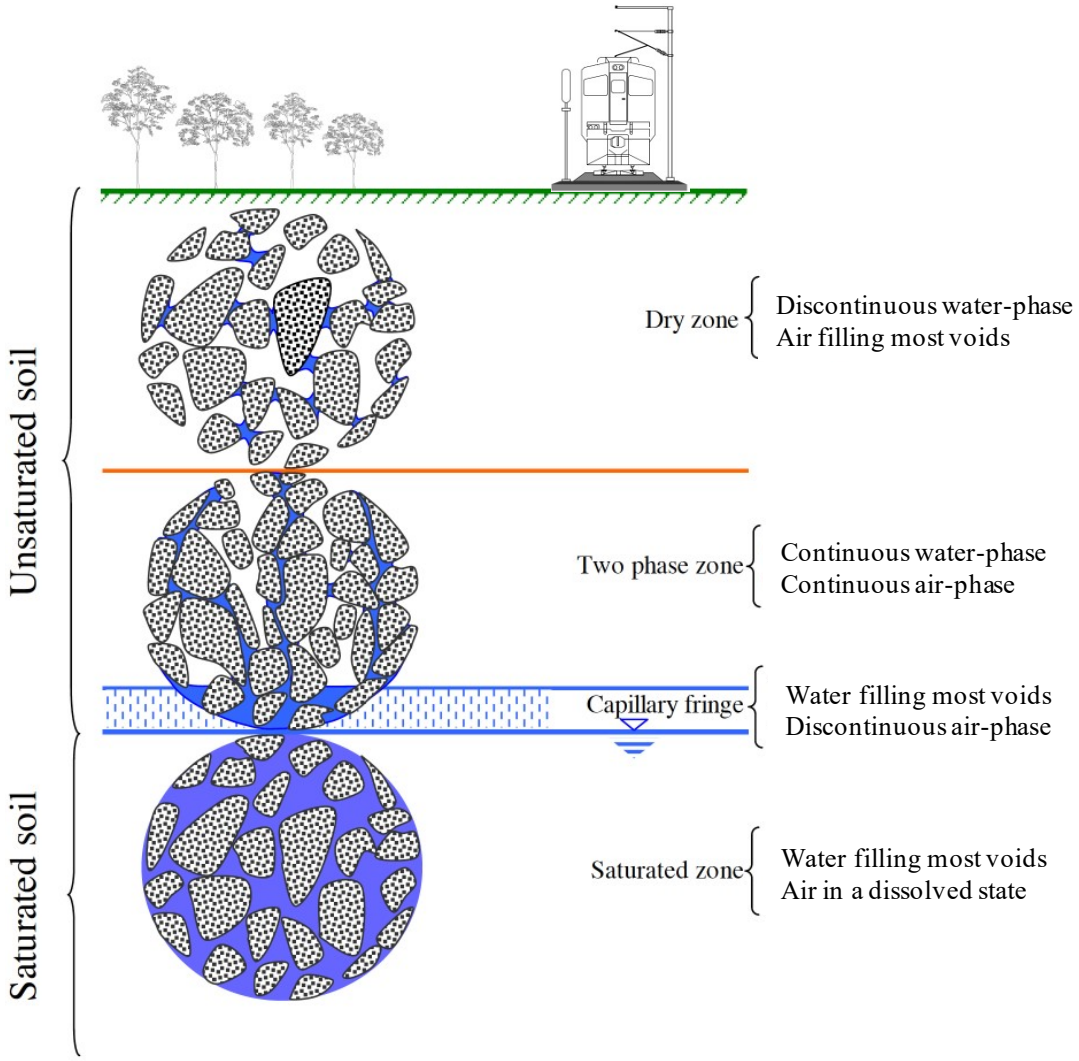

Figure 2-6: Unsaturated and saturated soil conditions in a railway foundation (Modified from Perez-Ruiz, 2009)

2.5.1 SUCTION IN UNSATURATED SOILS

Toll (2012) explained that suction in unsaturated soils consists of matric suction and osmotic suction. Matric suction is due to the surface tension forces at the interfaces (or menisci) between the water and gas (or air) which is as a result of capillarity action. Osmotic suction is caused by the presence of

dissolved salts in the pore water. The numerical sum of the osmotic suction and matric suction is equal to the total suction of unsaturated soils as shown in Equation (2-16).

$$\psi_t = \psi_o + \psi_m \tag{2-16}$$

Where:

ψ_t = total suction,

ψ_o = osmotic suction,

ψ_m = matric suction.

Fredlund and Rahardjo (1993) stated that for most geotechnical engineering applications, it is reasonable to assume that the greater contribution to the total suction in a soil will be from the matric suction component, such that total suction is approximately equivalent to matric suction as shown in Equation (2-17).

$$\psi_t \approx \psi_m \tag{2-17}$$

2.5.2 SOIL-WATER-RETENTION-CURVE OF UNSATURATED SOILS

A soil-water-retention-curve (SWRC), also called Soil Water Characteristic Curve (SWCC) is a measure of the matric suction as a function of the degree of saturation or gravimetric water content, which describes the hydro-mechanical behaviour of unsaturated soils. Briaud (2013) presented data which indicate that the shape of the primary SWRC is largely dependent on the soil type as depicted in Figure 2-7. There are distinctive stages during desaturating of unsaturated soils as explained by Vanapalli et al. (1999). The first stage is the boundary effect zone, followed by the transition zone and lastly residual zone of saturation. The boundary effect stage originates at a degree of saturation of 100% where the matric suction is zero and ends at the air entry value of the soil. The air entry value is essentially matric suction which causes desaturation of the largest pores. Upon reaching the air entry value, the soil undergoes a transition state where the degree of saturation linearly decreases as the suction exponentially increases. During the transition state, the connectivity of the water in the soil pores continues to reduce until there is a relatively small change in the degree of saturation, which leads to the residual state of saturation. In the residual stage of saturation, the water in the soil pores becomes completely discontinuous and the removal of the water by means of drainage becomes difficult. The relationship between matric suction and volumetric water content for the clays, silts and sands is shown in Figure 2-8. Based on the figure, it is evident that the air entry value of clays is mostly higher than that of sands. Furthermore, in case of clayey soils, a small change in the moisture content is required to mobilise high matric suctions.

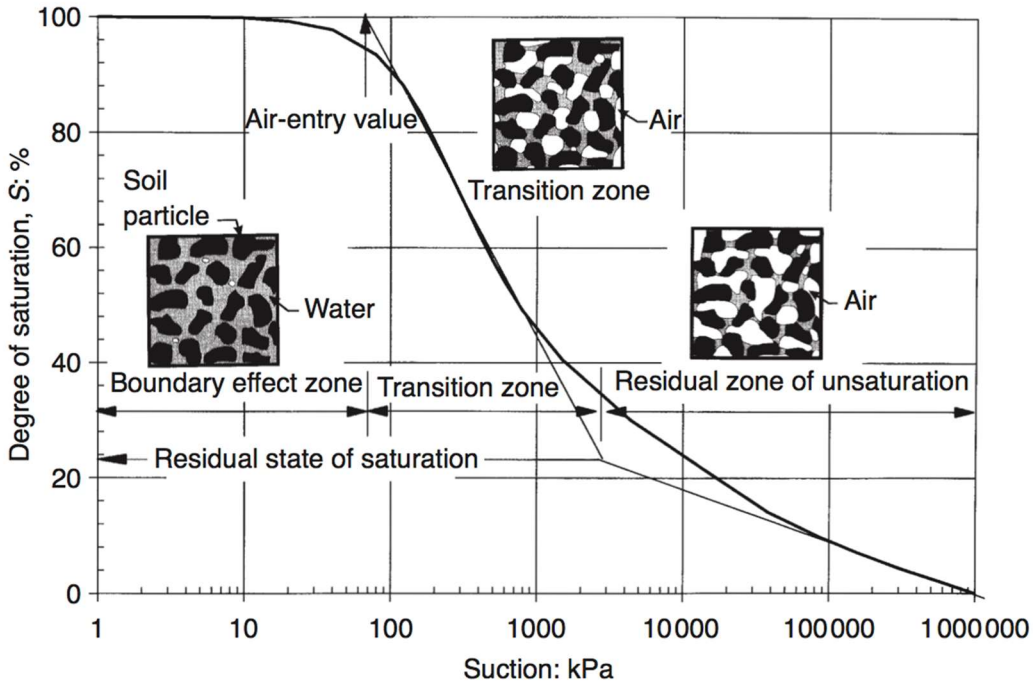

Figure 2-7: Stages of soil desaturation described by soil-water-retention-curve (Vanapalli et al., 1999)

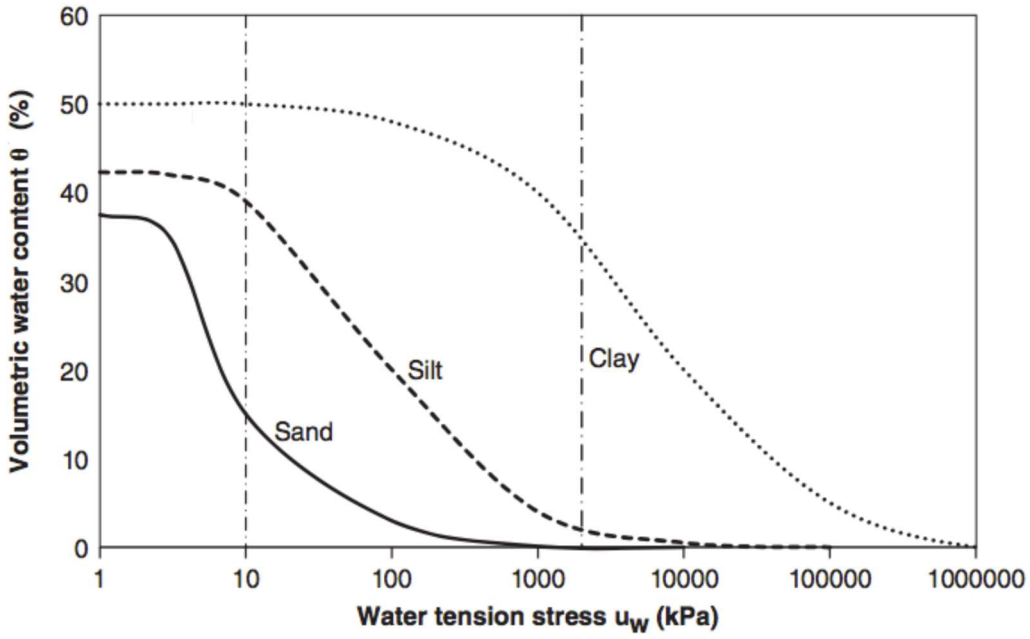

Figure 2-8: Soil water retention curve related to soil type (adapted from Briaud, 2013)

2.5.3 SOIL BEHAVIOUR DURING UNSATURATED SOIL CONDITIONS

The effect of unsaturated soil conditions on the soil behaviour has been widely published. The first effect of unsaturated soil conditions is collapsibility. Numerous researchers including Alonso et al. (1989), Rust et al. (2005; 2008) amongst others maintain that an unsaturated soil is inherently collapsible upon wetting and loading. Subsequently Alonso et al. (1990) developed the load-collapse

curve which is a constitutive equation which quantifies the collapse behaviour of unsaturated soil as a function of matric suction and net mean stress. The second effect of unsaturated soil conditions is on the shear strength. Various researchers agree that unsaturated soil conditions tend to increase the shear strength of a soil. To this effect, Fredlund et al. (1978) developed the Extended Mohr Coulomb failure envelope which quantifies the increase in shear strength as a function of matric suction. Later, Alonso et al. (1990) developed a critical state model for unsaturated soils called the Barcelona Basic Model, whereby the increase in shear strength is quantified by the intercept term. Other models which acknowledge the increase in shear strength of unsaturated soil were developed by Toll (1990), Wheeler and Sivakumar (1995) and Ng and Menzies (2007) to mention a few. Lastly Toll (1990) maintained that contrary to saturated soil where the fabric is destroyed during shear, the fabric of unsaturated soils is supported by suction which produces packets within the soil skeleton.

2.5.4 DEFORMATION STATE VARIABLES OF UNSATURATED SOILS

Deformation state variables play a very important role in understanding the volumetric behaviour of unsaturated soils. Fredlund and Rahardjo (1993) stated that the deformation state variables describe the movement and change of each phase in a multiphase system such that the law of conservation of mass is always satisfied. The conservation of mass is written in volumetric terms such that the total volume change relative to the total volume is equal to the sum of the volume change associated with each phase as represented by Equation (2-18).

$$\frac{\Delta V_t}{V_t} = \frac{\Delta V_s}{V_t} + \frac{\Delta V_w}{V_t} + \frac{\Delta V_a}{V_t} + \frac{\Delta V_c}{V_t} \tag{2-18}$$

Where:

V_t = total volume,

ΔV_t = total volume change,

ΔV_s = volume change of solid phase,

ΔV_w = volume change of water phase,

ΔV_a = volume change of air phase,

ΔV_c = volume change of contractile skin.

In Equation (2-18), the change of volume of the solid phase is assumed to be zero and the volume change of the contractile skin is assumed to be insignificant relative to the total volume change. This implies that the total volume change is equivalent to the volume change of the voids as represented by Equation (2-19), which is a reduction of Equation (2-18).

$$\Delta V_t = \Delta V_w + \Delta V_a \tag{2-19}$$

In Equation (2-19), the term ΔV_w represents the water phase deformation state variable and the term ΔV_a is the air phase deformation state variable and collectively they represent the deformation state variables of unsaturated soils. In the case of drained behaviour, the ΔV_w and ΔV_a are both nonzero because the water is permitted to leave the system. In the case of undrained and constant water tests, the ΔV_w is equal to zero as the water is not permitted to leave the system, given that water is incompressible and ΔV_a is always non-zero due to the high compressibility of the air phase. In the case of undrained and constant water content tests, the deformation state variable is solely dependent on the volume change of the air phase as shown in Equation (2-20).

$$\Delta V_t = \Delta V_a \tag{2-20}$$

2.5.5 STRESS STATE VARIABLES OF UNSATURATED SOILS

The matric suction and net normal stress, represented by Equation (2-21) and (2-22) respectively, were initially proposed by Fredlund and Morgenstern (1977) and have been accepted by various researchers as stress state variables for unsaturated soils (Alonso et al., 1990; Toll, 1990; Wheeler and Sivukumar, 1995; Housby, 1997; Ng and Menzies, 2007). Fredlund and Morgenstern (1977) stated that these stress state variables for an unsaturated soil found their origin in the equilibrium equations of the soil structure and contractile skin.

$$s = u_a - u_w \tag{2-21}$$

$$\bar{\sigma} = \sigma - u_a \tag{2-22}$$

Where:

s = matric suction,

$\bar{\sigma}$ = net normal stress,

σ = total normal stress,

u_a = pore air pressure,

u_w = pore water pressure.

Fredlund and Rahardjo (1993) presented the inequality in Equation (2-23) as the limiting stress state conditions for unsaturated soils. If the pore air pressure is increased above the total normal stress, an explosion of the sample may occur. If the pore water pressure exceeds the pore air pressure, the sample tends to saturate and the degree of saturation will approach 100%. Lastly, if the pore water pressure exceeds the total normal stress, the sample becomes unstable and may exhibit liquefaction.

$$\sigma > u_a > u_w \tag{2-23}$$

As a reader of soil mechanics at Imperial College London, Bishop (1961a) initially suggested the use of the effective stress principle for unsaturated soils based on a single equation with an empirical χ-factor. However, Jennings and Burland (1962) discovered that the collapsible behaviour of unsaturated

soils is essentially a reversal of the behaviour predicted by the effective stress principle. Matyas and Radhakrishna (1968) showed that the collapse behaviour caused by a decrease in the suction caused by wetting cannot be explained based on the principle of effective stress. As such, Fredlund and Morgensten (1977) proposed that total normal stress, pore air pressure and pore water pressure should be combined to formulate two independent stress state variables. The fundamental principle is that a suitable set of independent stress state variables are those that produce no distortion or volume change of an element when the individual pressures (for example σ, u_a and u_w) are changed by an equal amount and the stress state variables are kept constant. The criterion was tested experimentally through null tests by Fredlund and Morgenstren (1977), where the pore air, pore water and total pressure were varied by equal amounts and the resultant change in total volume and water volume was zero, which validates matric suction and net normal stress as suitable stress state variables. Fredlund (1979) stated that the combination of matric suction and net normal stress are satisfactory for most engineering applications.

2.5.6 CRITICAL STATE OF UNSATURATED SOILS

The critical state of unsaturated soils was initially proposed by Alonso et al. (1987) whilst studying the load-collapse behaviour of unsaturated soils, which subsequently led to the development of the Barcelona Basic Model by Alonso et al. (1990). The Barcelona Basic Model is a critical state constitutive model for unsaturated soils. From Section 2.4.3 of this thesis, the critical state line of saturated soils for shear stress was shown to be a projection on the void ratio line by Roscoe et al. (1958). Similarly, Alonso et al. (1987; 1990) showed that the projection of the load-collapse curve from the $S{:}p$ plane to the $q{:}p$ plane is the critical state line of unsaturated soils for shear stress, as shown in Figure 2-9, with the formulation represented by Equations (2-24), (2-25) and (2-26).

$$q = M(s)\bar{p} + \mu(s) \tag{2-24}$$

$$\bar{p} = p - u_a \tag{2-25}$$

$$p = \frac{\sigma_1 + 2\sigma_3}{3} \tag{2-26}$$

Where:

q = deviator stress,

$\bar{p}$ = net mean stress,

p = total mean stress,

M(s) = slope of the critical state line as a function of matric suction,

$\mu(s)$ = intercept term of critical state line as a function of matric suction,

σ_1 = total major principal stress,

σ_3 = total minor principal stress.

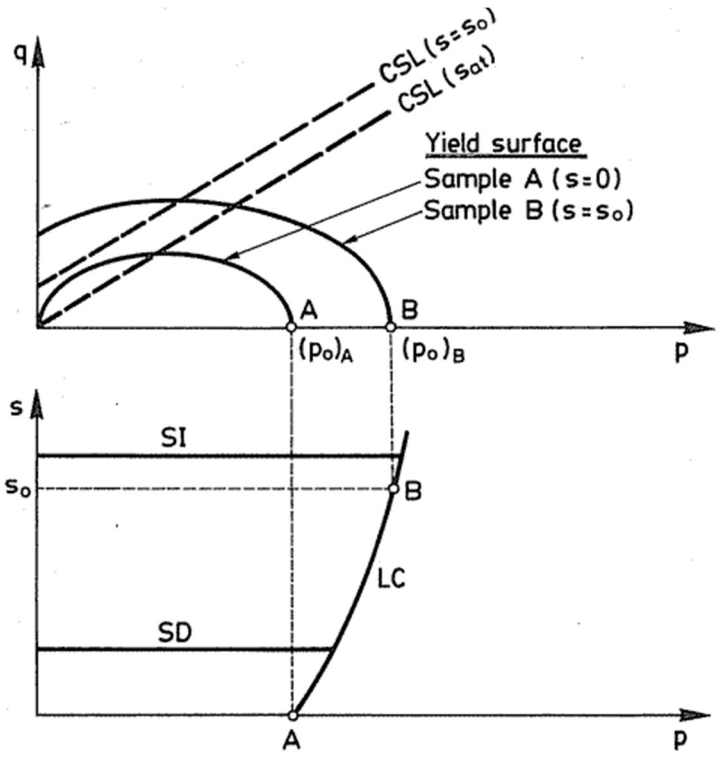

Figure 2-9: Projection of the critical state line for unsaturated soils in $q{:}\,p$ plane from the load-collapse (LC) curve in $p{:}\,S$ plane (Alonso et al., 1990)
Note: CSL = critical state line; s = matric suction; LC = load collapse; SI = suction increase; SD = suction decrease.

The net mean stress is defined using stress state variables for unsaturated soils as proposed by Fredlund and Morgenstern (1977) through the Cambridge stress invariants as shown by Schofield and Wroth (1968). In the Barcelona Basic Model, the slope of the critical state line for unsaturated soils is assumed to be equal to that of saturated soils, such that $M = M(s)$. This assumption has been accepted by numerous authors including Wheeler and Sivakumar (1995), Maatouk et al. (1995), Wang et al. (2002) and Chiu and Ng (2003). The assumption implies that the slope of the critical state line for unsaturated soils is independent of the matric suction in the soil and the matric suction creates an intercept term which increases the deviator stress or shear strength.

Toll (1990) presented a framework for the shear behaviour of unsaturated soils which considers the effect of the net mean stress and the matric suction to the deviator stress of unsaturated soils, as shown in Equation (2-27).

$$q = M_a \bar{p} + M_w s \tag{2-27}$$

Where:

M_a = total stress ratio,

M_w = suction ratio.

Contrary to the Barcelona Basic Model, Toll (1990) argued that based on test results from suction-controlled triaxial tests, the slope of the critical state line for unsaturated soils varies with degree of saturation which was confirmed by Toll and Ong (2003) and Futai and Almeida (2005). However, a direct comparison of Equation (2-27) developed by Toll (1990) with Equation (2-24) by Alonso et al. (1990) indicates that $M(s)\bar{p}$ is similar to $M_a\bar{p}$ and $\mu(s)$ is similar to $M_w s$. With this comparison, both models agree that the deviator stress of an unsaturated soil is higher than that of a saturated soil and the increase in deviator stress is directly related to the increase in the matric suction.

2.6 TRIAXIAL TESTING OF SATURATED SOILS

The triaxial test apparatus was developed by Bishop (1961b) whilst studying the pore pressures and effective stresses in saturated soils as suggested by Terzaghi (1943). Subsequently, Bishop and Henkel (1962) stated that the main function of the triaxial test is simply to obtain the relationship between shear strength and effective normal stress. Over the years with the advancement of measurement techniques and equipment, Craig (1983; 1997; 2004) and Knappet and Craig (2014) consistently maintained that the triaxial test has become the most widely used laboratory device suitable for all types of saturated soils. The main results from a triaxial test include volumetric and shear behaviour which can be represented by means of Mohr circles and stress paths. A stress path is a curve which represents successive stress points (Lambe, 1967).

2.6.1 MEASUREMENT OF VOLUMETRIC BEHAVIOUR OF SATURATED SOILS

The measurement of the volumetric behaviour of saturated soils is determined by the amount of deaired water leaving or entering the soil sample. The deaired water can be measured using a volume change indicator connected to a hydraulic pressure controller or a twin burette (Head, 1998). The importance of volume change behaviour is that it is associated with all forms of drained tests, inclusive of saturation, consolidation and shearing. During saturation, a decrease in volume is indicative of collapse behaviour caused by wetting and application of cell pressure and an increase in volume is indicative of swelling caused by the presence of expansive mineralogical particles and an application of the cell pressure below the swell pressure. During isotropic testing for normal consolidation and overconsolidation behaviour, a decrease in volume is associated with compression during the loading stress path and an increase in volume is associated with swelling during the unloading stress path. During drained shear testing, a decrease in volume is indicative of contraction behaviour and an increase in volume is indicative of dilation behaviour of the soil sample.

2.6.2 MEASUREMENT OF SHEAR BEHAVIOUR OF SATURATED SOILS

The measurement of shear behaviour of saturated soils is determined by measuring the axial load applied to the soil sample. The three types of shear tests for saturated soils are unconsolidated undrained (UU), Consolidated undrained (CU) and Consolidated drained (CD). An unconsolidated drained test is physically impossible because drainage inevitably leads to consolidation. The choices between unconsolidated and consolidated depends on the initial stress states and the stress history in the soil. The choice between drained and undrained depends on the type of material and rate of pore pressure dissipation during load application, as summarised in Table 2-3. Lambe (1967) stated that stress paths can be used as a visualization of the behaviour of the soil during triaxial testing. Typical stress paths for effective stress test are shown in Figure 2-10, where contraction is represented by effective stress paths moving towards the left as shown in Figure 2-10(a) and dilation is represented by stress paths in the right direction as shown in Figure 2-10(b).

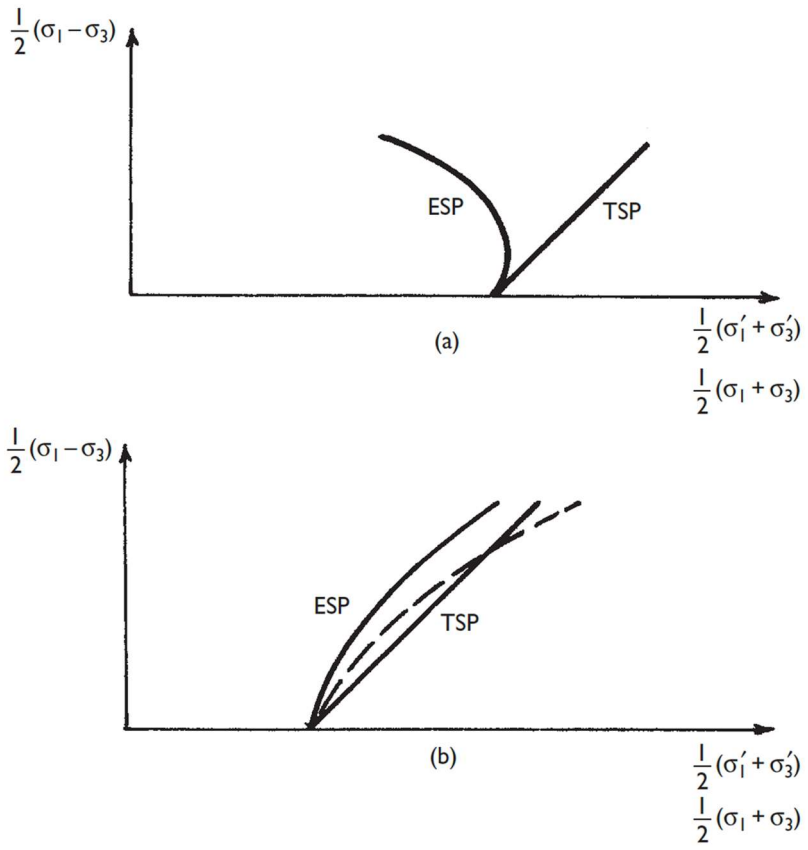

Figure 2-10: Stress paths for triaxial tests on saturated soils (a) contraction in normally consolidated soils (b) dilation in overconsolidated soils (Craig, 2004) (Note: ESP = effective stress path; TSP = total stress path.)

Table 2-3: Types of triaxial tests for saturated soils (after Craig, 2004)

Test Type	Consolidation Prior to Shearing Process	Pore water Drainage	Shearing Process	
			Pore water Pressure	Pore water Pressure
Consolidated Drained	Yes	Yes	C	M
Consolidated Undrained	Yes	No	M	CV
Unconsolidated Undrained	No	No	M	CV

Note: C = controlled, M = measured, CV = constant volume.

The application of an axial load ultimately leads to a state of perfect plasticity, which can be represented by the Mohr-Coulomb envelope or the critical state line. According to Terzaghi (1943), the Mohr-Coulomb envelope is represented by a straight line, which mathematically depends on cohesion, effective normal stress and the angle of internal friction. According to Atkinson and Bransby (1978), the critical state line is represented by a straight line which mathematically depends on the mean effective stress and effective angle of internal friction. In this context, shear failure is characterised by a state of large shear distortion with no change in stress or volume. Shear failure can be reached by means of dilation or contraction, depending on the initial conditions of the soil. Dilation is common in overconsolidated clays and dense sands while contraction is common in normally consolidated clays and loose sands.

2.7 TRIAXIAL TESTING OF UNSATURATED SOILS

Fredlund and Rahardjo (1993) and Fredlund et al. (2012) maintained that similar to saturated soils, a triaxial apparatus is also the appropriate equipment for measurement of the mechanical behaviour of unsaturated soils. Due to the presence of pore air in unsaturated soils, the triaxial apparatus for testing unsaturated soils requires modification for the control and measurement of the pore air. The first modification is the installation of a high air entry disk to introduce the matric suction by means of axis translation. The second modification involves the use of various methods for the measurement of the total volume. These modifications are discussed in the following paragraphs of the thesis.

2.7.1 MATRIC SUCTION BY AXIS TRANSLATION

Matric suction is defined as the difference between the greater pore air pressure and the lesser pore water pressure. Toll (2013) explained that pore water pressure below –100 kPa leads to cavitation, which impedes the accurate measurement of the matric suction in the soil using conventional transducers. Axis translation is a technique used to control and measure the matric suction without

causation of cavitation. According to Lu and Likos (2004), axis translation involves elevating the pore air pressure, while maintaining the pore water pressure at a measurable value below the pore air pressure. Axis translation is achieved by separating the pore air pressure and pore water using materials with high air entry values. As an example, a matric suction of 150 kPa can be achieved when the pore air pressure in the soil sample is 500 kPa and the pore water is 350 kPa. In principle, triaxial testing at an elevated backpressure relative to the cell pressure, is also a form of axis translation. Bishop and Henkel (1957) showed that the effective stress in a fully saturated soil remains unchanged even when testing is conducted at an elevated backpressure. Hilf (1948) also showed that the matric suction in a soil remains unchanged when it is achieved by means of axis translation. A high entry air disk is required to separate the pore air and pore water pressure. The air entry value is the matric suction value at which the pore air will pass through the disk. It is computed from Kelvin's equation based on the maximum pore in the disk as shown in Equation (2-28) with the properties of respective high air entry disks are shown in Table 2-4.

$$(u_a - u_w)_d = \frac{2T_s}{R} \tag{2-28}$$

Where:

$(u_a - u_w)_d$ = air entry value of disk,

T_s = surface tension of the air water interface or meniscus,

R = radius of largest pore in the disk.

Table 2-4: Properties of high air entry disks (Fredlund and Rahardjo, 1993)

Air Entry Value (Bar)	Bubbling pressure (psi)*	Approximate porosity (%)	Maximum pore size (μm)	Saturated permeability (m/s)
low	-	-	-	1×10^{-4}
0.5	7 – 9	50	6.0	3.11×10^{-7}
1	19 – 28	45	2.5	8.10×10^{-8}
2	32 – 42	38	1.3	6.93×10^{-9}
3	46 – 70	34	0.7	2.50×10^{-9}
5	80	31	0.5	1.21×10^{-9}
15	220	32	0.16	2.59×10^{-11}

Note: *1 psi = 6.78948 kPa

2.7.2 MEASUREMENT OF VOLUMETRIC BEHAVIOUR OF UNSATURATED SOILS

Laloui et al. (2006) stated that the knowledge of volume changes during a triaxial test is essential when analysing the mechanical behaviour of soils. However, Ng et al. (2002) maintained that the accurate measurement of the total change in volume of unsaturated soil samples is more complicated than the same measurement on a saturated soil specimen. The compression of the pore air in the soil creates an additional pore air volume change component in addition to the volume change of the pore water.

Several measurement techniques have been developed as summarised by Alva-Hurtado and Selig (1982), Geiser et al. (2000) and recently by Ahmadi-Naghadeh and Toker (2012) in three categories, namely: (i) cell liquid measurement, (ii) direct air and water volume measurement and (iii) direct measurement.

In the *cell liquid measurement* method, the change in volume of the soil sample is related to the variation of the liquid in the triaxial cell, by monitoring the volume of liquid surrounding the specimen. The method is limited to measuring the total change in volume of the soil sample. The method was developed by Bishop and Henkel (1962) using a single cell triaxial, where the air pressure and water pressure are controlled at the top and bottom of the sample, respectively. Bishop and Donald (1961) introduced an additional inner cell to eliminate errors related to expansion and creep associated with the single cell triaxial. Wheeler (1988) developed a double walled triaxial apparatus and Sivakumar (1993) developed the twin cell triaxial apparatus. The volume change of the sample in a double walled and twin celled triaxial apparatus is deduced from the liquid exchange between the inner and outer chamber. In order to improve the accuracy of the volume change measurement, Ng et al. (2002) modified the twin cell triaxial by introducing a bottle shaped open ended inner cell. The volume change of the soil samples is deduced from the pressure differential between the water inside the bottle shaped inner chamber and the water inside a reference manometer in the outer chamber using a differential pressure transducer. Mendes et al. (2012) recommended the use of glass in the inner cell wall to avoid the problems associated with the adsorption of water by perspex.

In the *air and water measurement* method, the change in volume of the soil sample is deduced by measuring the change in air volume and change in water volume independently. The total volume change of the soil sample is therefore the sum of the change in air volume and water volume. However, the method is successful when the air phase is continuous throughout the sample (Laloui et al, 2006). Adams et al. (1996) evaluated the use of a digital pressure volume controller as an air volume change indicator. They concluded that the pressure volume controller is satisfactory as an air volume change measurement device, provided there is no leakage from the tubes. To reduce the errors associated with changes in atmospheric pressure, temperature and air compressibility in the tube, Geiser (1999) proposed the usage of a mixed air water interface controller that allows reduction of air volume to the tubing.

In the *direct measurement* method, commonly referred to as local measurements, the measurements for sample deformation are taken directly on the sample. Hoyos et al. (2008) stated that there are three approaches which can be followed. The *first* approach involves the attachment of displacement sensors directly on the sample to measure axial and radial deformations as shown by Clayton et al. (1989). The *second* approach involves noncontact devices such as lasers, whereby laser sweeping over the entire

sample enables measurement of the sample volume change as shown by Romero et al. (1997). The *third* approach involves image processing to measure the change in volume of the sample with time as shown by Gachet et al. (2003).

2.7.3 MEASUREMENT OF SHEAR BEHAVIOUR OF UNSATURATED SOILS

The triaxial testing procedure for the shear behaviour of unsaturated soils is the same as that of saturated soils – the only difference is that the triaxial apparatus must be modified to measure or control the pore air pressure (Briaud, 2013). According the Fredlund and Rahardjo (1993), the five types of shear tests for unsaturated tests are unconsolidated undrained (UU), constant water content (CW), consolidated undrained (CU) and consolidated drained (CD) and unconfined compression (UC) as summarised in Table 2-5. Similar to saturated soils, the choices between each respective test also depend on the initial stress states and pore pressure dissipation expected in-situ. However, the dissipation of pore pressures in unsaturated soils involves the pore air and pore water. In a drained test both the pore air and pore water are drained and in a constant water content test, the drainage pore air is drained while the pore water remains undrained. During undrained tests, the pore air and pore water are undrained. The stress paths for each type of triaxial test are shown in Figure 2-11. A stress path trajectory from point A to point B along the axis of the matric suction indicates a change in the matric suction where the pore air and (or) pore water must be measured during the testing. This occurs in constant water content tests, consolidated undrained tests, unconsolidated undrained and unconfined compression tests as shown Figure 2-11. In these four tests, the drainage of the pore air and (or) pore water is not permitted and the stress path originates from a position of high matric suction to low matric suction where failure takes place. The point of shear failure can be represented by the Extended Mohr-Coulomb model or the critical state model.

Table 2-5: Types of triaxial tests for unsaturated soils (adapted from Fredlund and Rahardjo, 1993)

Test Type	Consolidation Prior to Shearing Process	Drainage		Shearing Process		
		Pore air	Pore water	Pore air Pressure	Pore water Pressure	Soil Volume Change
Consolidated drained	Yes	Yes	Yes	C	C	M
Constant water content	Yes	Yes	No	C	M	M
Consolidated undrained	Yes	No	No	M	M	M
Undrained	No	No	No	M	M	M
Unconfined compression	No	No	No	M	M	M

Note: C = controlled, M = measured.

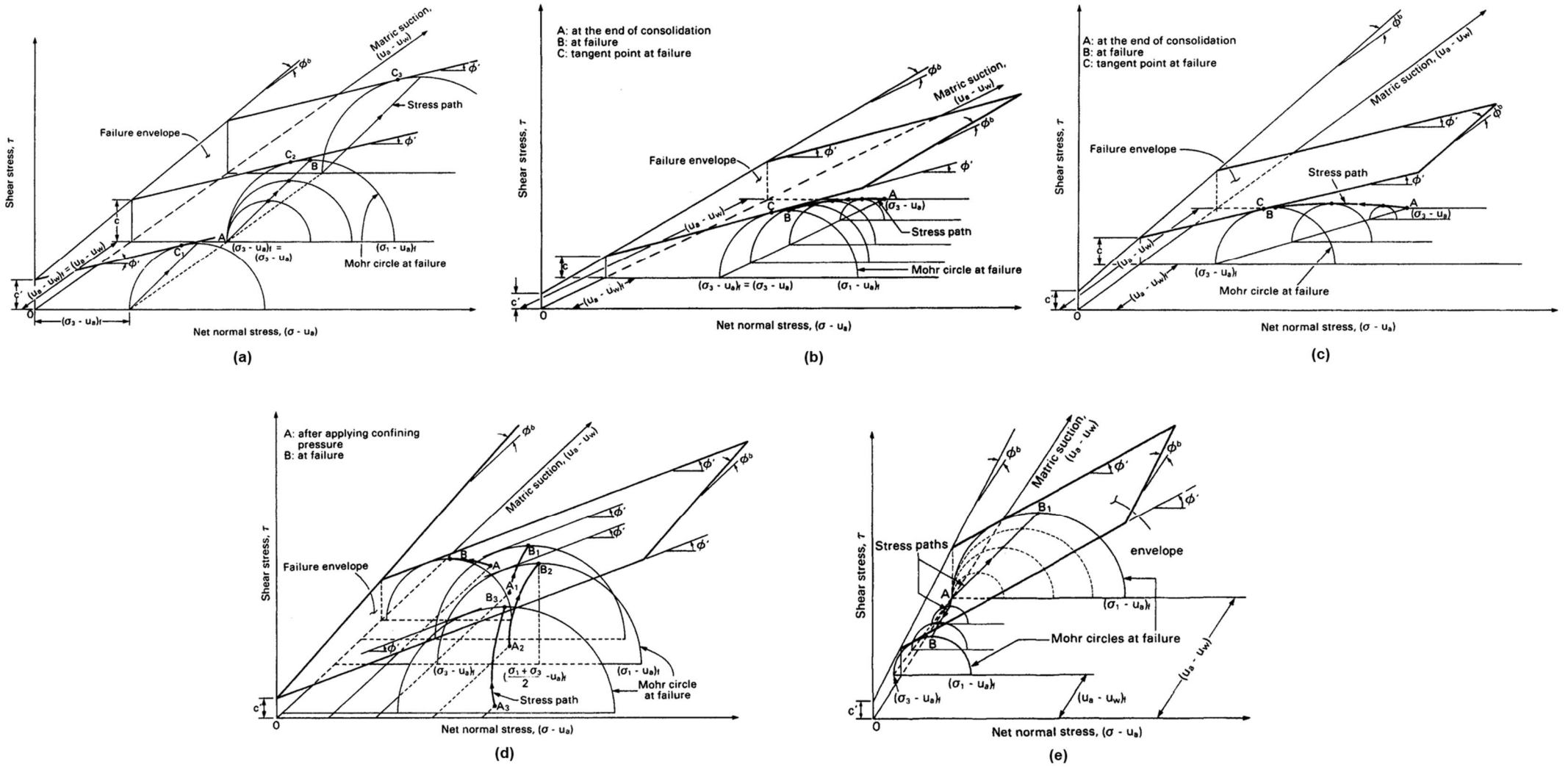

Figure 2-11: Stress paths for various unsaturated triaxial tests: (a) consolidated drained; (b) constant water content; (c) consolidated undrained; (d) unconsolidated undrained (e) unconfined compression (Fredlund and Rahardjo, 1993)

2.8 DISCUSSION

The literature presented in this chapter commenced with a broad discussion on the existing railway network in South Africa and track components on the network, which led to the definitions of the superstructure and substructure. The discussion on the superstructure highlights the importance of increased axle loading. The discussion on the substructure touched on various topics including foundation behaviour, design methods and saturated soils, leading to the important and relevant placement of unsaturated soil conditions in railway foundation engineering. The rationale for increased axle loading in the transportation of freight is shown to be economic and safety related under the banner of road-to-rail. The rationale for unsaturated soil conditions is that it is the predominate field condition for shallow railway foundations in arid to semi-arid conditions.

It is well accepted that saturated soil conditions can be regarded as the worst-case scenario for the design of shallow foundations. It therefore inherently means that unsaturated soil conditions are beneficial for shear strength. However, in the design of railway foundations, this assertion that unsaturated soil conditions are beneficial is based on “best practice” or “rule of thumb” without the inclusion of the principles of unsaturated soil mechanics. This is understandable, because unsaturated soil mechanics is a relatively new study field in geotechnical engineering with no available testing standards nor globally accepted constitutive relationships for the engineering parameters. The Extended Mohr-Coulomb model by Fredlund et al. (1978) and the critical state model by Alonso et al. (1990) and other models by Toll (1990), Wheeler and Sivukumar (1995) and Chui and Ng (2003) acknowledged that unsaturated soil conditions improve the shear strength of the soil because of the presence of matric suction in the soil skeleton. However, there are no research studies to date which have shown how unsaturated soil conditions improve the shear strength of railway foundation materials when subjected to increased axle loading. The knowledge or concept of matric suction in railway foundation materials is still vague and its role in improving the shear strength is not well understood.

As stated in the title of the thesis, this study aims to delve into the effects of increased axle loading on saturated and unsaturated railway foundation materials. As railway loads are cyclic due to the moving train, this study also aimed to illustrate how this cyclic nature can be characterised using finite element analysis and mathematical formulations. As railway foundations are predominately unsaturated, this study also aims to use the appropriate laboratory equipment required for testing both saturated and unsaturated soils and to present the scientific evidence that describes the behaviour of saturated and unsaturated soils under increased axle loading.

CHAPTER 3
CHARACTERISATION AND FINITE ELEMENT MODELLING OF CYCLIC RAILWAY LOADING

3.1 RAILWAY CYCLIC LOADING

According to Li et al. (2016), a railway track foundation is subjected to static, cyclic and dynamic loading. The static loading consists of a summation of the live and permanent loading. The cyclic loading, also called repeated loading, represents the static loading moving at a certain speed caused by a passing train. The dynamic loading is transient in nature arising from track and vehicle irregularities. This research focuses on static and cyclic loading which is directly related to increased axle loading. In this study, the use of finite element modelling is identified as an appropriate approach to characterise the cyclic nature of the railway loading. The main objective of the model is to estimate the magnitude and distribution of stress within the respective formation layers. For such an analysis, a linearly elastic closed form solution which satisfied both equilibrium and compatibility conditions under specific boundary conditions is appropriate. Given the complexity of soil behaviour, the advantage of this approach is that it is not prescriptive to a specific failure criteria or mechanism. However, in the case of a railway foundation where the respective layers are placed in stratified formation, a multi-layer analysis is more realistic (Brown, 1996).

The objectives of this chapter are as follows: (1) to describe the parameters of cyclic loading, (2) present the finite element model that was developed, (3) present the post processing results obtained from the analyses, and lastly (4) characterise the cyclic loading used as initial stress input values in the laboratory testing. These values are characterised by evaluating the distribution of stresses within the respective pavement layers and the use of equations proposed by Li et al. (2016).

3.2 CHARACTERISATION OF RAILWAY CYCLIC LOADING

O'Reilly and Brown (1991) defined cyclic loading as a system of loading which exhibits a degree of regularity both in its magnitude and in its frequency. From the fundamentals of physics, Halliday et al. (2005) stated that a regular or repetitive event is based on time. According to Li et al. (2016), the definition of cyclic loading consists of the following descriptors: (1) shape, (2) magnitude, (3) frequency and (4) total loading cycles.

3.2.1 SHAPE OF CYCLIC LOADING

The shape of cyclic loading depends on the spacing between the individual wheel loads, as depicted in Figure 3-1. The shape depicted in Figure 3-1(a) is representative of a train with short spacing between the wheel loads. The shape depicted in Figure 3-1(b) originates from a train with long spacing between the wagons. Li (1994) concluded that under field conditions, the shape of cyclic loading has been found to be a haversine wave and (or) a trapezoidal wave. However, other studies have indicated that under laboratory conditions, a sinusoidal wave can be used to represent cyclic loading.

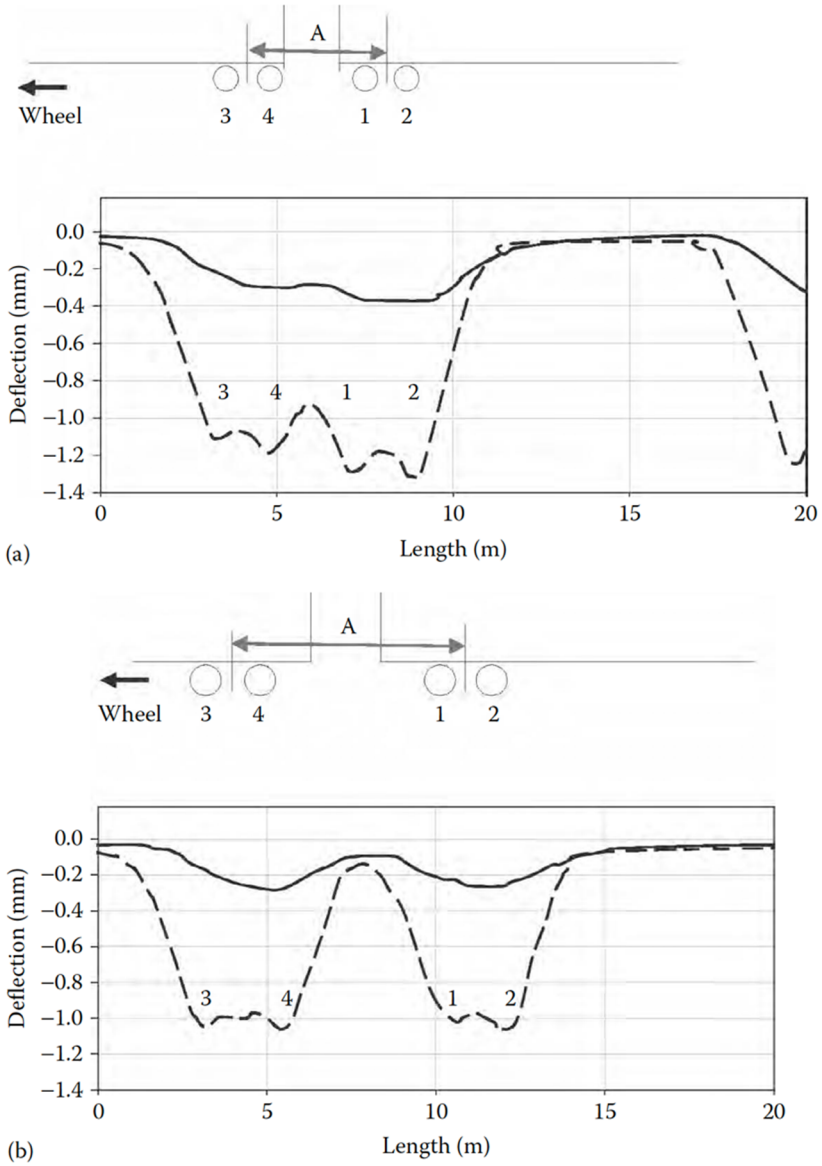

Figure 3-1: Shape of cyclic loading for (a) short coupling (b) long coupling between wagons (Li et al., 2016)

3.2.2 MAGNITUDE OF CYCLIC LOADING

The *magnitude* of cyclic loading under triaxial stress conditions consist of confining stress, initial deviator stress and cyclic deviator stress. For the purpose of shear strength and stiffness testing in a triaxial apparatus, the pattern of cyclic loading in the field shown in Figure 3-1 needs to be translated to a pattern which can be utilised in a laboratory setting, as depicted in Figure 3-2.

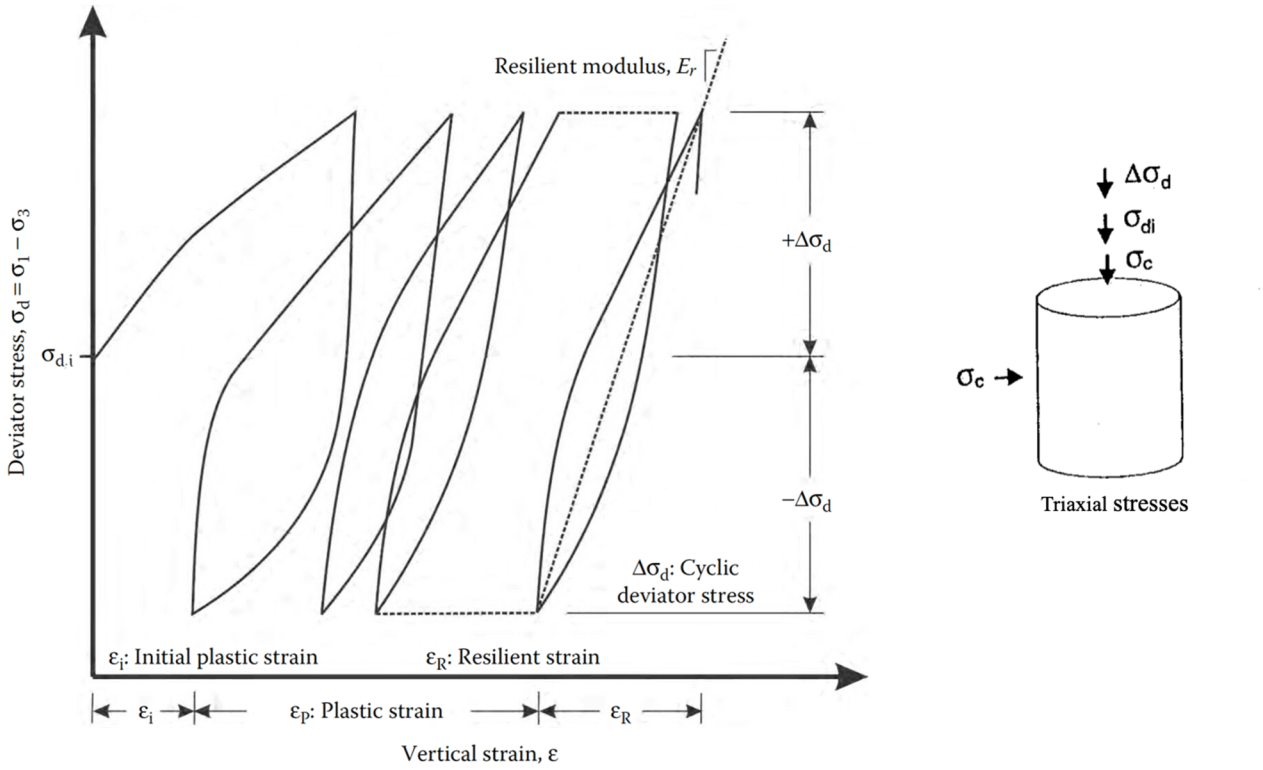

Figure 3-2: Characteristics of cyclic loading under triaxial laboratory conditions (adapted from Selig and Waters, 1994)

The confining stress represents the effect of the overburden pressure and remains constant during cyclic loading. The initial deviator stress represents the midpoint of a single loading cycle. The cyclic deviator stress consists of two equivalent but opposite stresses which represent the boundary points of cyclic loading between minimum and maximum stresses. The initial deviator stress and cyclic deviator stress can be calculated using Equation (3-1) and Equation (3-2).

$$\sigma_{di} = \frac{\sigma_{max} + \sigma_{min}}{2} \tag{3-1}$$

$$\Delta\sigma_d = \frac{\sigma_{max} - \sigma_{min}}{2} \tag{3-2}$$

Where:

σ_{di} = initial deviator stress,

$\Delta\sigma_d$ = cyclic deviator stress,

σ_{max} = maximum vertical pressure,

σ_{min} = minimum vertical pressure.

The maximum and minimum vertical stress respectively can be measured in the field or calculated using computer modelling, such as finite element analysis. In practice the maximum vertical stresses originate from the wheel loads, whilst the minimum vertical stresses originate from the seating loading or overburden pressure. The minimum and maximum vertical stresses can be estimated by field measurements or finite element modelling, of which the former has been adopted in this study. Selig and Chang (1981) stated that it is important to differentiate between isotropic loading (also called symmetrical or one-way loading) and anisotropic (non-symmetrical two-way loading). During anisotropic loading, $|\Delta\sigma_d| < \sigma_{di}$, and the soil experiences compression stresses only. During isotropic loading (two-way loading), $|\Delta\sigma_d| > \sigma_{di}$, and the soil experiences both compression and extension stresses, which causes shear stress reversal. Selig and Chang (1981) concluded that during isotropic loading, the cyclic axial strain is greater due to stress reversal and during anisotropic loading the permanent axial strain, as depicted in Figure 3-3. Railway loading on a railway foundation is anisotropic due to the seating load and reduced load intensity with depth.

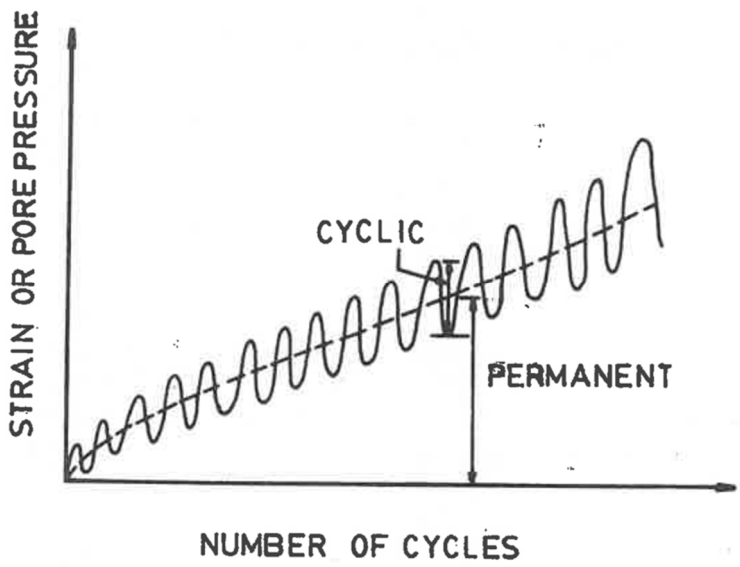

Figure 3-3: Permanent and cyclic strain or cyclic pore pressure (Selig and Chang, 1981)

Li et al. (2016) indicated that Equations (3-3) to (3-8) can used to translate the triaxial stresses into field stresses, or verse versa. In the translation it is assumed that the octahedral normal and shear stresses in the field are equal to octahedral normal and shear stresses in the triaxial. As such, Equation (3-7) can be used to calculate the triaxial axial stress and Equation (3-8) can be used to calculate the triaxial radial (or confining stress) based on field measurements.

$$I_1 = \sigma_x + \sigma_y + \sigma_z \tag{3-3}$$

$$I_2 = \sigma_x\sigma_y + \sigma_x\sigma_z + \sigma_y\sigma_z - \tau_{xy}^2 - \tau_{xz}^2 - \tau_{yz}^2 \tag{3-4}$$

$$\sigma_{\text{oct(f)}} = \frac{I_1}{3} \tag{3-5}$$

$$\tau_{\text{oct(f)}} = \left[-\frac{2}{3}\left(I_2 - \frac{I_1^2}{3}\right)\right]^{1/2} \tag{3-6}$$

$$\sigma_a = \sigma_{\text{oct(f)}} + \sqrt{2}\,\tau_{\text{oct(f)}} \tag{3-7}$$

$$\sigma_r = \sigma_{\text{oct(f)}} + \frac{1}{\sqrt{2}}\tau_{\text{oct(f)}} \tag{3-8}$$

Where:

$\sigma_{\text{oct(f)}}$ = octahedral normal stress in the field,

$\tau_{\text{oct(f)}}$ = octahedral shear stress in the field,

σ_a = triaxial axial stress,

σ_r = triaxial radial (or confining) stress,

σ_x = normal stress in x-direction,

σ_y = normal stress in y-direction,

σ_z = normal stress in z-direction,

τ_{xy} = shear stress in xy-plane,

τ_{xz} = shear stress in xz-plane,

τ_{yz} = shear stress in yz-plane.

3.2.3 FREQUENCY

Another important parameter of cyclic loading is the duration of a single load application, commonly known as *frequency*. In relation to railway loading, Li et al. (2016) stated that the frequency of wheel load application depends on the operating train speed and the influence length as expressed in Equations (3-9) and (3-10). The influence length is the distance between the approaching wheel that starts to have an influence for the element of concern and the leaving wheel that still has an influence on the same element. In order words, it is the distance between zero stresses or strains experienced by a soil element during the passage of a train or load application.

$$f = \frac{1}{t} \tag{3-9}$$

$$t = \frac{L}{V} \tag{3-10}$$

Where:

f = frequency of the loading,

t = time duration between load applications,

V = speed of a passing train and

L = influence length between adjacent axles.

3.2.4 TOTAL LOADING CYCLES

In general, total loading cycles represents the number of load cycles required for a foundation to reach a certain failure criterion. Li et al. (2016) indicated that the number of load cycles are related to number of wheel loads. In other words, a single load cycle can represent one or more wheel loads depending on the spacing between the wheels or axles, in accordance with the influence length in Equation (3-10). For example, in the case of grouped loading, as depicted in Figure 3-1(a), one load cycle represents four wheel loads and similarly in Figure 3-1(b), one load cycle here represents two wheel loads. Lourens and Maree (1997) further stated that it is common to group a number of wheel loads in a single load cycle. The relationship between total load cycles and wheel loads determines the total gross tonnage of a railway corridor, as represented by Equation (3-11).

$$N_a = \frac{10^6}{n(P_s)} \tag{3-11}$$

Where:

N_a = number of axles per million gross tonnage,

P_s = static wheel load per tonne,

n = wheel loads per cycle.

3.3 FINITE ELEMENT MODEL OF RAILWAY LOADING

According to Potts (2003), a conventional finite element model is characterised by the following aspects:

- Equilibrium conditions,
- Compatibility conditions,
- Constitutive behaviour and
- Boundary conditions.

The *equilibrium conditions* describe the overall and internal equilibrium. The overall equilibrium is associated with resolving forces and moments. The internal equilibrium is associated with stress fields in the form of differentials of stress components which satisfy the collection of differential equations shown in Equation (3-12).

$$\begin{aligned}\frac{\partial \sigma_x}{\partial x}+\frac{\partial \tau_{yx}}{\partial y}+\frac{\partial \tau_{zx}}{\partial z}+\gamma=0\\ \frac{\partial \tau_{xy}}{\partial x}+\frac{\partial \sigma_y}{\partial y}+\frac{\partial \tau_{zy}}{\partial z}=0\\ \frac{\partial \tau_{xz}}{\partial x}+\frac{\partial \tau_{yz}}{\partial y}+\frac{\partial \sigma_z}{\partial y}=0\end{aligned} \quad (3\text{-}12)$$

Where:

γ = self-weight.

The *compatibility conditions* describe the displacements and strains, essentially to ensure that if movement of a body occurs under loading, discontinuities and overlapping does not occur within the model. The displacements throughout the body during load application should satisfy a collection of strain equations shown in Equation (3-13).

$$\begin{aligned}\varepsilon_x=-\frac{\partial u}{\partial x}, \quad \varepsilon_y=-\frac{\partial v}{\partial y}, \quad \varepsilon_z=-\frac{\partial w}{\partial z}\\ \gamma_{xy}=-\frac{\partial v}{\partial x}-\frac{\partial u}{\partial y}, \quad \gamma_{yz}=-\frac{\partial w}{\partial y}-\frac{\partial v}{\partial z}, \quad \gamma_{xz}=-\frac{\partial w}{\partial x}-\frac{\partial u}{\partial z}\end{aligned} \quad (3\text{-}13)$$

Where:

u = displacement in x-direction,

v = displacement in y-direction,

w = displacement in z-direction,

ε_x = normal strain in x-direction,

ε_y = normal strain in y-direction,

ε_z = normal strain in z-direction,

γ_{xy} = shear strain in xy-plane,

γ_{yz} = shear strain in yz-plane,

γ_{xz} = shear strain in xz-plane.

The *constitutive behaviour* describes the stress strain relationship of the material. The constitutive behaviour also provides a link between equilibrium and compatibility. The constitutive behaviour is expressed as shown in Equation (3-14).

$$\{\Delta\sigma\}=[D]\{\Delta\varepsilon\} \quad (3\text{-}14)$$

Where:

$\{\Delta\sigma\}$ = increments of stress components $=\left[\Delta\sigma_x,\Delta\sigma_x,\Delta\sigma_x,\Delta\tau_{xy},\Delta\tau_{xz,}\Delta\tau_{yz}\right]^T$,

$\{\Delta\varepsilon\}$ = increments of strain components $=\left[\Delta\varepsilon_x,\Delta\varepsilon_y,\Delta\varepsilon_z,\Delta\gamma_{xy},\Delta\gamma_{xz,}\Delta\gamma_{yz}\right]^T$ and

$[D]$ = assumed relationship between $\{\Delta\sigma\}$ and $\{\Delta\varepsilon\}$, for example, Young's modulus of elasticity.

The relationship between stress and strain components depends on the assumed material behaviour. Popular material behaviour of soils that has been published are isotropic elasticity, anisotropic elasticity and elastoplastic, amongst others. In this study, $[D]$ is assumed to be an isotropic linear elastic matrix, mainly to obtain the stress distribution as shown in Equations (3-15) and (3-16).

$$[D] = \begin{bmatrix} 1/E & -\nu/E & -\nu/E & 0 & 0 & 0 \\ -\nu/E & 1/E & -\nu/E & 0 & 0 & 0 \\ -\nu/E & -\nu/E & 1/E & 0 & 0 & 0 \\ 0 & 0 & 0 & 1/G & 0 & 0 \\ 0 & 0 & 0 & 0 & 1/G & 0 \\ 0 & 0 & 0 & 0 & 0 & 1/G \end{bmatrix} \quad (3\text{-}15)$$

$$G = \frac{E}{2(1+\nu)} \quad (3\text{-}16)$$

Where:

E = Young's modulus of elasticity,

ν = Poisson's ratio,

G = Shear modulus.

The *boundary conditions* of the model define the constraints under consideration (Potts, 2003). These conditions can range from the displacement and rotational constraints, geometry constraints, sequence of loading, excavations, construction or any other predefined conditions.

3.4 DESCRIPTION OF TRACK STRUCTURE MODEL

The finite element model of the railway track structure that was developed for this study is depicted in Figure 3-4. The dimensions used for the track components represents those currently in service on the South African freight railway lines for a conventional track with a gauge of 1065 mm. The superstructure consists of 60 kg/m rails, PY prestressed concrete sleepers spaced at 650 mm centre-to-centre and a ballast depth of 300 mm. The rails are modelled as rectangular sections with a base width of 140 mm and height of 138.5 mm which is representative of the second moment of area of a 60 kg/m rail. The sleepers are modelled as a rectangular box with a length, width and height of 2200, 270 and 200 mm respectively. The substructure consists of a 200 mm subballast layer and a 2800 mm subgrade layer. The typical material properties of each component are shown in Table 3-1. A Poisson's ratio of 0.5 is ideal for undrained conditions but may lead to nonconvergence of the numerical solution. In order

to prevent convergence problems, a value of 0.49 was used as indicated by numerous authors including Potts and Zdravkovic (1999), Gräbe (2002) and Powrie et al. (2007) amongst others.

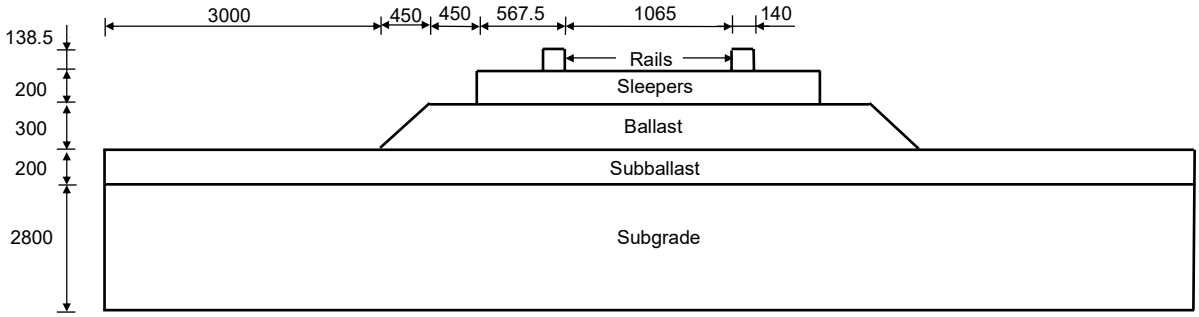

Figure 3-4: Lateral view of finite element discretisation, not to scale (dimensions in mm)

Table 3-1: Material properties of track components

Track component	Young's modulus (MPa)	Poisson's ratio	Density (kg/m^3)
Rails	205 000	0.30	7850
Sleepers	34 000	0.30	2400
Ballast	200	0.35	1800
Subballast (0 – 200 mm)	120	0.49	2000
Subgrade (200 – 3000 mm)	100	0.49	2000

The three-dimensional model is meshed using eight node linear hexahedron elements with full integration of average strain in each element. Due to the triangular shape of the ballast profile, wedged hexahedron elements are used in ballast layer with tie condition to the subballast layer for continuity. The model consisted of 187 050 elements and 197 762 nodes. The track length is 19.770 m with 31 sleepers. The finite element mesh in an isometric view is shown in Figure 3-5.

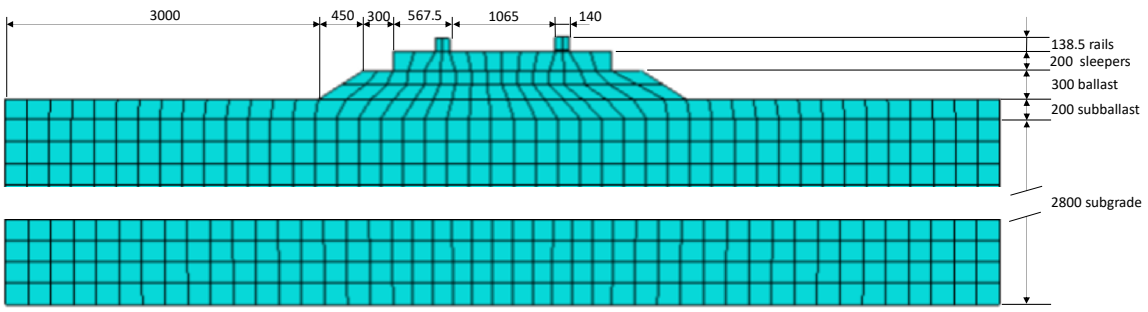

Figure 3-5: Finite element mesh (dimensions in mm)

The loading conditions of the finite element model are based on the axle loading of 20, 26, 30, 32.5 and 40 tonnes and the spacing between the wheel loads. The spacing of the wheel loads are based on the

critical wagon type which constituted the majority of the fleet. The spacing of the effective four wheels are depicted in Figure 3-6. The grouping of the four axles forms the basis of the loading conditions which were applied in the model, as shown in Figure 3-6. Fixed boundary conditions in three-dimensional space were selected as shown in Figure 3-7. The boundary conditions were selected, such that, they do not influence the stresses at the point of interest, which is in the middle of the track structure.

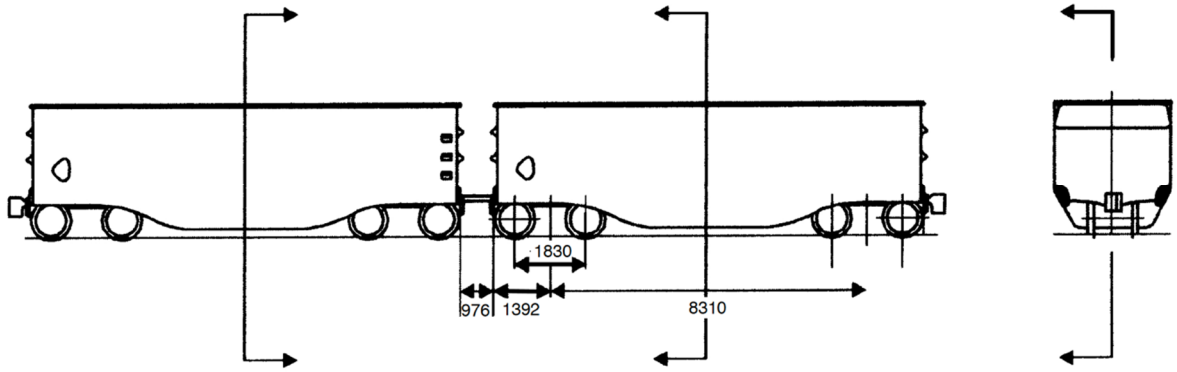

Figure 3-6: Wheel spacing of the critical wagons

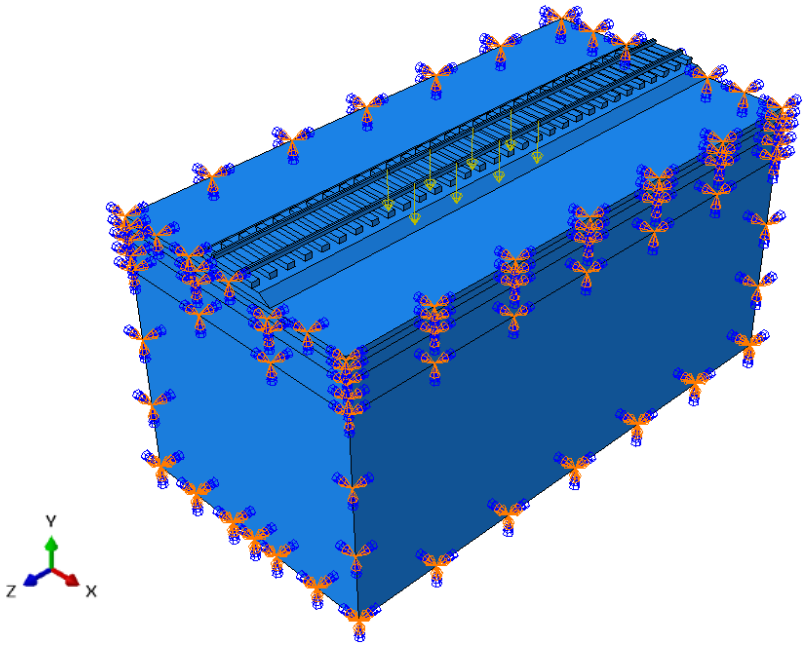

Figure 3-7: Boundary conditions and loading configuration (Note: Direction of load starts at tail of arrow)

3.5 POST PROCESSING OF RESULTS

The post processing results obtained from the finite element modelling and analysis are presented in this section. The results are presented by means of the distribution of the vertical and transverse stresses

as a function of the depth within a railway foundation measured from the formation level. The results have been expressed by normalisation with axle load per tonne to accommodate all five axle loading cases in a single graph.

3.5.1 VERTICAL STRESS DISTRIBUTION

The vertical stress can be viewed as the major principal stress in a conventional triaxial apparatus, which is related to the deviator stress. In the model, the vertical stress acts in the direction parallel to the y-axis, as shown in Figure 3-8, which represents the half space of the model. The distribution of the vertical stresses along the longitudinal axis in z-direction are plotted in terms of stress contours and also depicted in Figure 3-8. The maximum stresses occur at the formation level. The distribution of the vertical stresses in the longitudinal axis is shown graphically in Figure 3-9. The respective graphs highlight a significant trend regarding the distribution of the vertical stresses in a railway foundation with depth. It confirms that closer to the formation level, the stress distribution from each sleeper resembled that of point loads acting on a beam. Furthermore, the magnitude of the vertical stresses decreases with depth where at a depth of 2000 mm, the stress distribution tends to become uniform as shown in Figure 3-9.

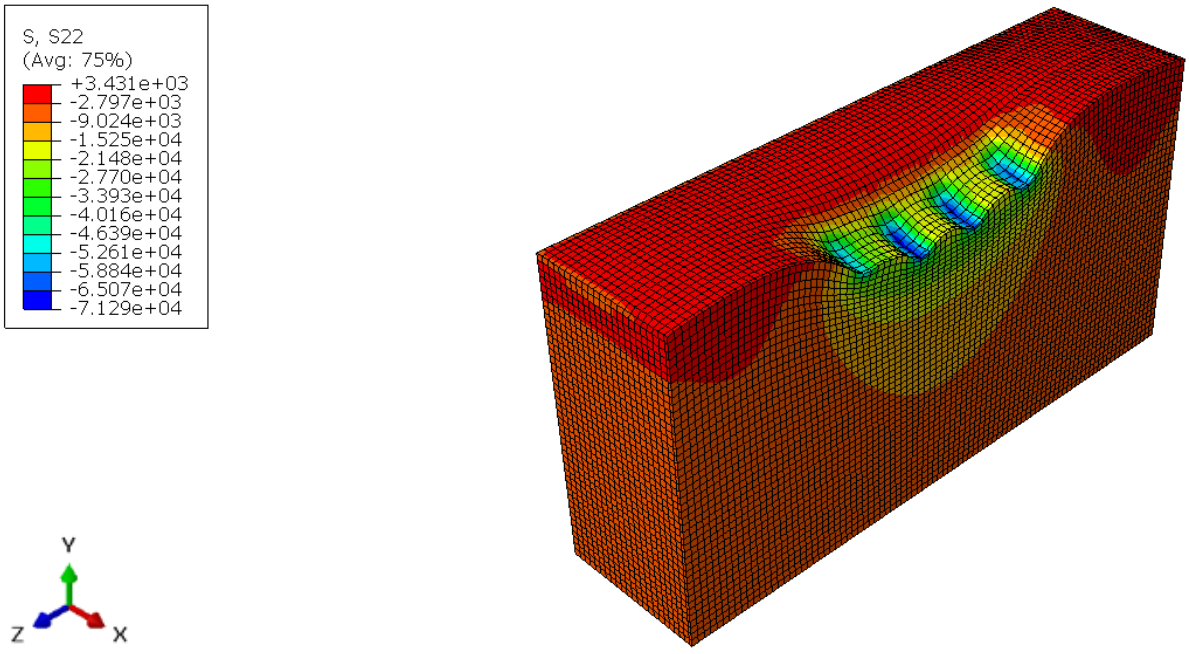

Figure 3-8: Typical contour plot of the vertical stress distribution along the longitudinal plane for 20 tonnes per axle (Note: stress in N/m^2)

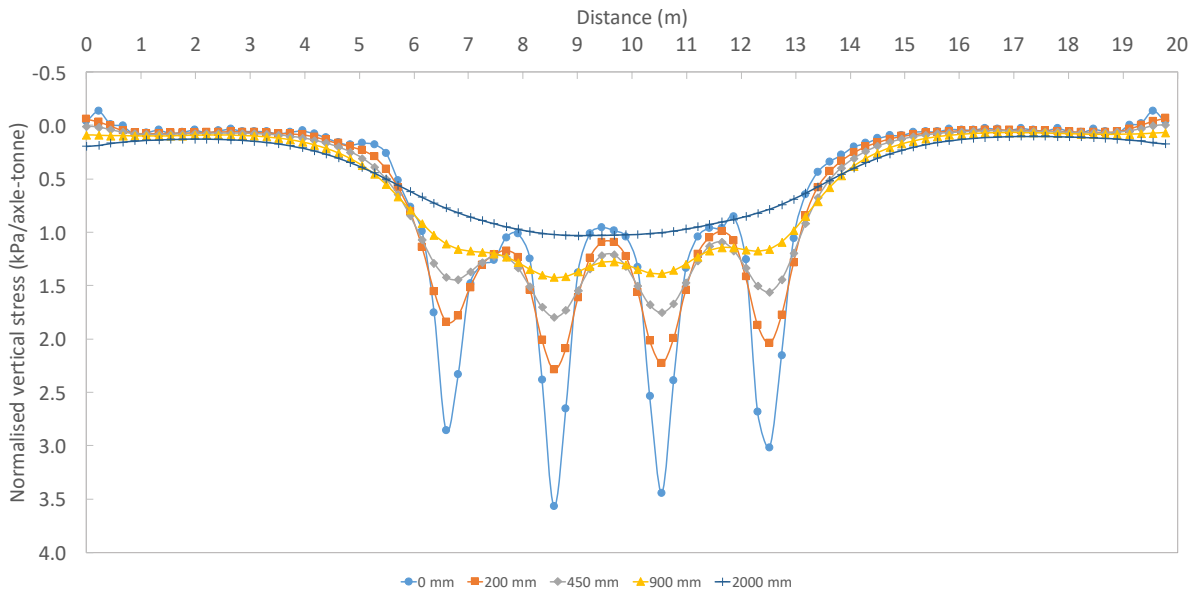

Figure 3-9: Vertical stress distribution along longitudinal axis at depth 0 – 2000 mm (Note: 0 mm represents formation level at top of subballast)

3.5.2 TRANSVERSE STRESS DISTRIBUTION

The transverse stresses can be viewed as the intermediate or minor principal stresses in a conventional triaxial apparatus, which are related to the confining stresses. The transverse stresses in the x-direction were found to be approximately equal in magnitude to the longitudinal stresses in the z-direction. The distribution of the transverse stresses along the longitudinal axis, plotted in terms of stress contours are depicted in Figure 3-10. The maximum vertical stresses occur at the sleeper edge and the maximum transverse stresses also occur at the edge of the sleeper combined with uplift stresses adjacent to the track. The distribution of the transverse stresses along the longitudinal axis are graphically depicted in Figure 3-11. The transverse stresses follow the same trend as the vertical stresses, meaning, the maximum stresses occur at the formation level and decreases with depth and becomes uniform at a depth of 2000 mm.

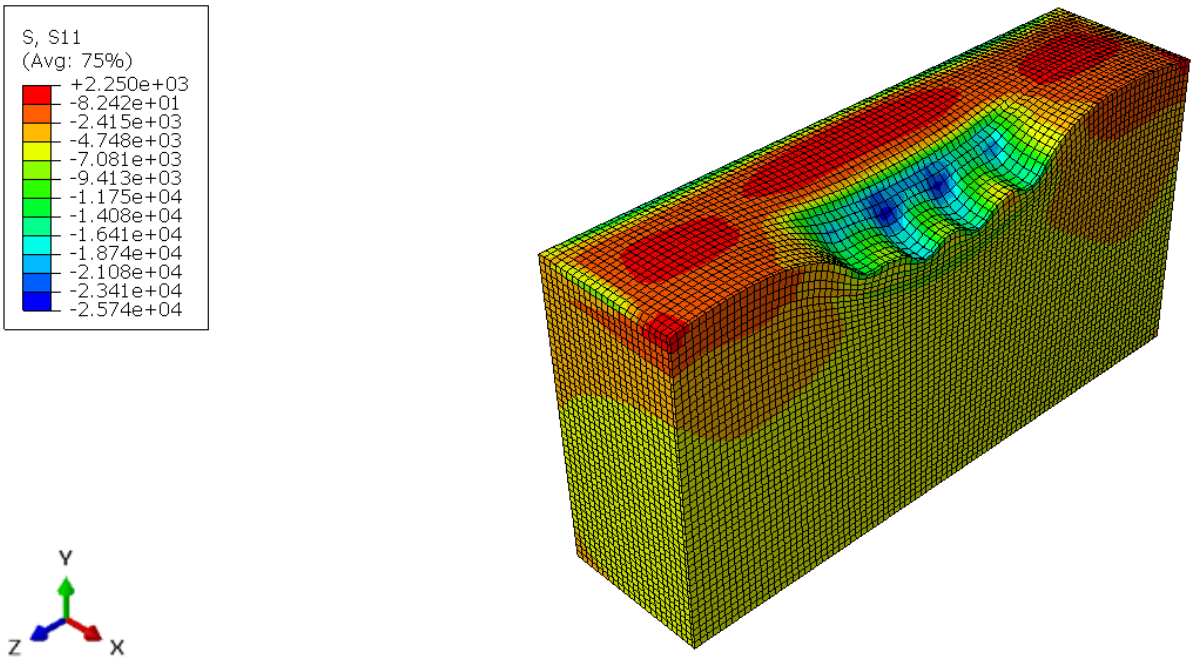

Figure 3-10: Typical contour plot of transverse stress distribution along longitudinal plane for 20 tonnes per axle (Note: stress in N/m^2)

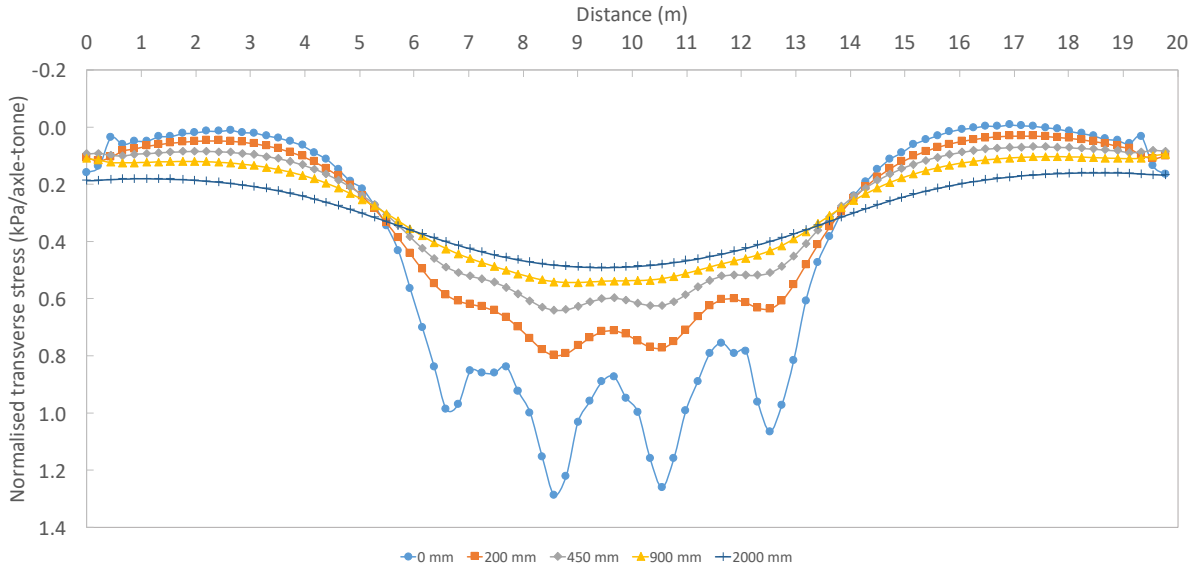

Figure 3-11: Transverse stress distribution along longitudinal axis at depth 0 – 2000 mm (Note: 0 mm represents formation level at top of subballast)

3.6 RAILWAY LOADING FOR CYCLIC TRIAXIAL TESTING

The loading in a triaxial apparatus consists of confining stresses and deviator stresses. The confining stresses are assumed to be constant because the change of stresses in the transverse and longitudinal direction are small relative to that in the vertical direction. The deviator stress which represents train

loads are cyclic and therefore characterised as such. A discussion of the methodology followed in the characterisation of the cyclic loading is presented in this section.

3.6.1 CONFINING STRESSES

In the finite element model and analyses, the confining stresses are assumed to be represented by the transverse stresses. Numerous studies have shown that the confining stresses in shallow foundation structures such as railway foundations are very low. Shahu et al. (2000) reported that the confining stress in a railway foundation is between 20 to 40 kPa and Miller et al. (2000) reported values of 14 to 35 kPa. Gräbe (2002) reported that the confining stress on a railway formation is 30 kPa. Based on the results from the finite element model of this study, the transverse stress, which represent the confining stress is 1.4 kPa per tonne at a depth of 0 mm for the subballast material and 0.8 kPa per tonne at a depth of 200 mm for the subgrade material as shown in Figure 3-11. Based on the results, the effective normal stress in the experimental work is kept constant at a value of 30 kPa for all test materials and axle loading cases.

3.6.2 DEVIATOR STRESSES

The parameters required to describe cyclic loading are discussed in Section 3.1. This subsection presents the magnitudes of each parameter required to describe the cyclic loading for each axle loading case which are cumulatively presented in Table 3-2 for the subballast material and Table 3-3 for the subgrade material. The theory about the *shape* of cyclic loading is presented in Section 3.1.1. A sinusoidal wave shape is adopted based on the stress distribution obtained from the finite element analysis, which is depicted in Figure 3-9 and Figure 3-11. The shape of the cyclic loading tends towards the shape of a sinusoidal curve. The theory about the *magnitude* of cyclic loading is presented in Section 3.1.2. The magnitude of cyclic loading depends primarily on the minimum and maximum vertical stresses. The minimum stresses are the hydrostatic state or the seating pressure, which consists of the surcharge loads, including rails, sleepers, ballast and the overburden pressure. At a depth of 0 mm, the seating pressure is calculated to be 6 kPa. At depths of 200 mm, the seating pressure is calculated to be 10 kPa. The maximum stresses obtained from the finite element analysis are presented in Figure 3-9 and Figure 3-11 for the subballast and subgrade materials respectively. The initial deviator stress and cyclic deviator stress are calculated using Equations (3-1) and (3-2). The results of the magnitudes for axle loading of 20, 26, 30, 32.5 and 40 tonnes per axle are presented in Table 3-2 for the subballast material and in Table 3-3 for the subgrade material. The theory about the *frequency* of cyclic loading is presented in Section 3.2.3. The frequency is calculated using Equation (3-10) and Equation (3-9). The influence length is taken as 19.0 m from Figure 3-9. Train speeds from 60 km/h to 80 km/h are selected as being representative, which result to a frequency in the range of 0.877 Hz to 1.170 Hz, respectively,

with an average value of 1.024 Hz. For practical reasons, a frequency of 1.0 Hz is selected for testing purposes for all materials and axle loading cases.

Table 3-2: Cyclic loading for the subballast material at a depth of 0 mm

Axle load (tonnes)	Cyclic loading on subballast material				
	Max stress (kPa)	Min stress (kPa)	Initial stress (kPa)	Cyclic amplitude (kPa)	Frequency (Hz)
20.0	77.4	6.0	41.7	35.7	1.0
26.0	98.8	6.0	52.4	46.4	
30.0	113.1	6.0	59.6	53.6	
32.5	122.0	6.0	64.0	58.0	
40.0	148.8	6.0	77.4	71.4	

Table 3-3: Cyclic loading for the subgrade material at a depth of 200 mm

Axle load (tonnes)	Cyclic loading on subgrade material				
	Max stress (kPa)	Min stress (kPa)	Initial stress (kPa)	Cyclic amplitude (kPa)	Frequency (Hz)
20.0	57.2	10.0	33.6	23.6	1.0
26.0	71.3	10.0	40.7	30.6	
30.0	80.6	10.0	45.3	35.3	
32.5	86.5	10.0	48.3	38.3	
40.0	104.2	10.0	57.1	47.1	

3.7 DISCUSSION

In this chapter, the characterisation of cyclic railway loading has been carried out by means of finite element modelling and analysis. The chapter commenced with a general definition of cyclic loading and delved into a general discussion on the theory of finite elements. Thereafter, the finite element model of the track structure together with the track components related to the study which was developed in ABAQUS is presented followed by the post-processing. In the post-processing, the vertical and transverse stress distribution are presented by means of graphs and stress contours. The graphs indicate the shape and magnitude of cyclic loading together with the locations of maximum and minimum stresses. The frequency of cyclic loading is based on the average train speed between 60 and 80 km/h. The importance of the vertical stress is that it represents the axle loading on a railway track and the transverse stress represents the overburden pressure.

In the last section of the chapter, the post-processing results are used to translate the cyclic loading for triaxial testing, where the vertical stress is the deviator stress and the transverse stress is the confining stress (or mean stress). For a shallow foundation structure such as a railway foundation, the confining stress is 30 kPa. The magnitude of cyclic loading acting on the subballast and subgrade materials for each axle loading case were calculated as in presented in Table 3-2 and Table 3-3. In the chapter on experimental work, the cyclic loading from this chapter is used as input values for triaxial testing.

CHAPTER 4
LABORATORY EQUIPMENT

4.1 OVERVIEW OF LABORATORY EQUIPMENT

The laboratory equipment consisted of the following five main components, namely: (1) water deaerator system, (2) triaxial testing system, (3) unsaturated testing system, (4) local instrumentation and (5) data capturing software. An overview of the laboratory equipment is shown schematically in Figure 4-1 and photographically in Figure 4-2. Each component of the laboratory equipment is described in detail in this chapter of the thesis.

4.2 WATER DEAERATOR SYSTEM

A Nold deaerator system was developed for the removal of free and dissolved air in the testing water. The use of deaired water was mainly to ensure accurate measurement of volume change of the sample, stable pressure targets of the pressure controllers and to prevent the movement of the dissolved air through the latex membrane. The Nold deaerator consisted of a 10 litre air and watertight perspex tank connected to a rotating disk and a 1.5 cfm vacuum pump. The triaxial cell was filled with deaired water from the tank under gravity flow.

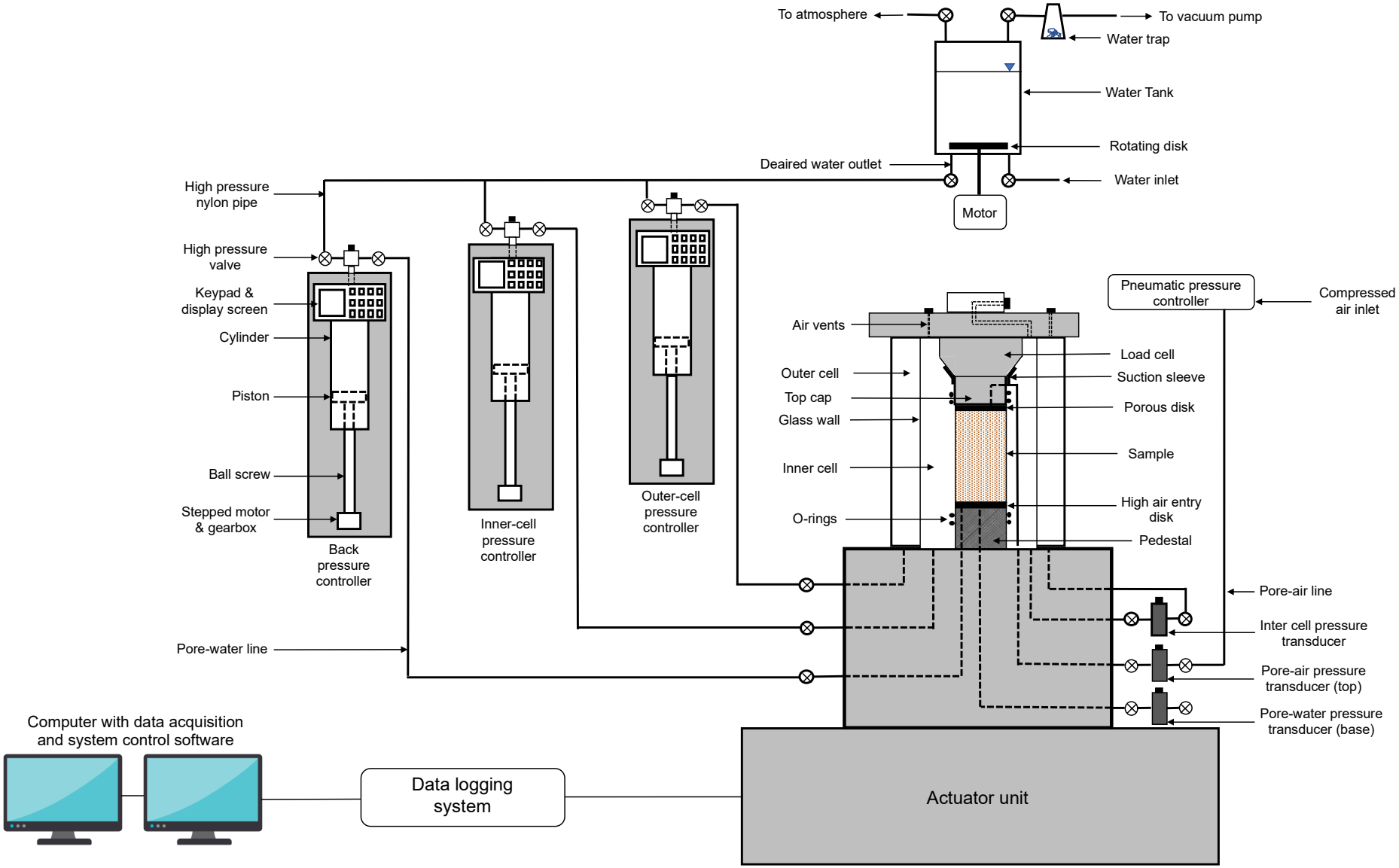

Figure 4-1: Schematic representation of test equipment (not to scale)

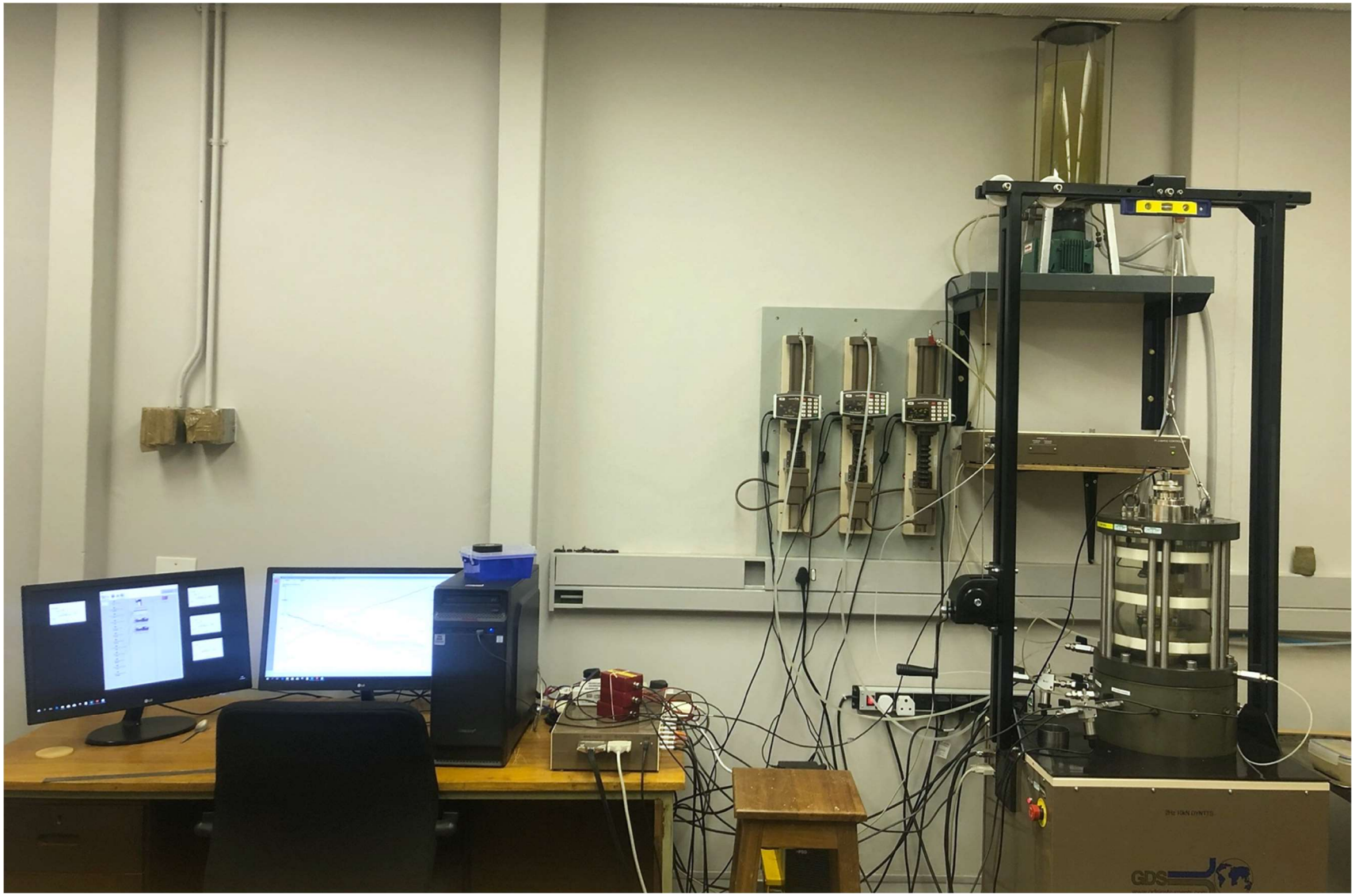

Figure 4-2: Photographic representation of test equipment

4.3 TRIAXIAL TESTING SYSTEM

The triaxial testing system manufactured by GDS Instruments was the Dynamic Triaxial Testing (DYNTTS) hardware. It consisted of the actuator unit, triaxial cell, hydraulic pressure controllers, pressure transducers, data logging unit and the data acquisition and control software. Each component is described in the following subsections.

4.3.1 ACTUATOR UNIT AND LOAD CELL

The actuator unit is capable of monotonic loading up to a maximum load of 10 kN and cyclic loading to a maximum frequency of 2 Hz also with a maximum load of 10 kN. The thrust cylinder in the actuator unit is connected to the axial ram through a balanced ram, as shown in Figure 4-3. The balanced ram compensates the volumetric displacement of the loading ram, caused by the upward and downward movement into the triaxial cell, such that the net volume change in the cell is zero. The axial displacement ram is connected to the sample pedestal for measurement of global displacement during displacement-controlled tests. The loading on the sample was measured by an internal submersible loadcell shown in Figure 4-4, which was attached to the top cap of the sample for stress-controlled and load-controlled tests. The technical properties and calibration data of the axial ram and loadcell are presented in Table 4-1 and Table 4-2 respectively.

Table 4-1: Technical properties and calibration data of the axial displacement ram

Serial number	21867
Maximum displacement (mm)	100
Sensitivity (mm/count)	0.000125
Counts (per rotation)	8000

Table 4-2: Technical properties and calibration data of the loadcell

Serial number	57825
Maximum load (kN)	10
Excitation voltage (V)	10
Full scale	30
Zero output (mV)	0.034
Sensitivity (N/mV)	486.7
Non-linearity (% FS)	±0.018
Hysteresis (% FS)	- 0.029

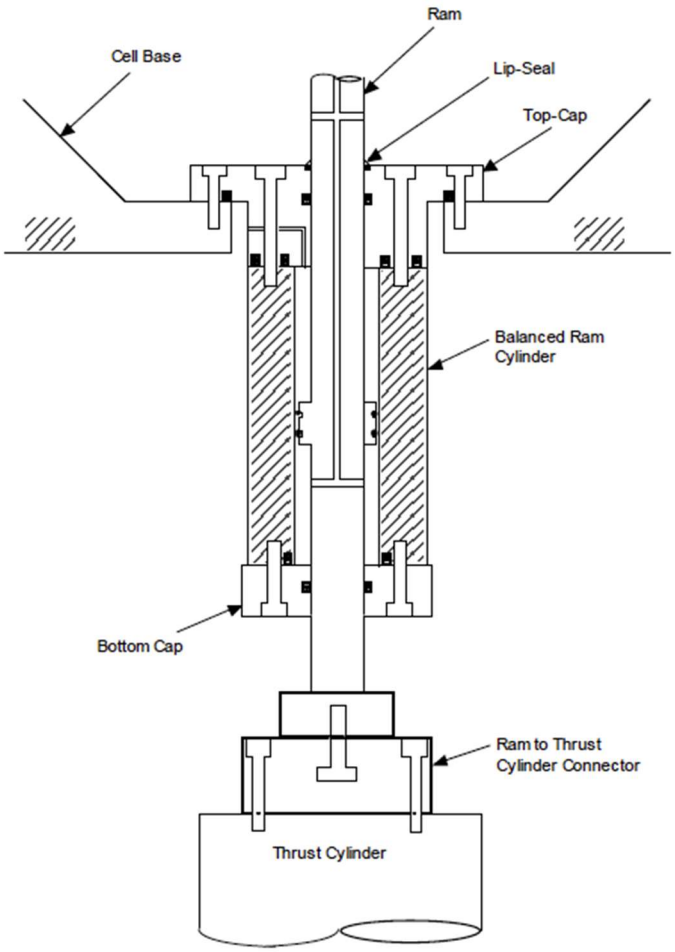

Figure 4-3: Configuration on the balanced ram attached to the thrust cylinder in the actuator unit

Figure 4-4: Internal submersible load cell (Courtesy of GDS Instruments)

4.3.2 TRIAXIAL CELL

The triaxial cell that was attached to the actuator unit had a cylindrical body. The main function of the triaxial cell was to contain the deaired water used for the cell pressure and the soil sample during testing. The acquired triaxial cell for the system was double walled with an outer and inner cell. The inner and outer cell were connected to each other monolithically and were internally separated by a cylindrical glass wall. The inner and outer cells were externally connected by a nylon pipe with control valves for single cell or double cell setup. For high frequency cyclic loading, the triaxial cell can be operated as a single cell by keeping the inter-cell valve open. The maximum working pressure of the triaxial cell is 2 000 kPa. At all times, care was taken to ensure that the pressure difference between the inner and outer cell did not exceed 50 kPa to prevent fracture of the inner glass.

4.3.3 HYDRAULIC PRESSURE CONTROLLERS

Standard Digital Pressure Controllers (STDDPCs) were used as pressure controllers to control and measure the backpressure and cell pressure. The controllers used hydraulic actuators, powered by a stepper motor to measure and regulate the deaired water pressure and volume. The controllers operated by pressurising the water in the cylinder by a piston. The piston was activated by the motor and gearbox connected by the ball screw, as instructed from the control software or the command keypad. The pressure in the water was measured by means of an integral solid state pressure transducer. The volume change of water in the cylinder was measured by the number of steps of the piston movement in the rectilinear direction as counted by the stepper motor. The process of operation is illustrated in Figure 4-5. The maximum working pressure of each controller was 2 000 kPa and the volume capacity was 200 000 mm^3. The controllers were calibrated in terms of quanta, measured by the number of steps or counts. The technical properties and the calibration data are shown in Table 4-3.

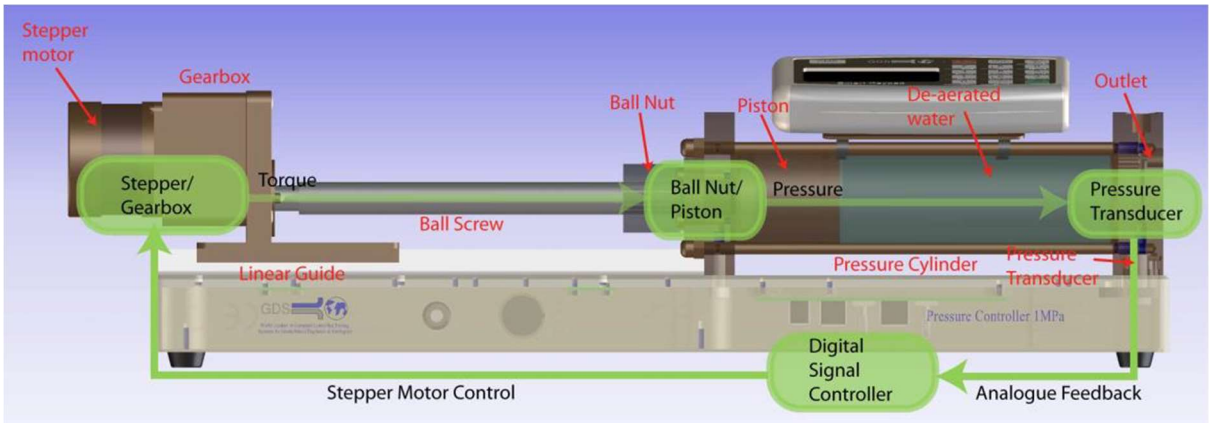

Figure 4-5: Operation of hydraulic pressure transducer (Courtesy of GDS Instruments)

Table 4-3: Technical properties and calibration data of the hydraulic pressure controllers

Parameter	Pressure controller		
	Backpressure	**Inner cell**	**Outer cell**
Serial number	21179	21178	21456
Maximum pressure (kPa)	2000	2000	2000
Volume capacity (mm^3)	200 000	200 000	200 000
Pressure quanta (kPa/count)	0.000543	0.000542	0.000544
Pressure offset (kPa)	1.0	8.0	3.0
Volume quanta (mm^3/count)	0.0626	0.0626	0.0626

4.3.4 PORE PRESSURE TRANSDUCERS

Pore Pressure Transducers (PPTs) were used to measure the pressures at the relevant positions independent of the pressure controllers. The triaxial testing system was fitted with three pressure transducers. The pore water pressure transducer was installed at the base of the triaxial cell with a connection through the pedestal into the bottom of the sample to measure the pore water pressure. The pore air pressure transducer was also installed at the base of the triaxial cell, with a connection through the top cap into the top of the sample to measure the pore air pressure in the sample during testing at unsaturated soil conditions or the top pore water pressure during testing at saturated soil conditions. The technical properties and calibration data of each pressure transducer are shown Table 4-4.

Table 4-4: Technical properties and calibration data of pressure transducers

Parameter	Pressure transducer		
	Backpressure	**Pore air**	**Outer cell**
Serial number	461 997	501264	483462
Maximum pressure (kPa)	2000	1000	2000
Excitation voltage(V)	10	10	10
Zero output (mV)	0.060	0.030	0.020
Full output (mV)	99.970	99.880	99.870
Sensitivity (kPa/mV)	20.006	10.012	20.026
Non-linearity (% of FS)	±0.053	±0.015	±0.053
Hysteresis (% of FS)	0.010	0.000	0.000

4.3.5 LOCAL DISPLACEMENT INSTRUMENTATION

Local displacement instrumentation was used to measure the total volume of the sample. As discussed in Section 2.6, the change in the total volume of a soil sample in an unsaturated condition cannot directly be related to the change in water volume as measured by the volume change indicator of the backpressure controller due to the presence of pore air in the voids. To overcome this deficiency, local displacement instrumentation was used to measure the radial displacement (for radial strain) and vertical displacement (for vertical strain), which were related mathematically to obtain total volume change. Linear Variable Differential Transformers (LVDTs) were used for the measurement of radial and vertical displacement of the sample. The radial displacement instrumentation was installed onto the sample by attaching an LVDT to a radial calliper (or collar) as shown in Figure 4-6. The radial calliper together with the LVDT were thereafter attached to the mid-height of the sample membrane using epoxy. The vertical displacement instrumentation was installed onto the sample by attaching the LVDTs to the top and bottom vertical clamp as shown in Figure 4-7. The vertical clamps together with two pairs of LVDTs were thereafter attached to the middle third of the sample. For data transfer, each connection between the LVDT and the data logging unit was supplemented by an amplifier and power supply unit. The technical properties and calibration data of each LVDT is shown in Table 4-5.

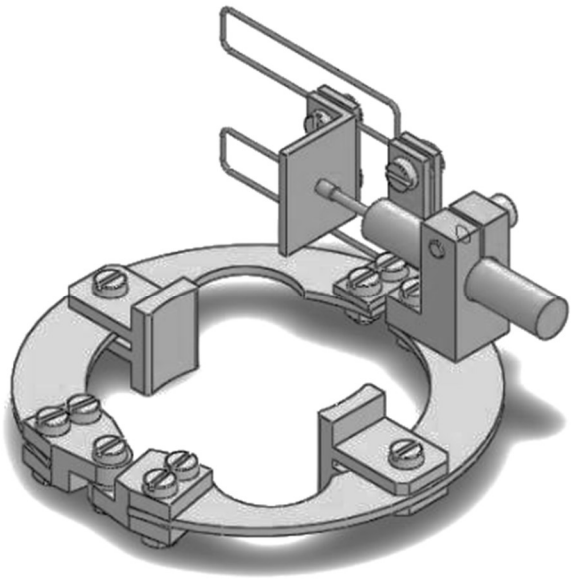

Figure 4-6: Cylindrical collar with LVDT for measurement of radial strains

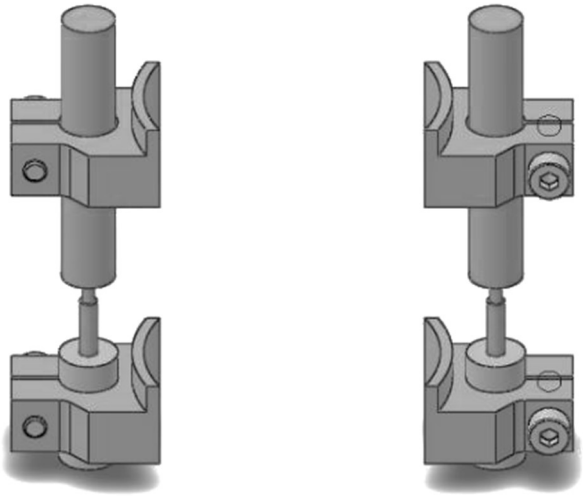

Figure 4-7: Vertical clamps with LVDTs for measurement of axial strains

Table 4-5: Technical properties and calibration data of local displacement instrumentation

Parameter	Vertical 1	Vertical 2	Radial
Serial Number	199469 (216411)	199468 (216410)	199464 (216409)
Full scale (V)	10	10	10
Range (mm)	±5	±5	±5
Linearity (%)	(0.29)	(0.26)	(0.31)
Sensitivity (mm/mV)	0.001022	0.001008	0.001005

4.3.6 DATA LOGGING UNIT

The data logging unit was a datalogger used to record the measurement data from each measuring instrument. The datalogger was referred to as the serial data acquisition pad, or serial pad, as depicted in Figure 4-8. The datalogger was equipped with 8 channels of 16-bit data acquisition and configurable gain range depending on the full scale of the measuring device. Each channel of the datalogger was fitted with a LEMO port to connect with the measuring device or system. The wire configuration of the LEMO plug and socket is shown in Figure 4-9. Storage of data to a computer hard drive was facilitated by the data acquisition software through an RS232 serial communication cable via the Comm port. The channel connection of each measuring device is shown in Table 4-6.

Figure 4-8: Serial data acquisition pad with 8 channels

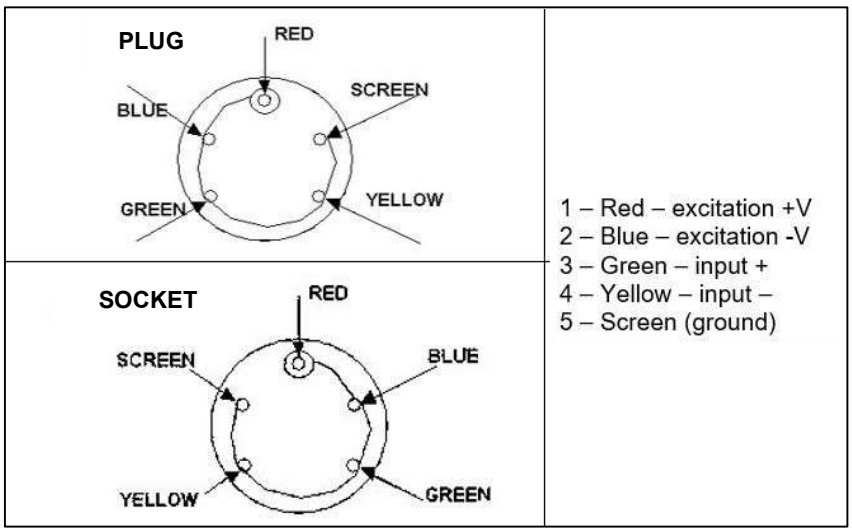

Figure 4-9: Wire configuration for LEMO plug and socket for local instrumentation

Table 4-6: Connection of measuring devices into data logger channels

Channel number	Transducer name
Channel 0	Load cell
Channel 1	Pore water pressure transducer
Channel 2	Pore air pressure transducer
Channel 3	Outer cell pressure transducer
Channel 4	Local vertical 1
Channel 5	Local vertical 2
Channel 6	Local vertical 3
Channel 7	Pore air controller

4.4 UNSATURATED TESTING SYSTEM

The testing of unsaturated soils necessitated modifications of the triaxial testing system by adding a pedestal with a high air entry disk and a pneumatic pressure controller. The modification equipment is described in the following subsections. Auxiliary modification included the installation of a heavy duty air conditioning unit in the testing room to maintain a constant temperature.

4.4.1 HIGH AIR ENTRY DISK

The high air entry disk was used to separate the pore air pressure from the pore water pressure in order to induce matric suction in the soil using the axis-translation technique as discussed in Section 2.6. The high air entry disk, depicted in Figure 4-10, was essentially a porous ceramic material which allowed the passage of water and prevented the flow of air, provided the difference between pore air pressure and pore water pressure (or matric suction) remained below the air entry value of the disk. The disk was machined to fit into the sample pedestal and the edges were sealed off with epoxy to prevent leakage. The water compartment below the high air entry disk was grooved spirally to serve as a channel to remove entrapped air bubbles. At all times, the uplift force acting on the disk from the backpressure controller was maintained such that it did not exceed 50 kPa to prevent cracking of the disk. In between tests, the disk was kept saturated by application of a backpressure of 10 kPa.

Figure 4-10: High air entry disk (Courtesy of GDS Instruments)

4.4.2 PNEUMATIC PRESSURE CONTROLLER

The Pneumatic Pressure Controller (PPC) shown in Figure 4-11 was used to introduce the pore air into the soil sample which was required for unsaturated soil conditions. The air pressure in the controller

was controlled by two solenoid valves with a built-in pressure transducer between them. The one valve was for inflow and the other was for outflow of air. The inflow valve allowed air pressure supplied by an external air compressor into the pneumatic pressure controller and the outflow valve released the required air pressure into the sample. The built-in pressure transducer measured the air pressure in the controller and regulated the control mechanism by opening and closing the inlet and outlet valves, depending on the required pore air pressure as instructed via the data control software. The data transfer for the control mechanism was facilitated by an analogue signal transmitted by the serial bus from the PC and software. The technical properties and calibration data of the pneumatic pressure controller are shown in Table 4-7.

Figure 4-11: Pneumatic Pressure Controller (Courtesy of GDS Instruments)

Table 4-7: Technical properties and calibration data of pneumatic pressure controller

Serial number	21270
Maximum pressure (kPa)	1 000
Excitation voltage (V)	10
Full span output (mV)	9940.4
Sensitivity (kPa/mV)	0.1006

4.5 DATA ACQUISITION AND SYSTEM CONTROL SOFTWARE

The control software was called GDSLab. The functions of the software were to control the system, execute different tests, display the live results and store the test results into datafiles. A test was initiated by setting up a station within the software, which allowed the test to be executed and controlled using test modules and stages. Manual control of a test was done using control panels for each device built within the software, shown in Figure 4-12. The live results were displayed in an instantaneous format as shown in Figure 4-13 or in graph format as shown in Figure 4-14. The software captured the raw and processed data from the datalogger and stored it as a datafile (.gds) which was opened as a comma separated value (.csv) file. Data processing was done in a spreadsheet and plotting was done with scientific software, called SigmaPlot.

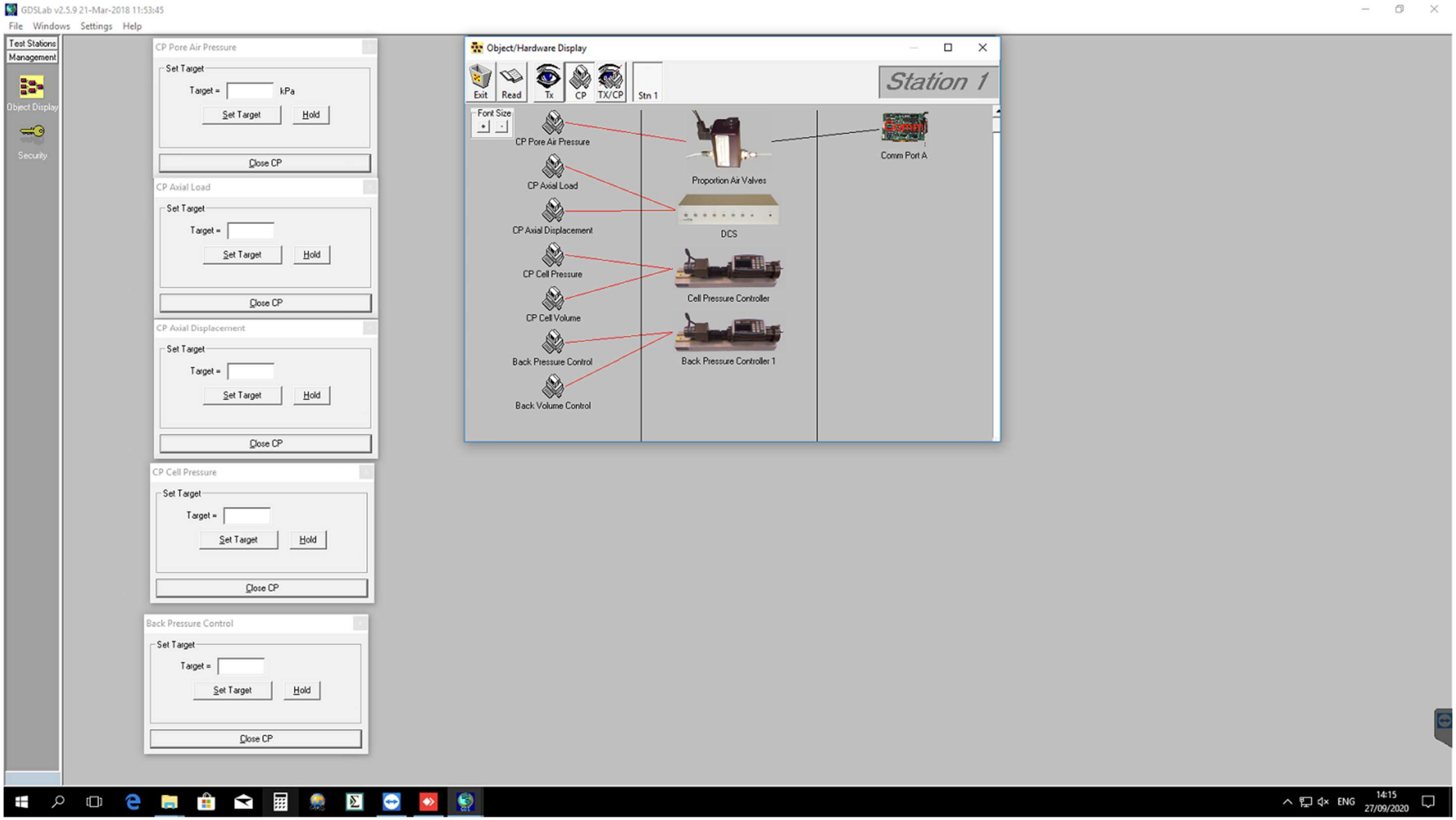

Figure 4-12: Control panels of devices in the control software

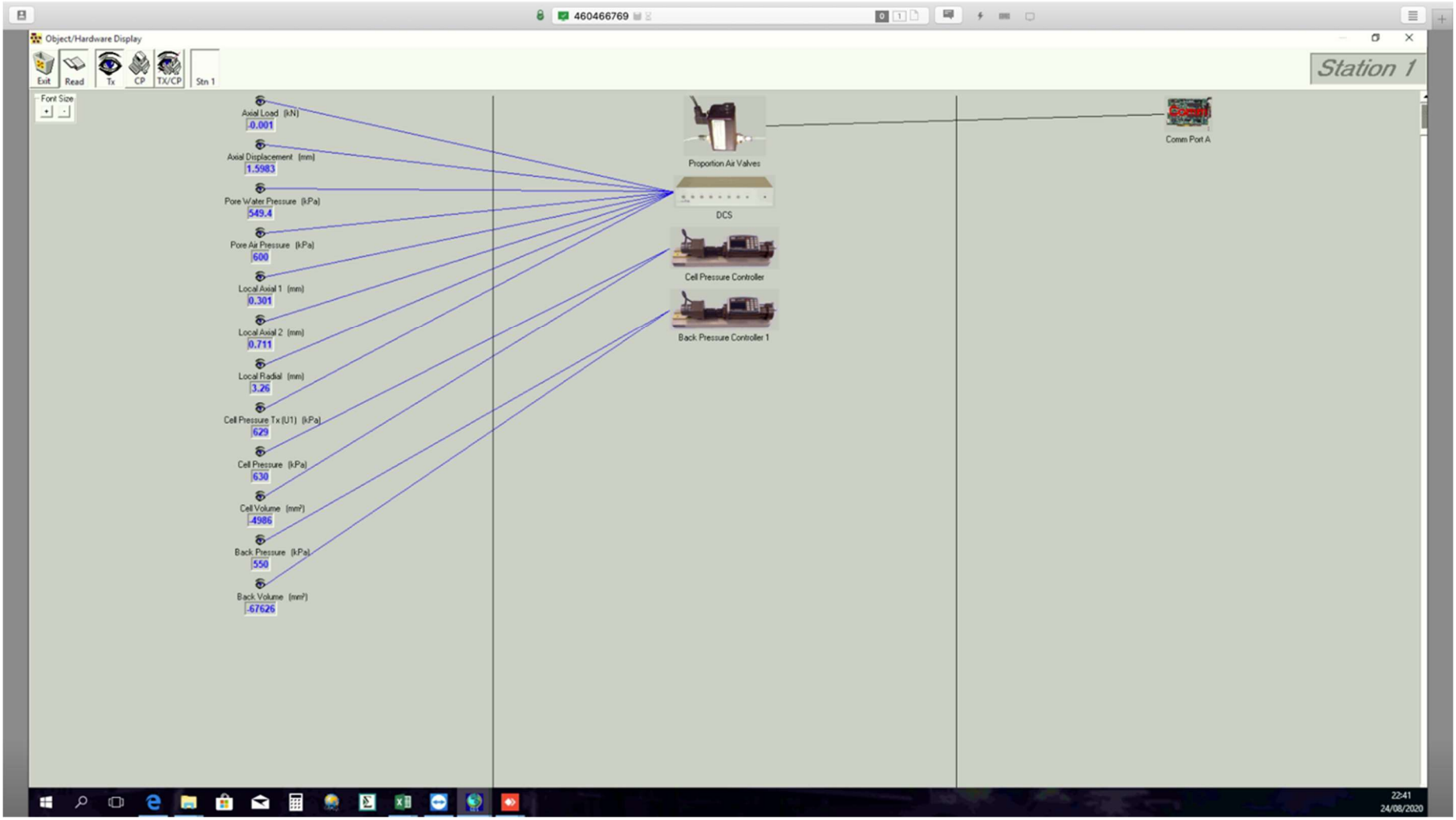

Figure 4-13: Display of instantaneous results and control panel of the data acquisition software

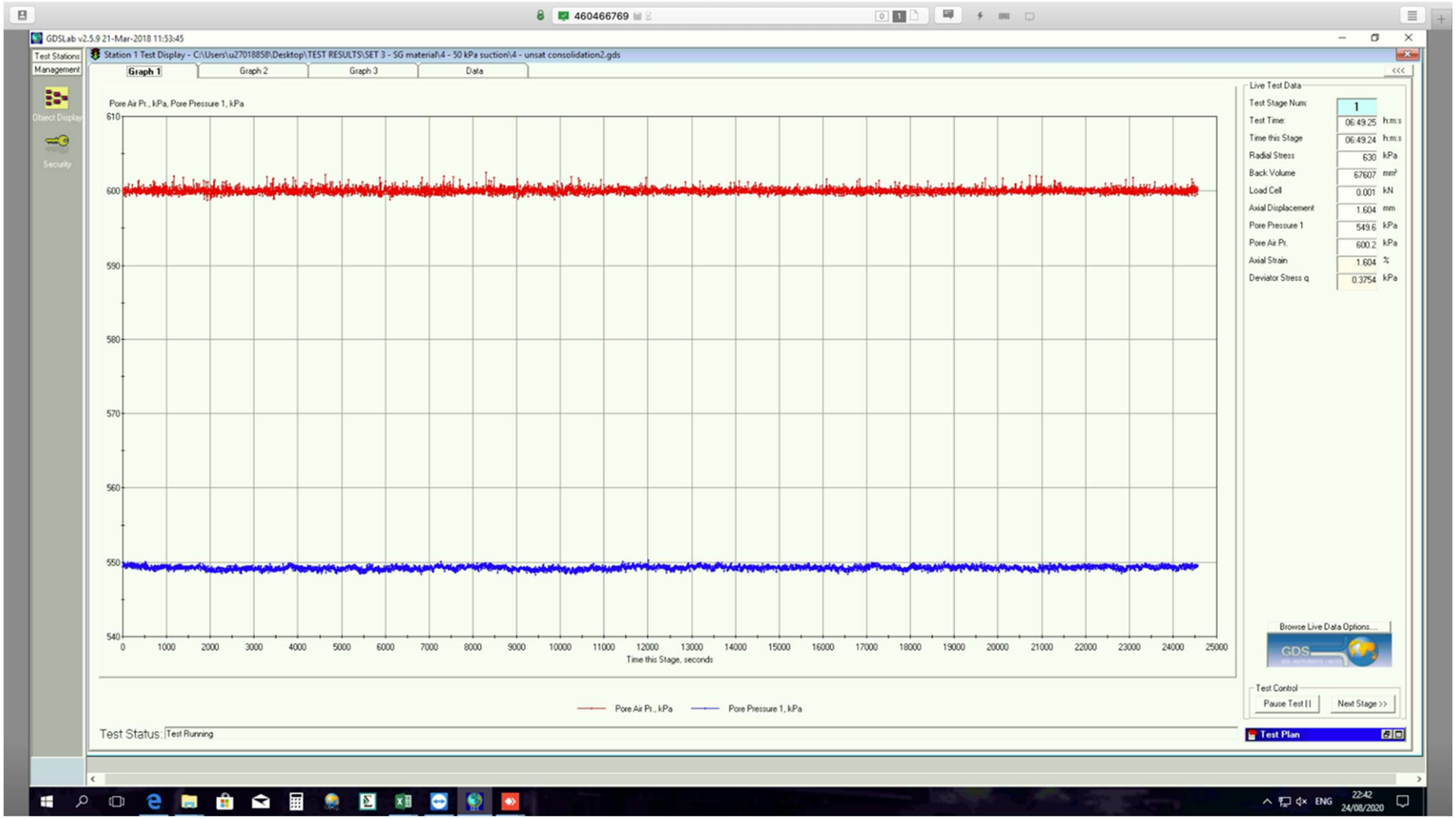

Figure 4-14: Graphical display of live results

4.6 DISCUSSION

In this chapter the laboratory equipment is presented and each component is discussed in detail. The chapter commenced with a presentation of the schematic diagram showing each component of the laboratory equipment. The schematic diagram is supplemented by a photograph of the laboratory equipment showing the real-life view of each component. The main components of the system include the actuator unit, triaxial cell, hydraulic pressure controllers, local instrumentation and the data logging unit. Auxiliary components for testing unsaturated soils include the pedestal with high air entry disk and a pneumatic pressure controller. The technical specifications and calibration values of each components are also presented. Lastly, the data acquisition and control software are presented. In the next chapter, the laboratory equipment is utilised to carry out the experimental work.

CHAPTER 5
EXPERIMENTAL WORK

5.1 TEST METHODOLOGY

The test methodology of the experimental work was carried out by conducting experiments in the laboratory using the laboratory equipment presented and described in Chapter 4 of this thesis. The test procedure undertaken included a series of planned tests executed as outlined by the diagram in Figure 5-1 with the sample description and loading procedure highlighted in Table 5-1.

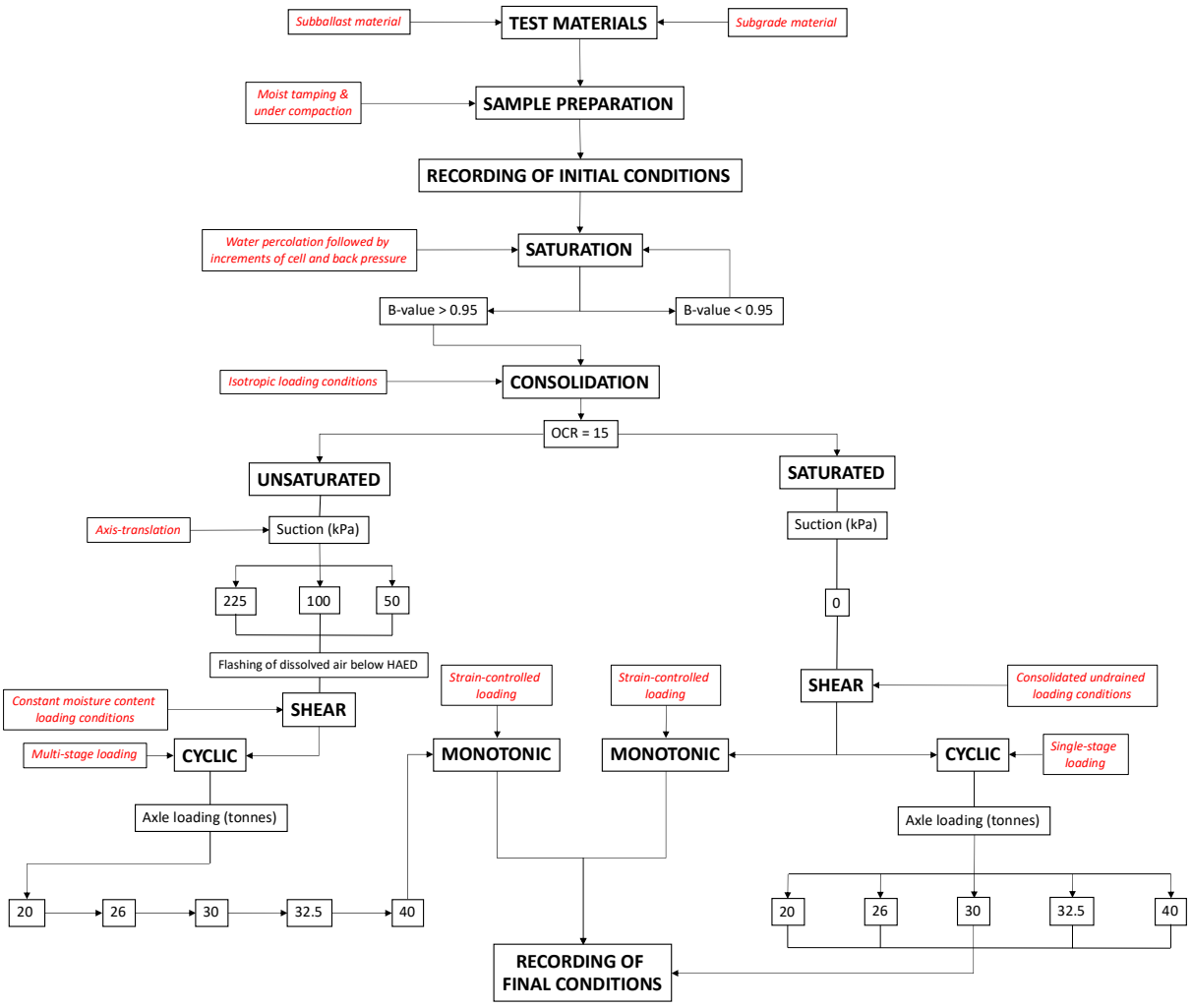

Figure 5-1: Test procedure of experimental work

Table 5-1: Summary of sample description and loading procedure for the test programme

Loading	Sample	Material	Soil conditions		Loading sequence
			Consolidation	Matric suction	
Monotonic only	SB-s-00	Subballast	15	-	Shear of 0 - 10 % strain
	SG-s-00	Subgrade	15	-	
Cyclic only	SB-s-20	Subballast	15	-	Single stage of cyclic shear of 0 - 20 tonnes
	SB-s-26		15	-	Single stage of cyclic shear of 0 - 26 tonnes
	SB-s-30		15	-	Single stage of cyclic shear of 0 - 30 tonnes
	SB-s-32.5		15	-	Single stage of cyclic shear of 0 - 32.5 tonnes
	SB-s-40		15	-	Single stage of cyclic shear of 0 - 40 tonnes
	SG-s-20	Subgrade	15	-	Single stage of cyclic shear of 0 - 20 tonnes
	SG-s-26		15	-	Single stage of cyclic shear of 0 - 26 tonnes
	SG-s-30		15	-	Single stage of cyclic shear of 0 - 30 tonnes
	SG-s-32.5		15	-	Single stage of cyclic shear of 0 - 32.5 tonnes
	SG-s-40		15	-	Single stage of cyclic shear of 0 - 40 tonnes
Cyclic and monotonic	SB-u-50	Subballast	15	50	Multi-stage of cyclic shear 0 - 20 tonnes + RT + 0 - 26 tonnes + RT + 0 - 30 tonnes + RT + 0 - 32.5 tonnes + RT + 0 - 40 tonnes + RT + 0 - 10% monotonic shear to 10% strain
	SB-u-100		15	100	
	SB-u-225		15	225	
	SB-u-50	Subgrade	15	50	
	SB-u-100		15	100	
	SB-u-225		15	225	

RT = rest period for equilibration of the pore water pressure to the respective matric suction

5.2 TEST MATERIALS

A railway track foundation consists of a subballast and a subgrade layer as discussed in Chapter 2. Test materials with properties representative of the subballast and subgrade layers were obtained and used as test materials for the experimental work. The physical material properties of the subballast and subgrade materials are presented in Table 5-2 and the particle size distribution graphs are shown in Figure 5-2. The maximum particle size of the final test materials was limited to sand particles with maximum size of 2 mm for the following reasons:

- general soil mechanics principles have shown that the failure behaviour of foundation materials is dominated by the sand, silt and clay particles,
- larger particles would have resulted in rough surfaces and membrane penetration during the application of cell pressure,
- larger particles would have resulted in stress concentrations and localisation around the sharp edges.

The particle size analysis and soil classification were conducted in accordance with the SANS 3001:GR1 and SANS 3001:GR3 specification. The Atterberg limits (LL, PL, PI and SL) were determined in accordance to the SANS 3001:GR10. The specific gravity or particle density was determined by based on diffraction principle using the Malvern Mastersizer 2000.

Table 5-2: Physical properties of the test materials

Material property	**Material**	
	Subballast	**Subgrade**
% gravel	2	1
% sand	75	67
% silt	18	29
% clay	5	3
Description	Silty sand	Silty sand
Liquid limit (%)	17	25
Plastic limit (%)	20	34
Plasticity index (%)	3	9
Linear shrinkage (%)	2	4
Specific gravity	2.89	2.64
Grading modulus	1.30	1.09

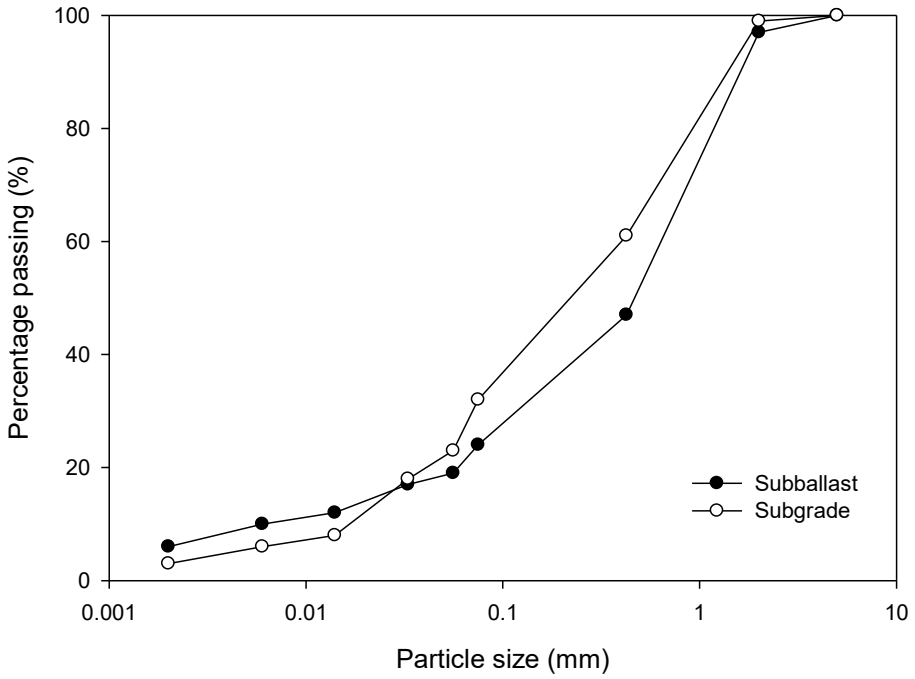

Figure 5-2: Particle size distribution of test materials

5.3 SAMPLE PREPARATION

The sample preparation procedure and the sequence of the procedures which were followed to setup the sample in the triaxial cell is shown in Figure 5-3. The samples were prepared in the steel mould with an internal diameter of 50 mm and a height of 100 mm as illustrated in Figure 5-3(a). The sample size was based on the size of the maximum particle size of 2 mm together with the size of the pedestal and the high air entry disk. Two latex membranes with an aluminium foil slotted between them was used to prevent permeation of the pore air through the membrane and to expedite the equilibration of the suction pressure throughout the sample as recommended by Dunn (1965) and Fredlund and Rahardjo (1993), as illustrated in Figure 5-3(b) and Figure 5-3(c). The positions of the vertical and radial local instrumentation were marked on the middle third and midway heights of the sample, shown in Figure 5-1(d). O-rings were used to prevent leakage of water between the sample and the triaxial cell as shown in Figure 5-3(e). The local instrumentation was attached to the sample membrane using epoxy followed by the measurement of the original height as shown in Figure 5-3(f). Illustration of the local instrumentation consisting of a radial collar for radial displacement and two sets of clamps for vertical displacement is shown in Figure 5-3(h). A suction sleeve was installed to ensure adhesion of the top cap to the load cell during cyclic loading as shown in Figure 5-3(i).

Figure 5-3: Sample setup procedure: (a) mass recording after reconstitution (b) sample placement on pedestal (c) wrapping of aluminium (d) measurement for local instrumentation (e) placement of O-rings on second latex membrane, (f) attachment of radial calliper and top cap (g) measurement of dimensions between vertical claps, (h) illustration of local instrumentation, (i) installation of suction sleeve

The samples were reconstituted by means of moist tamping in order to reconstitute the soil fabric of compacted materials (Kuervis and Vaid, 1988). The reconstitution of the samples in the mould was carried out by means of undercompaction for uniformity and repeatability of the physical characteristics throughout the whole sample (Ladd, 1978). The undercompaction percentage of each layer was calculated based on Equation (5-1) and the height of each layer was calculated based on Equation (5-2).

$$U_n = U_{ni} - \left[(n_l - 1) \times \left(\frac{U_{ni} - U_{nt}}{n_t - 1}\right)\right] \quad (5\text{-}1)$$

and

$$H_n = \frac{H}{n_t} \times \left[(n_l - 1) \times \left(1 + \frac{U_{ni}}{100}\right)\right] \quad (5\text{-}2)$$

Where:

n_l = number of the layer of soil sample in consideration

n_t = total number of layers of soil sample,

U_n = undercompaction percentage of n-th layer,

U_{ni} = undercompaction percentage of initial layer (0 to 15% for dense to loose sample),

U_{nt} = undercompaction percentage of the last layer (usually 0%),

H_n = height of the n-th layer of sample,

H = height of sample.

All samples were prepared in four layers compacted twice per layer, with an initial under-compaction of 6%, as shown in Table 5-3. All samples were also prepared at the same water content, density and compaction effort in order to qualify as identical (Fredlund and Rahardjo, 1993). The target density and moisture content at which the samples were prepared, are presented in Table 5-4. The initial physical conditions for each sample are shown in Table 5-5 and Table 5-6 for the subballast and subgrade materials, respectively.

Table 5-3: Under-compaction properties for sample preparation

Layer*	Under-compaction (%)	Height (mm)	Thickness(mm)
1	6	25.6	26.5
2	4	51.0	24.5
3	2	75.5	24.5
4	0	100.0	24.5

*layers are counted from the bottom to top of sample.

Table 5-4: Target properties for materials preparation

Material property	Material	
	Subballast	Subgrade
Bulk density (kg/m^3)	2200	1800
Water content (%)	6	6

Table 5-5: Initial conditions of subballast samples after preparation and B-value after saturation

Soil test conditions	Sample	Initial Water Content	Bulk Density (kg/m^3)	Void Ratio	Final B-value
Saturated	SB-s-00	0.063	2202	0.381	0.967
	SB-s-20	0.061	2224	0.365	0.973
	SB-s-26	0.064	2206	0.379	0.955
	SB-s-30	0.063	2220	0.369	0.969
	SB-s-32.5	0.061	2212	0.372	0.975
	SB-s-40	0.062	2223	0.367	0.972
Unsaturated	SB-u-50	0.061	2190	0.386	0.963
	SB-u-100	0.062	2214	0.373	0.964
	SB-u-225	0.060	2193	0.381	0.964

Table 5-6: Initial conditions of subgrade samples after preparation and B-value after saturation

Soil test conditions	Sample	Initial Water Content	Bulk Density (kg/m^3)	Initial Void Ratio	Final B-value
Saturated	SG-s-00	0.061	1806	0.552	0.974
	SG-s-20	0.064	1814	0.549	0.976
	SG-s-26	0.063	1830	0.534	0.971
	SG-s-30	0.061	1835	0.527	0.971
	SG-s-32.5	0.061	1792	0.563	0.979
	SG-s-40	0.064	1793	0.567	0.982
Unsaturated	SG-u-50	0.061	1825	0.534	0.988
	SG-u-100	0.060	1840	0.521	0.967
	SG-u-225	0.060	1803	0.553	0.964

5.4 SATURATION STAGE

The objective of the saturation stage was to eliminate the unknown presence of pore air and negative pore water pressure induced during sample preparation. Sample saturation commenced with the percolation (or flushing) of deaired water through the sample for a duration of 12 hours from the bottom pedestal to the top cap, which was open to atmosphere for free drainage. Percolation was carried out at 1 m head of deaired water pressure, supplied from the reservoir of the deaerator. After percolation, saturation was continued by means of increments of the cell pressure and backpressure as described by Black and Lee (1973). The pore pressure coefficient B (also known as B-value) was used as means to measure the degree of saturation as indicated by Skempton (1954). The B-value was calculated after each cycle of increment of the cell pressure based on Equation (5-3).

$$B = \frac{\Delta u_w}{\Delta \sigma_3} \tag{5-3}$$

Where:

B = B-value,

Δu_w = change in pore water pressure,

$\Delta \sigma_3$ = change in all round confining (or cell) pressure.

All samples were considered saturated once the calculated B-value was above 0.95 as specified by BS 1377. Samples tested at an unsaturated state were also initially saturated and then desaturated to a precise degree of saturation as measured by the water volume indicator of the backpressure controller. The saturation stage of the subballast and subgrade materials is depicted in Figure 5-4 and Figure 5-5, respectively. The final B-value of each sample is shown in Table 5-5 and Table 5-6 for the subballast and subgrade materials, respectively.

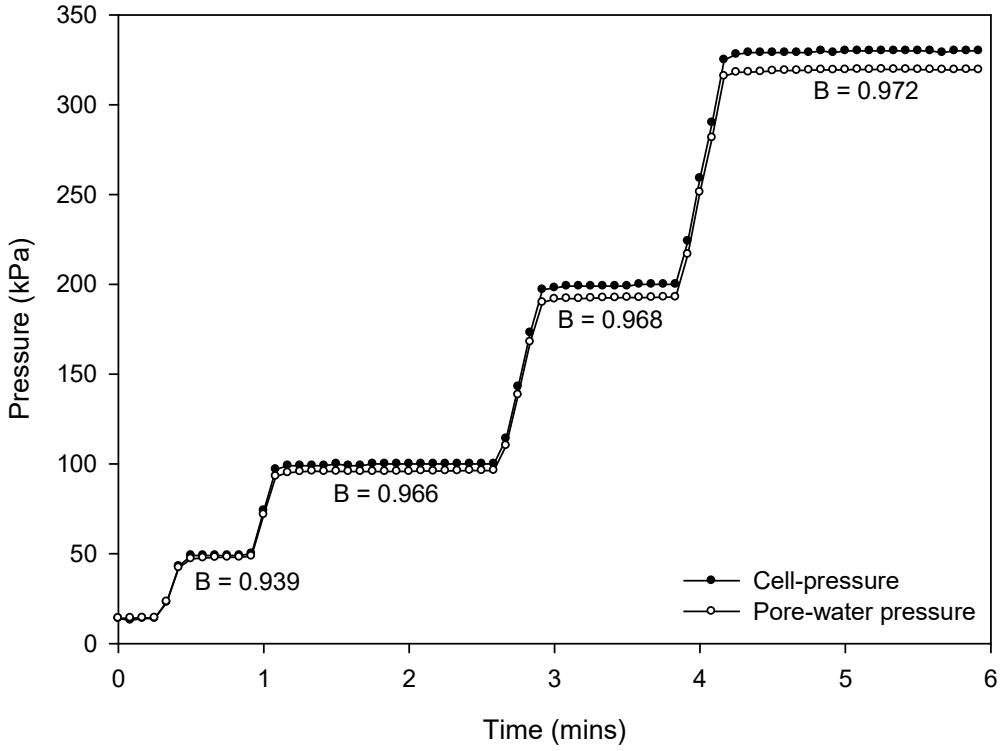

Figure 5-4: Typical saturation of subballast material

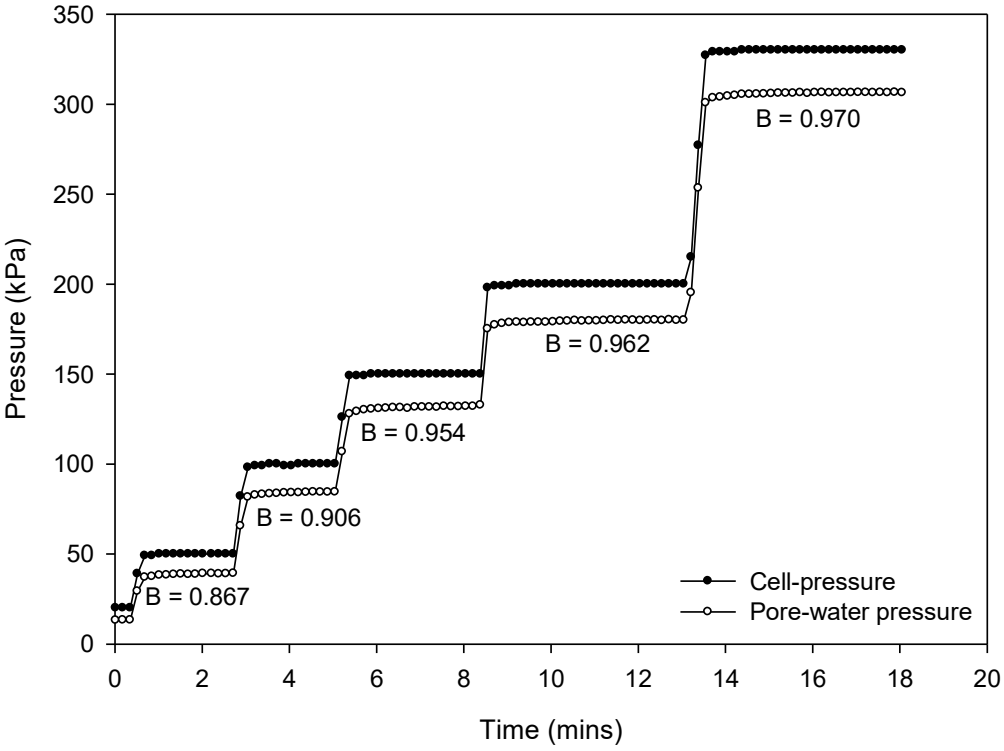

Figure 5-5: Typical saturation of subgrade material

5.5 SATURATED CONSOLIDATION STAGE

The objective of the consolidation stage under saturated soil conditions was to establish the initial conditions required for the shear stage of saturated and unsaturated samples. The initial conditions referred to the likely in-situ state of the soil in terms of the stress history confining stress. The stress history in the soil samples was measured by means of the overconsolidation ratio as represented in Equation (5-4). The saturated consolidation stage was carried out on all samples under the application of an isotropic pressure to the maximum effective normal stress based on Equation (5-4).

$$OCR = \frac{\sigma'_m}{\sigma'} \tag{5-4}$$

Where:

OCR = Overconsolidation ratio,

σ'_m = maximum effective normal stress,

σ' = current effective normal stress.

Railway materials are known to be heavily overconsolidated because of the effect of roller and vibratory compaction during construction. Field measurements by Gräbe (2002) from pressure plate tests conducted during the construction of a railway line indicated that the overconsolidation ratio on compacted railway foundation materials is between 14 and 16. Based on that, the subballast and subgrade materials were consolidated to an overconsolidation ratio of 15, meaning, to a maximum effective normal stress of 450 kPa with current effective normal stress reduced to 30 kPa. Typical results from the consolidation stage for the subballast and subgrade materials are shown in Figure 5-6 and Figure 5-7 respectively, with the consolidation properties for each material presented in Table 5-7.

Table 5-7: Saturated consolidation properties of the test materials

Material property*	**Material**	
	Subballast	**Subgrade**
Effective pre-consolidation (kPa)	450	450
Normal consolidation slope $(-\lambda)$	0.02	0.06
Recompression slope $(-\kappa)$	0.002	0.006

*average value of all samples tested with reference to Figure 5-6 and Figure 5-7

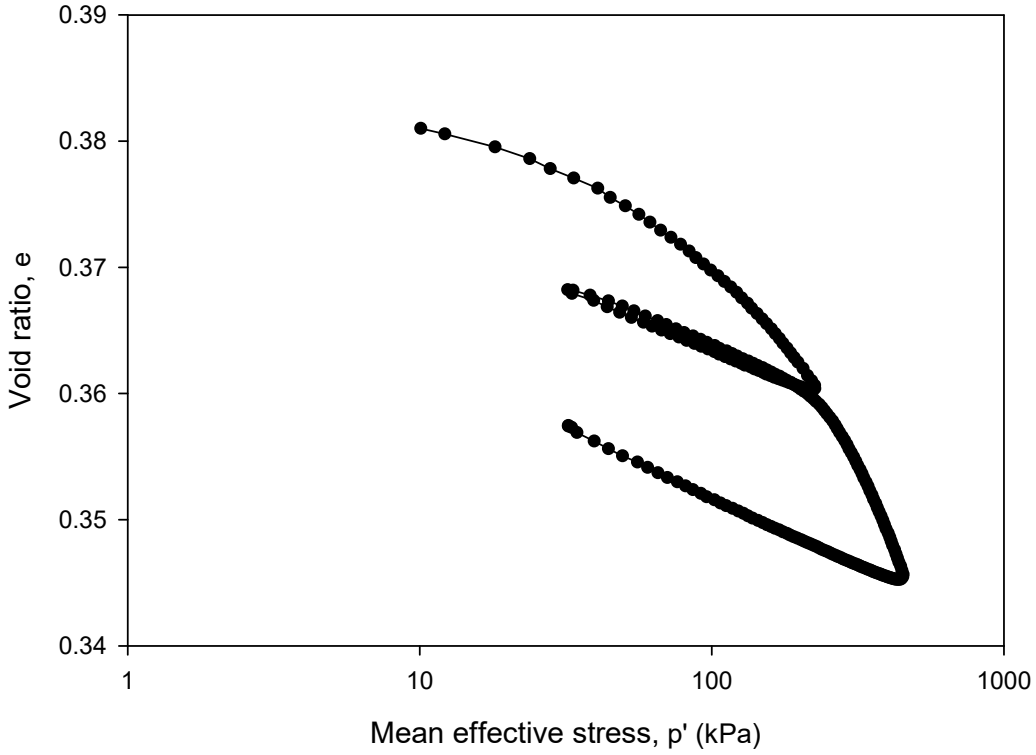

Figure 5-6: Typical consolidation compression of subballast material

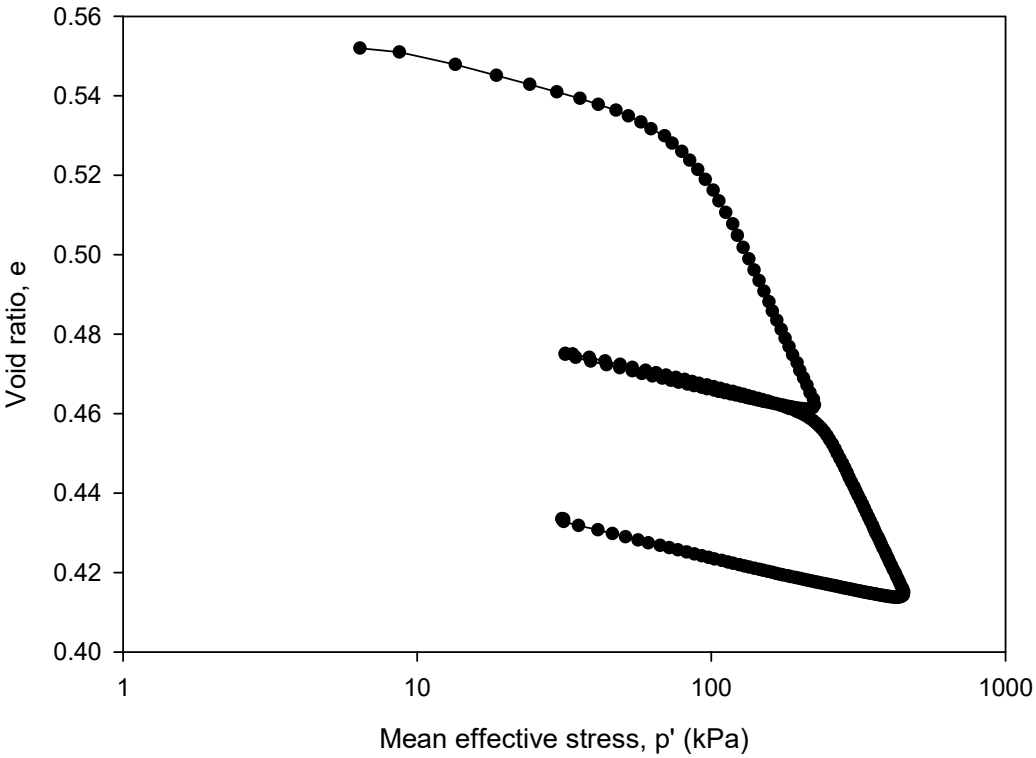

Figure 5-7: Typical consolidation compression of subgrade material

5.6 DESATURATION STAGE

The desaturation of soil samples was conducted by means of unsaturated consolidation and its main objective was to prepare the soil samples to a known suction value. The matric suction was determined based on Equation (5-5) and achieved by means of axis translation as discussed in Chapter 2. Three matric suction values of 50, 100 and 225 kPa were considered. As shown in Figure 5-1, all the samples were initially saturated and isotopically consolidated and the unsaturated consolidation stage was carried out immediately after the isotropic consolidation stage for the unsaturated part of the experimental test procedure. The reason for the saturation and saturated consolidation of all samples (saturated and unsaturated samples) was to ensure that desaturation was the only change in the soil conditions and stress history, to ensure accurate comparison of the results. Desaturation was conducted via axis translations by keeping the pore air pressure constant at 800 kPa and the pore water pressure at 750, 700 and 575 kPa to achieve matric suctions of 50, 100 and 225 kPa respectively, in accordance with Equation (5-5).

$$s = u_a - u_w \tag{5-5}$$

Where:

s = matric suction,

u_w = pore water pressure at base of sample,

u_a = pore air pressure at top of sample.

The graphs depicting the desaturation of the subballast and subgrade materials at various matric suction values are shown in Figure 5-8 and Figure 5-10, respectively, in terms of the specific water volume. Specific water volume was considered as the equilibration parameter (over water content alone) because it captures the change in volume of the sample by means of the void ratio and the change in water content by means of the degree of saturation as represented by Equations (5-6) and (5-7)

$$v_w = 1 + S_r e \tag{5-6}$$

$$S_r = \frac{V_w}{V_v} \tag{5-7}$$

Where:

v_w = specific water volume,

S_r = degree of saturation,

e = void ratio ($= V_v/V_s$),

V_w = volume of water,

V_v = volume of voids,

V_s = volume of solids.

Unsaturated soil conditions were achieved after equilibration, which involved the dissipation of the excess pore water, draining through the high air entry disk against the applied pore air pressure and cell pressure. Desaturation was complete after six days for the subballast material and after eight days for the subgrade material. Equilibration of the matric suction throughout the samples was assumed to be achieved under the following conditions:

- the rate of change of the specific water volume was below 0.001 per day (Wheeler and Sivakumar, 1995) and,
- the rate of change in volume represented by the degree of saturation and specific water volume was equal to zero (Airó Farulla and Ferrari, 2005).

The change in the degree of saturation during desaturation together with the final degree of saturation for both subballast and subgrade materials are shown in Figure 5-9 and Figure 5-11, respectively. According to Fredlund and Rahardjo (1993), long term testing (longer that 12 hours) under the application of pore air pressure can cause air diffusion through the high air entry disk, which may result in the loss of continuity of the pore water below the high air entry disk and erroneous measurements of the pore water pressure. To correct for air diffusion after the unsaturated consolidation stage, the trapped air bubbles underneath the high air entry disk were removed using the back pressure controller and an auxiliary hydraulic pressure controller by means of a flushing process as stated by Delage et al. (2008). The flushing process was achieved by setting the pressure of the back pressure controller at 5 kPa higher than that in the auxiliary hydraulic pressure controller for about 30 - 45 minutes to allow the diffused air to migrate to the auxiliary hydraulic pressure in preparation for the shear stage. To further minimise to possibility of air diffusion into the pore water, testing of unsaturated samples was conducted at a back pressure higher than 500 kPa.

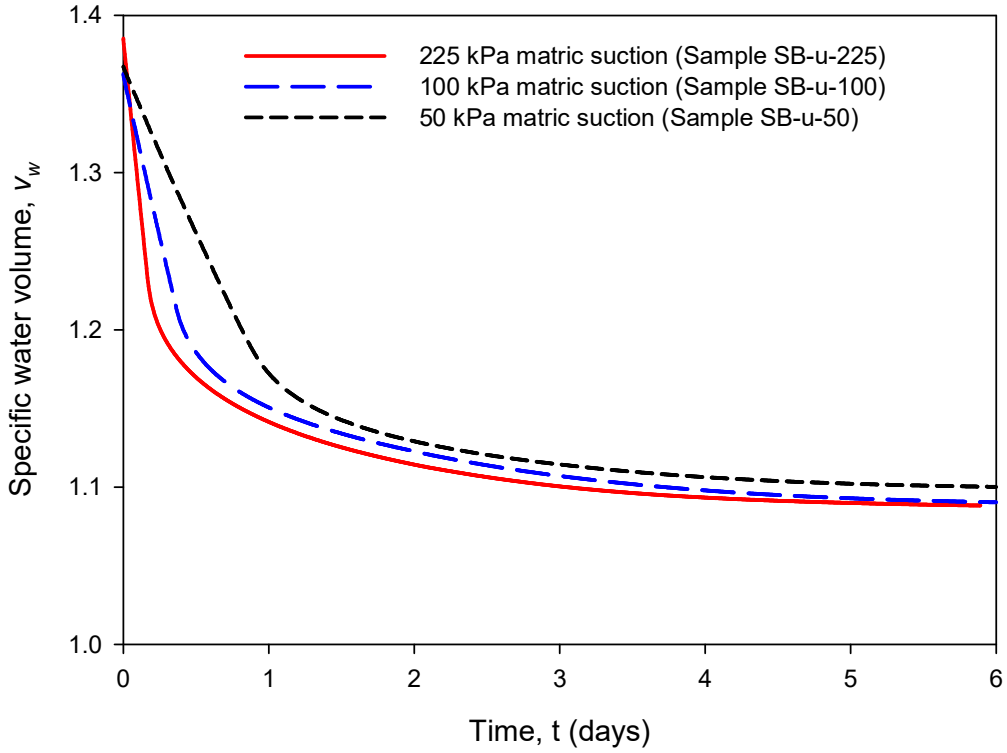

Figure 5-8: Variation of specific water volume during desaturation of subballast material at different matric suctions

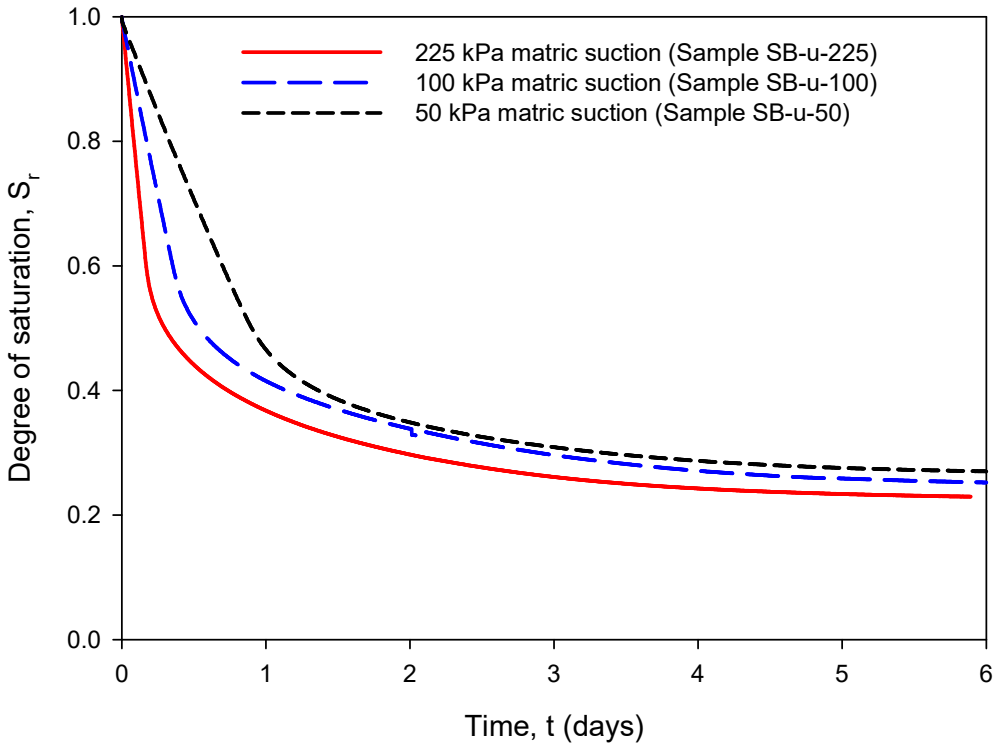

Figure 5-9: Variation of specific water volume during desaturation of subballast material at different matric suctions

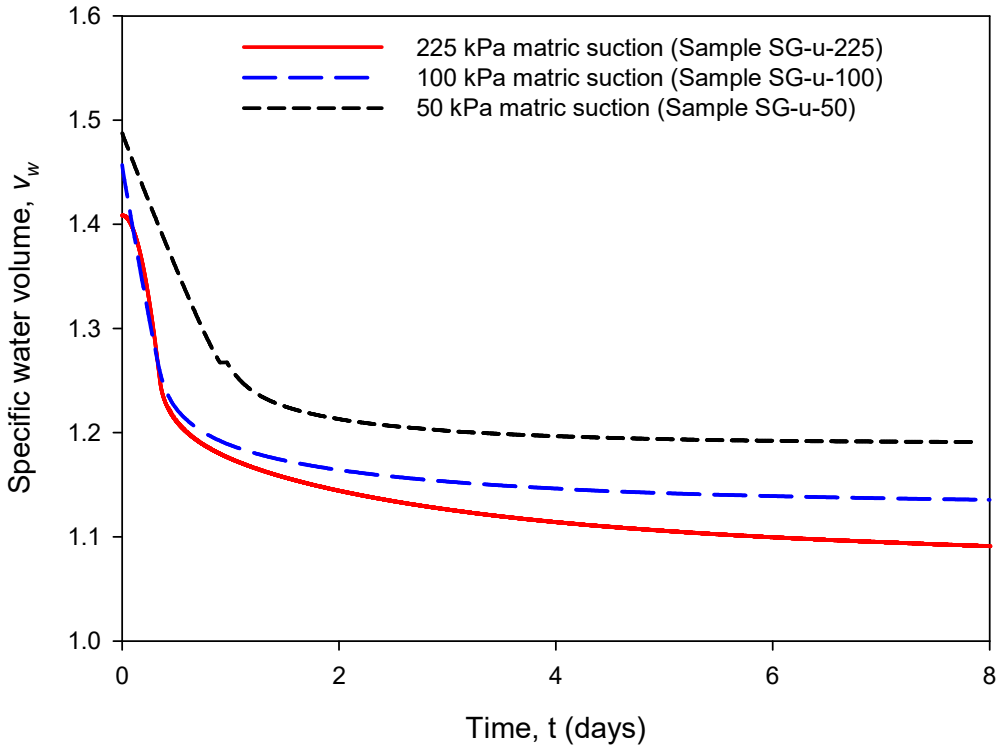

Figure 5-10: Variation of degree of saturation during desaturation of subgrade material at different matric suctions

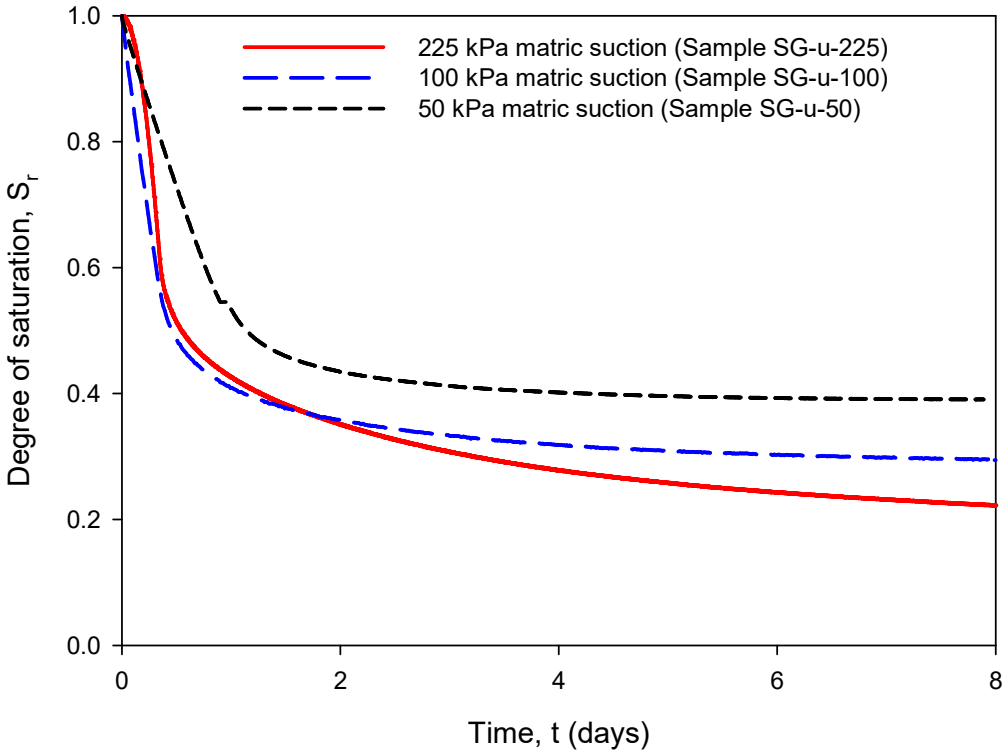

Figure 5-11: Variation of degree of saturation during desaturation of subgrade material at different matric suctions

5.7 SHEAR STAGE

The objective of the shear stage was to evaluate the strength and behaviour of the soil sample when subjected to an axial load or deviator stress. The shear stage of this study consisted of monotonic and cyclic loading tests. The monotonic loading tests were conducted on saturated and unsaturated soil samples under strain control settings of the triaxial apparatus. The monotonic shear tests were conducted at a strain rate of 0.05 percent per minute to a maximum strain of 10%. The strains were limited to 10% due to the limit of the local instrumentation. Strain controlled testing (as opposed to load or stress controlled) and slow strain rate of shearing were chosen in order to clearly obtain the peak shear strength (Lade, 2016) of the materials. The cyclic loading tests were also conducted for saturated and unsaturated soil conditions for the different axle load cases under load control settings of the test equipment. The cyclic shear tests were conducted at a loading frequency of 1 Hz and total number of load cycles of 2000. A typical heavy haul train in South Africa consists of 200 load cycles. The total number of 2000 loading cycles therefore represented a scenario where 10 trains transverse a track section with permanent development of pore water pressures and little dissipation thereof. The magnitudes of the cycle loading were applied to each sample as determined by the finite element modelling and analysis presented in Chapter 3. The axial load was corrected for each sample based on the current dimensions of the specific sample. The corrected area considered the effect of saturation, consolidation and desaturation on the radial and axial deformation, which were measured by the local instrumentation and calculated based on Equation (5-8). The magnitude and shape of the cyclic loading of each load case is shown in Figure 5-12 and Figure 5-13 for subballast and subgrade materials, respectively. The loading pattern of the cyclic loading was sinusoidal and its shape was acceptable as stipulated in the ASTM D5311/D5311M (2013) standard.

$$A_c = A_0\left(\frac{1-\varepsilon_v}{1-\varepsilon_a}\right) \tag{5-8}$$

Where:

A_c = corrected (or current) area,

A_0 = original (or initial) area,

ε_v = volumetric strain ($= \varepsilon_a + 2\varepsilon_R$),

ε_a = axial strain ($=\Delta H/H_0$),

ε_R = radial strain $\Delta R/R_0$)

ΔH = change in height,

H_0 = initial height,

ΔR = change in radius,

R_0 = initial radius.

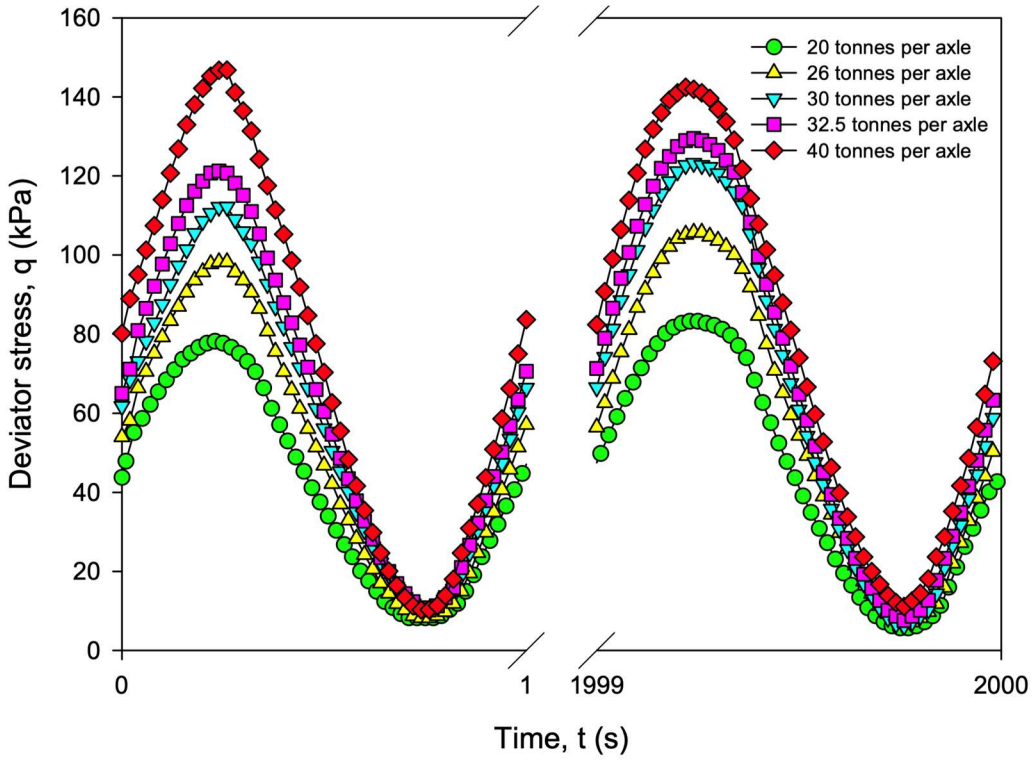

Figure 5-12: Cyclic loading applied to the subballast material

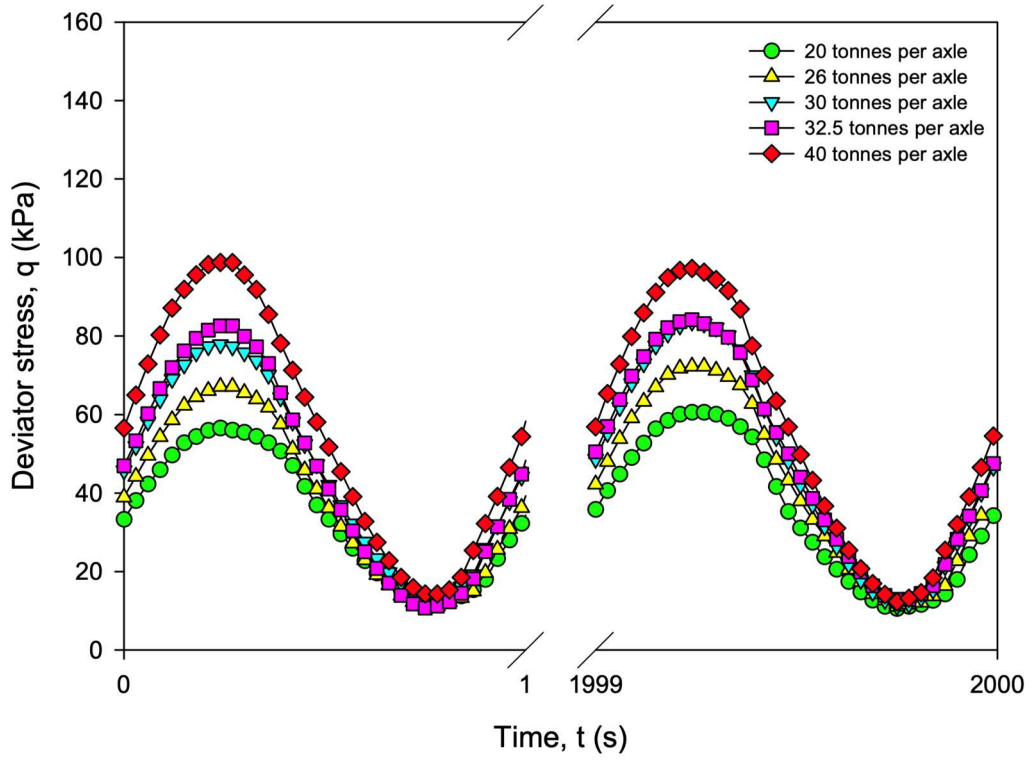

Figure 5-13: Cyclic loading applied to the subgrade material

5.8 PRELIMINARY RESULTS

The preliminary results from the experimental work are the measured parameters which are strains and pore pressures for saturated and unsaturated samples. The measured strains are permanent or plastic strains. The pore pressures for saturated samples are presented as excess pore water pressure whilst the pore pressures for unsaturated samples are presented as matric suction.

5.8.1 STRAINS OF SATURATED AND UNSATURATED SAMPLES

During the application of cyclic loading, the permanent deformations were consistently measured at a sampling rate of 100 Hz. The permanent deformation of the subballast and subgrade materials is plotted as shown in Figure 5-14 to Figure 5-17. Preliminary analysis of the permanent deformations indicated that for saturated samples, there was a direct relationship between axle loading and deformation, that is, increased axle loading resulted in increased deformations. In the case of the unsaturated samples, it is evident that the relationship between increased loading and deformation is more complex in that increased axle loading did not directly result in increased permanent deformation. The permanent deformations for a lower stress level (20 tonnes per axle) can be greater than that for a higher stress level (26 tonnes per axle). This trend is fairly consistent and indicative of initial stabilisation and particle reorientation due to the presence of air pockets in the voids of the soil. Further analysis and investigation of this trend are explored in Chapter 6.

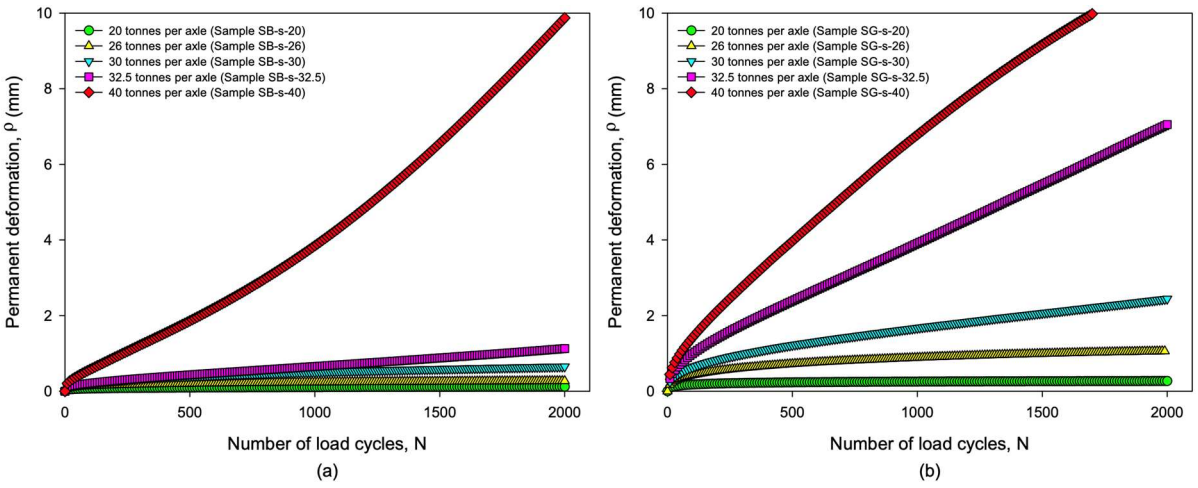

Figure 5-14: Permanent deformation of (a) subballast and (b) subgrade material under saturated soil conditions

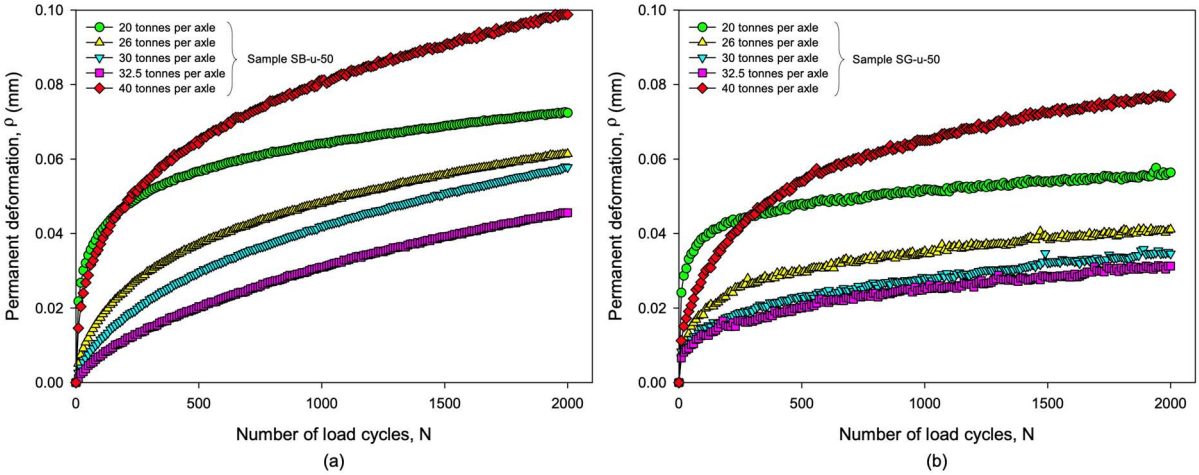

Figure 5-15: Permanent deformation of (a) subballast and (b) subgrade material under unsaturated soil conditions with 50 kPa initial matric suction

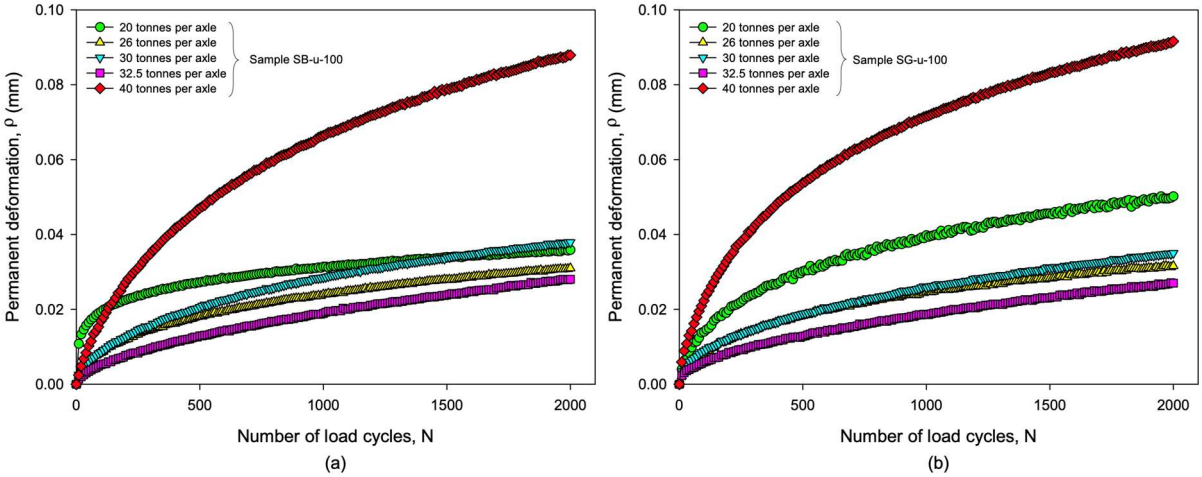

Figure 5-16: Permanent deformation of (a) subballast and (b) subgrade material under unsaturated soil conditions with 100 kPa initial matric suction

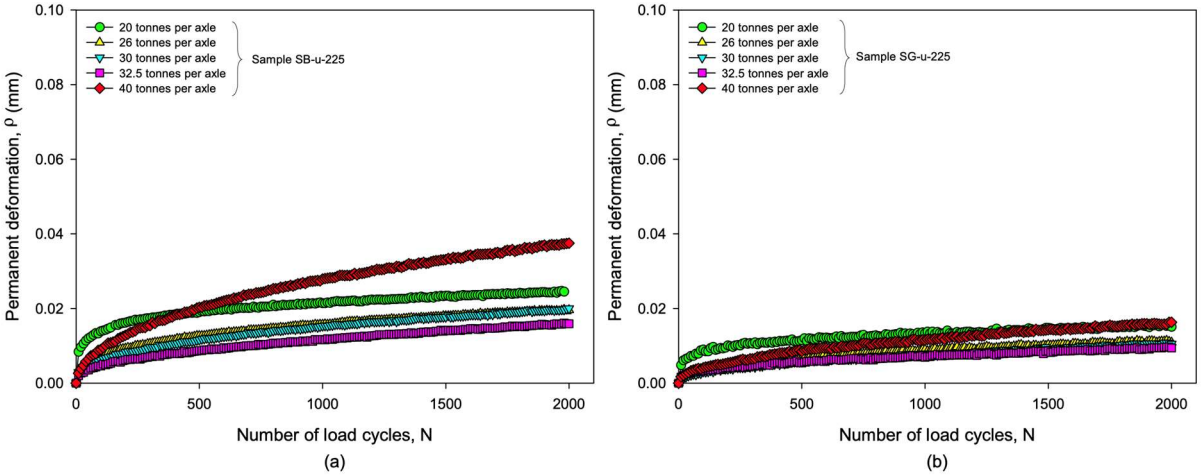

Figure 5-17: Permanent deformation of (a) subballast and (b) subgrade material under unsaturated soil conditions with 225 kPa initial matric suction

5.8.2 PORE PRESSURES OF SATURATED AND UNSATURATED SAMPLES

Pore air pressure and pore water pressure were also measured at a sampling rate of 100 Hz during cyclic loading. The preliminary results of the pore pressures were plotted and are shown in Figure 5-18 to Figure 5-21. The measured pore water pressures for saturated samples were reduced to excess pore water pressure based on Equation (5-9) and that of unsaturated samples were reduced to matric suction based on Equation (5-5). Preliminary analysis and inspection of the excess pore water pressure for saturated samples indicate a direct relationship between increased axle loading and the development of positive excess pore water pressure. In the case of unsaturated samples, it is evident that the loss of matric suction is directly related to the increase in the stress level. Further analysis and investigation of the effect of increased axle loading on the pore pressure of saturated and unsaturated soils commences in Chapter 6.

$$u_e = u_b - u \tag{5-9}$$

Where:

u_e = excess pore water pressure,

u_b = back pressure,

u = measured pore water pressure.

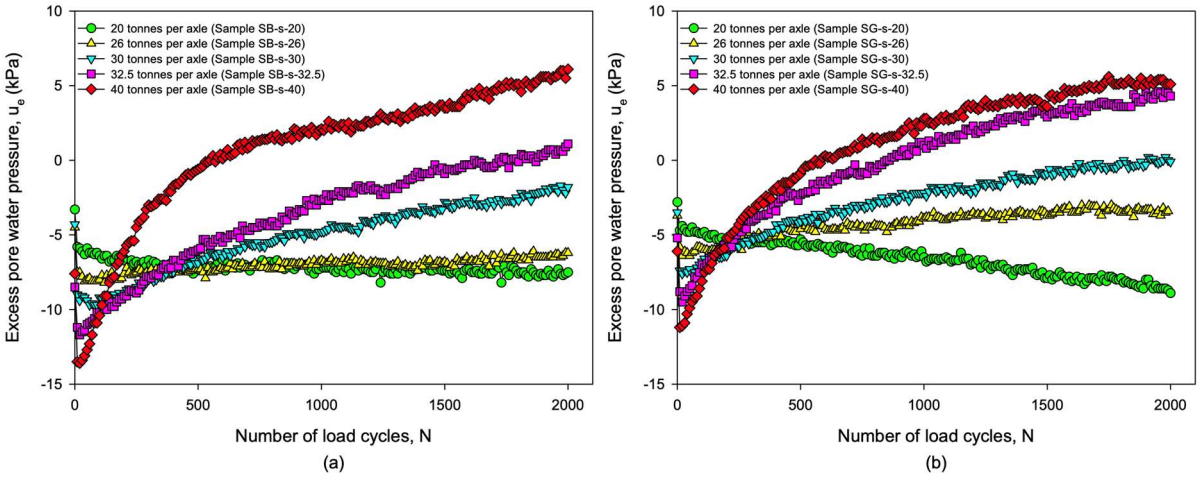

Figure 5-18: Change in excess pore water pressure of (a) subballast and (b) subgrade material under saturated soil conditions

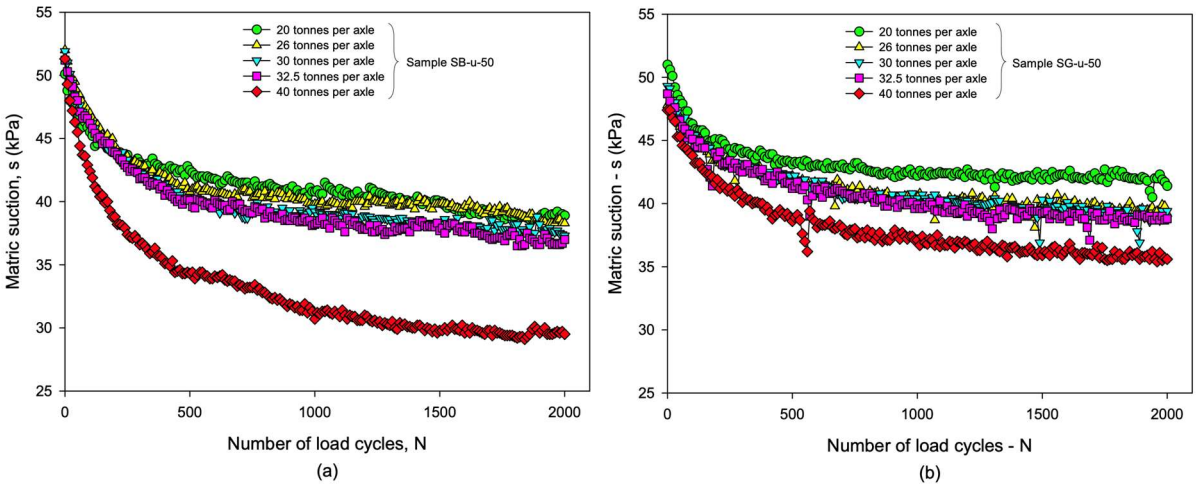

Figure 5-19: Change in matric suction of (a) subballast and (b) subgrade material under unsaturated soil conditions with 50 kPa initial matric suction

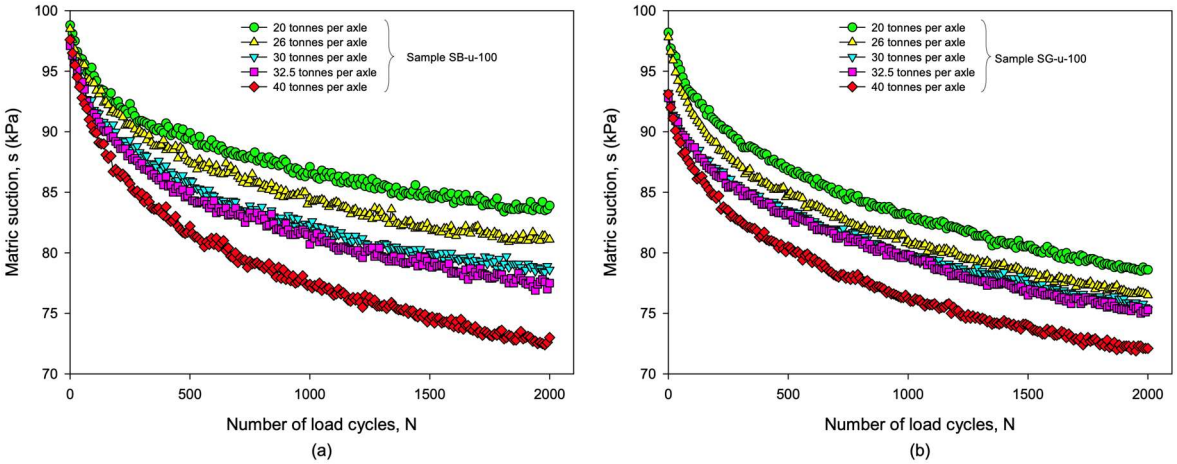

Figure 5-20: Change in matric suction of (a) subballast and (b) subgrade material under unsaturated soil conditions with 100 kPa initial matric suction

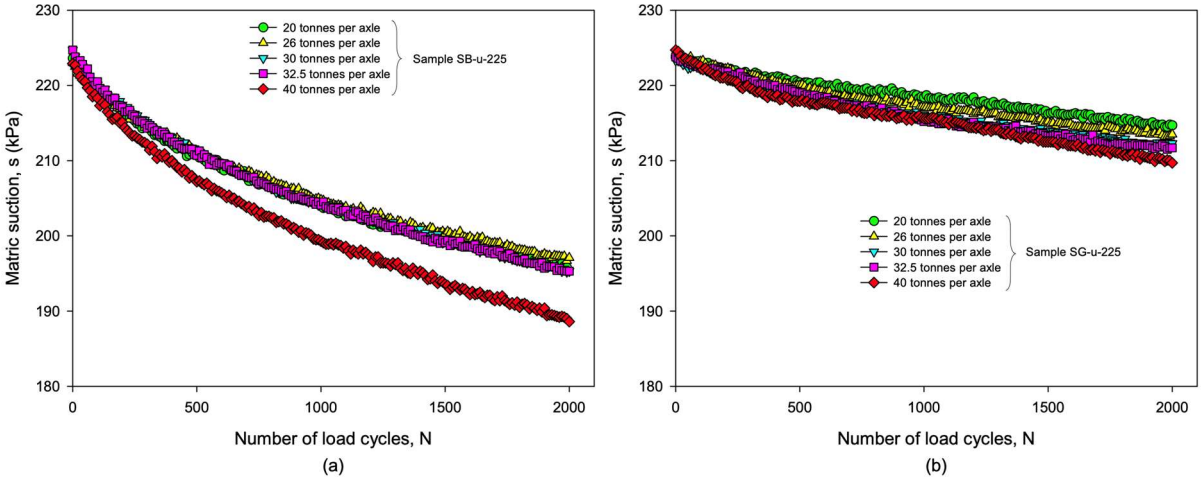

Figure 5-21: Change in matric suction of (a) subballast and (b) subgrade material under unsaturated soil conditions with 225 kPa initial matric suction

5.9 DISCUSSION

In this chapter of the thesis, the experimental work which was undertaken has been presented. The chapter commenced with a presentation of a diagram depicting the test stages and procedures together with a table highlighting the samples and the loading on each sample. Thereafter, procedures and results from each test stage, including sample preparation, saturation, consolidation, desaturation and shear stage, are presented and briefly discussed, as an introduction or preview of discussions in the following chapter, which consist of detailed analysis and interpretation of the results.

CHAPTER 6
INTERPRETATION AND DISCUSSION OF RESULTS

6.1 OVERVIEW OF RESEARCH METHODOLOGY

A cyclic triaxial apparatus was used to carry out experimental tests on 18 soil samples. The soil conditions were saturated in 12 of the samples and unsaturated in 6 of the samples. The experimental work and preliminary results are presented in Chapter 5 of this thesis. The cyclic triaxial apparatus used in the experimental work and described in Chapter 4, allowed for the testing of saturated and unsaturated soil conditions with monotonic and cyclic loading. The axle loading started from a base load of 20 tonnes per axle, followed by increased axle loading of 26, 30, 32.5 and 40 tonnes per axle. The characterisation of the increased axle loading for cyclic railway loading was carried out by means of finite element analysis as presented in Chapter 3. Saturated and unsaturated soil conditions are discussed in detail in the literature study in Chapter 2 of this thesis. The importance of unsaturated soil conditions in railway formation materials is highlighted as relevant and prevalent to railway foundations especially in arid to semi-arid regions. The importance of increased axle loading is also discussed in Chapter 2 with an emphasis placed on the benefits to the economy, environment and safety.

This chapter is therefore devoted to the analysis, interpretation and presentation of the test results from the experimental work and the discussion of the various investigated engineering parameters and trends. The chapter commences by presenting a summary of the experimental work with specific reference to the test procedures and stages undertaken (see Table 6-1). As shown in the table, the experimental work was carried out on two materials which were representative of the subballast and subgrade layers in a railway foundation. The experimental work was conducted in three main stages, namely initialisation, followed by desaturation, where necessary, and then shearing, which was either monotonic or cyclic. The initialisation stage involved saturation and consolidation mainly to establish known initial conditions such as stress history, density and phase properties within the soil matrix. The desaturation stage was carried out to introduce unsaturated soil conditions into the samples and induce matric suction by means of axis translation. Lastly, the shear stage was carried out to investigate the effect of increased axle loading on saturated and unsaturated railway foundation materials. The results presented in this chapter include monotonic test results, determination of shear strength and the effect of increased axle loading on saturated and unsaturated railway material by means of the stress states, resilient modulus, strains and pore pressures. The chapter closes with a discussion that summarises the findings and significance of this research.

Table 6-1: Summary of experimental work

Material	Soil conditions	Sample notation	Stage 1: Initialisation		Stage 2: Desaturation		Stage 3: Shear	
			Saturation, B-value	Consolidation, OCR	Degree of saturation (%)	Matric suction (kPa)	Cyclic, (stress expressed in tonnes per axle)	Monotonic, (strain level up to maximum strain)
Subballast	Saturated	SB-s-00	0.967	15	~100	-	-	CU up to 10%
		SB-s-20	0.973	15	~100	-	CU & SS @ 20	-
		SB-s-26	0.955	15	~100	-	CU & SS @ 26	-
		SB-s-30	0.969	15	~100	-	CU & SS @ 30	-
		SB-s-32.5	0.975	15	~100	-	CU & SS @ 32.5	-
		SB-s-40	0.972	15	~100	-	CU & SS @ 40	-
	Unsaturated	SB-u-50	0.963	15	26.7	50	CW & MS @ 20 →26 →30 →32.5→ 40	CW to 10%
		SB-u-100	0.964	15	24.9	100		
		SB-u-225	0.964	15	22.9	225		
Subgrade	Saturated	SG-s-00	0.974	15	~100	-	-	CU up to 10%
		SG-s-20	0.976	15	~100	-	CU & SS 0 @ 20	-
		SG-s-26	0.971	15	~100	-	CU & SS @ 26	-
		SG-s-30	0.971	15	~100	-	CU & SS @ 30	-
		SG-s-32.5	0.979	15	~100	-	CU & SS @ 32.5	-
		SG-s-40	0.982	15	~100	-	CU & SS @ 40	-
	Unsaturated	SB-u-50	0.988	15	39.0	50	CW & MS @ 20 →26 →30 →32.5→ 40	CW up to 10%
		SB-u-100	0.967	15	28.8	100		
		SB-u-225	0.964	15	20.9	225		

SB = subballast material, SG = subgrade material,
s = saturated soil conditions, u = unsaturated soils conditions,
CU = consolidated undrained test, SS = single-stage loading,
CW = constant water content test, MS = multi-stage loading.

6.2 MONOTONIC SHEAR TEST RESULTS

The monotonic shear tests were conducted on saturated and unsaturated materials under strain-controlled conditions in order to obtain the stress-strain behaviour, response of the pore water pressure and the stress states where the maximum deviator stress occurs. The strains were limited to 10% due to the full range of the local instrumentation. The saturated samples were sheared under consolidated undrained conditions where the pore air was not present and the pore water was undrained. The unsaturated samples were sheared under constant water content conditions, where the pore air was drained and the pore water was undrained.

The results from the monotonic shear tests are presented in Figure 6-1 and Figure 6-2 for the subballast and subgrade materials, respectively. During saturated soil conditions, where the matric suction was equal to 0 kPa, the subballast and subgrade materials presented linear-elastic-perfectly-plastic behaviour, where the linear elastic behaviour is followed by perfectly plastic behaviour as explained by Potts and Zdravkovic (1999). During unsaturated soil conditions, where the matric suction is greater than 0 kPa, both materials presented linear-elastic-strain-hardening behaviour, where linear elastic behaviour is followed by strain hardening as explained by Potts and Zdravkovic (1999). The most noticeable trend in the stress-strain relationship of the unsaturated subballast material is that the strain hardening and peak deviator stress are preceded by a load-collapse which resulted in a sudden decrease in the deviator stress at constant axial strain. The mode of failure is accompanied by the physical formation of multiple bifurcation and slip planes which resulted in the rupture and collapse of the sample as shown in Figure 6-3 for the subballast material, accompanied by a greater load-collapse. The mode of failure of the subgrade material is observed mainly to be barrelling as depicted in Figure 6-4, accompanied by a lesser load-collapse. The load-collapse is less prominent in the subgrade material with a plasticity index of 9%, as compared to the subballast material with a plasticity index of 3%. It is also evident that the load-collapse is proportional to the matric suction, that is, the higher the matric suction, the higher the magnitude of the collapse in the deviator stress.

The topic of load-collapse has been widely researched mainly under isotropic loading and wetting (or soaking) by numerous researchers including Jennings and Burland (1962), Matyas and Radhakrishna (1968) and Alonso et al. (1987; 1990), amongst others. The test results depicted in Figure 6-1 and Figure 6-2 confirm that load-collapse is indeed a phenomenon related to unsaturated soils. These results are evidence that load-collapse in unsaturated soils can also occur during shearing even if the water content and isotropic stress are constant. Furthermore, it is also evident that the shear strength of unsaturated soils, represented by the deviator stress, is much higher than that of saturated soils. The increase in the shear strength can be attributed to the strain hardening property in the test materials. However, the increase in the shear strength of non-plastic, sandy, unsaturated soils (subballast material in this study)

can induce brittle behaviour where the material suddenly ruptures and collapses followed by significant loss of shear strength, which Wheeler and Sivakumar (1995) termed the post-rupture shear strength.

The relationship between the pore water pressure and axial strain during monotonic shear loading is also presented in Figure 6-1 for the subballast material and in Figure 6-2 for the subgrade material. In the graph, the negative pore water pressure represents the matric suction in the soil samples. A consistent trend is that the pore water pressure for both materials during saturated and unsaturated soil conditions tend to converge and approach stability at large strains. For unsaturated materials, the stability commenced post the load-collapse and peak deviator stress stage. The stability of the pore water pressure indicates the presence of possible critical states, where the change in the pore water pressure remains zero during shearing. There is, however, a prominent difference in the behaviour of the response of the pore water pressure between saturated and unsaturated materials even though the pore water is undrained in both instances. The pore water pressure in saturated materials decreased with increasing monotonic shear loading mainly due to the initially heavily overconsolidated state of the samples. In the case of unsaturated materials, the pore water pressure consistently increased with increasing monotonic shear loading even though the materials were initially heavily overconsolidated. It is therefore important to keep in mind that in unsaturated soils, the presence of the pore air pressure can cause build-up of pore water pressures in an initially heavily overconsolidated soil when loaded at constant water content, as also discovered and explained by Rahardjo et al. (2004) based on triaxial tests on compacted residual soil sheared under constant water content conditions.

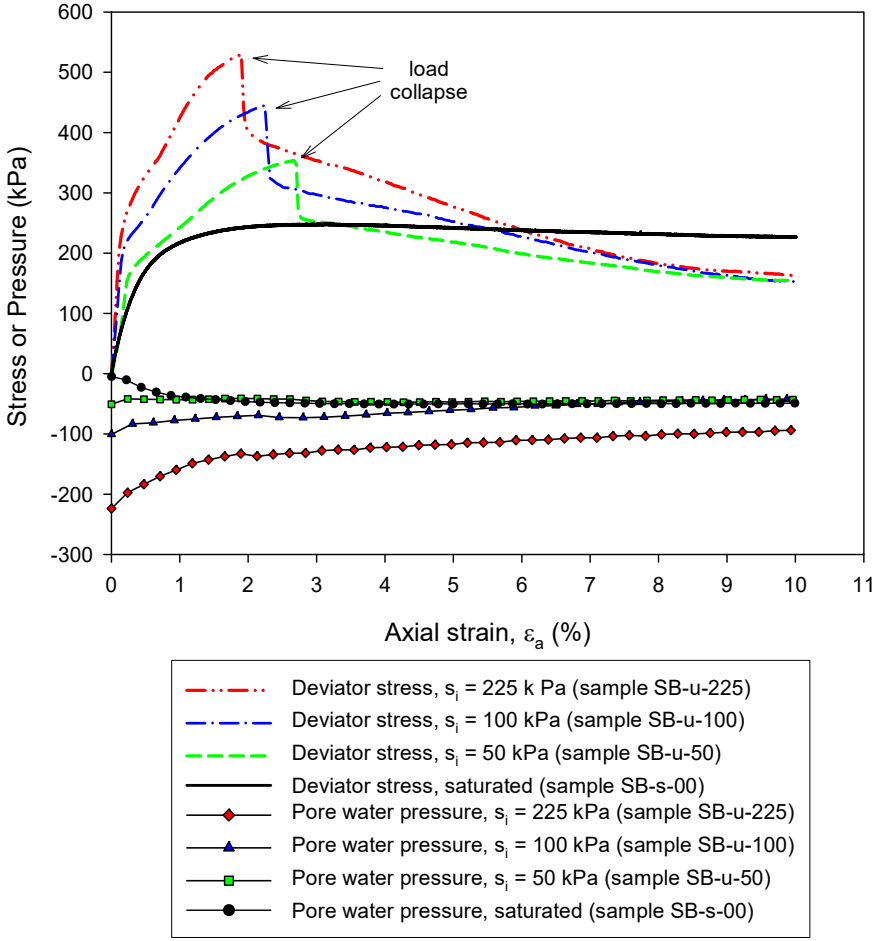

Figure 6-1: Stress vs strain and pore water pressure vs strain relationship of subballast material

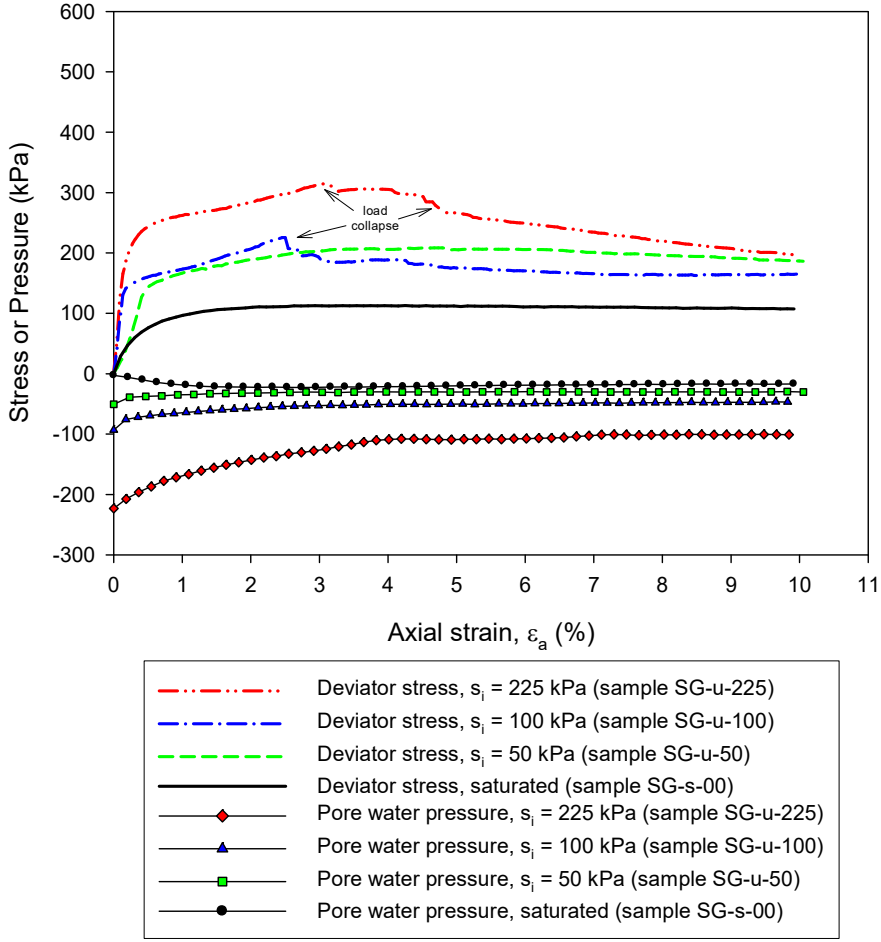

Figure 6-2: Stress vs strain and pore water pressure vs strain relationship of subgrade material

Figure 6-3: Failed sample of subballast material

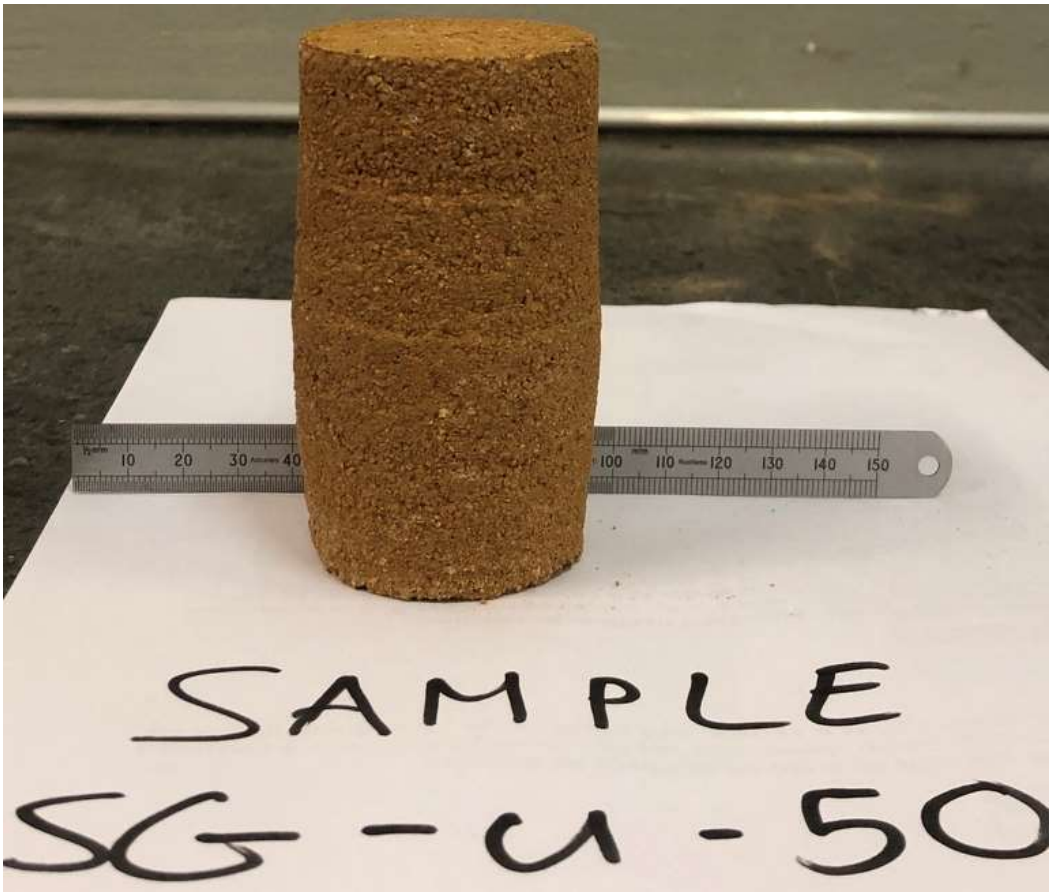

Figure 6-4: Failed sample of subgrade material

6.3 DETERMINATION OF SHEAR STRENGTH

The shear strength of a soil can be defined as the axial load or deviator stress at which failure is expected to occur. The direct link between shear strength and deviator stress is represented by Equation (6-1).

$$\tau = \frac{1}{2}q \tag{6-1}$$

Where:

τ = shear strength,

q = deviator stress.

In this study, the shear strength is represented by the deviator stress in order to investigate the effect of increased axle loading on the stress states. For saturated soils, the effective stress principle as proposed by Terzaghi (1936; 1943) and Terzaghi et al. (1996), is appropriate for analyses of stress paths and stress states. For unsaturated soils, the net stress principle as proposed by Fredlund and Morgensten (1978) is appropriate for analyses of stress paths and stress states. The reason for the use of different stress spaces is that the effective stress principle has been found to be inappropriate for analysis of stress states in unsaturated soils as discussed in Chapter 2. However, the concept of shear strength remains applicable to both saturated and unsaturated soils. The significance of shear strength for unsaturated soils remains equally important as it is for saturated soils, which can be quantified by the deviator stress in both cases, as shown in Equation (6-1).

6.3.1 SHEAR STRENGTH OF SATURATED SOILS BY EFFECTIVE STRESS ANALYSIS

The shear strength of the saturated soils can be determined using the effective stress principle and the critical state line for saturated soils as presented by Atkinson and Bransby (1978). It was calculated using Equations (6-2), (6-3) and (6-4), which represents the failure criterion (or failure envelope) for saturated soils.

$$q = Mp' \tag{6-2}$$

$$M = \frac{6\sin\phi'}{3-\sin\phi'} \tag{6-3}$$

$$\sin\phi' = \frac{\sigma'_1 - \sigma'_3}{\sigma'_1 + \sigma'_3} \tag{6-4}$$

Where:

q = deviator stress ($= \sigma'_1 - \sigma'_3$),

p' = mean effective stress ($= (\sigma'_1 + 2\sigma'_3)/3$),

M = slope of the critical state line for saturated soils,

ϕ' = effective angle of shearing resistance,

σ'_1 = effective major principal stress,

σ'_3 = effective minor principal stress.

The shear strength parameters for the saturated subballast and subgrade materials are shown in Table 6-2. The effective angle of shearing resistance for the subballast and subgrade materials were obtained from the plots in Figure 6-5 and the associated stress paths are shown in Figure 6-6.

Table 6-2: Shear strength parameters of saturated test materials

Shear strength parameter	**Material**	
	Subballast	**Subgrade**
Effective angle of shearing resistance, ϕ' (°)	37.5	30.5
Slope of the critical state line, M	1.50	1.20

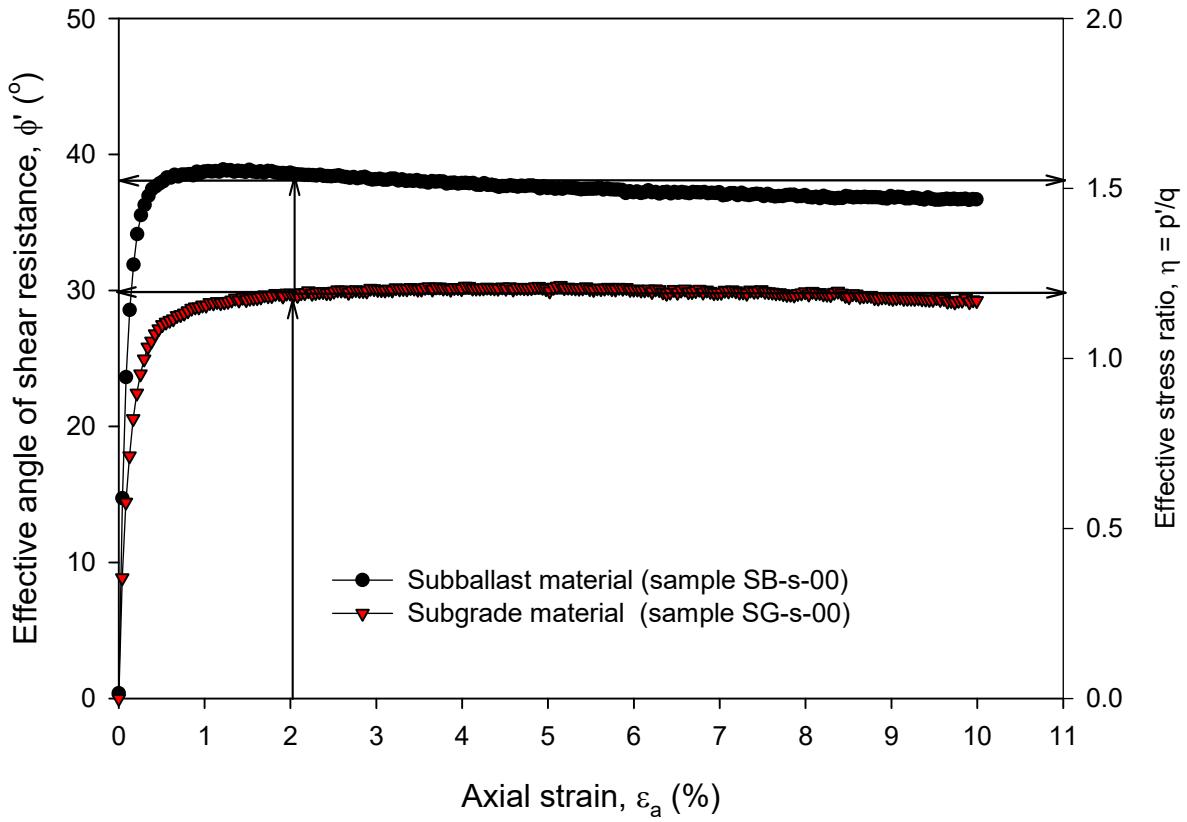

Figure 6-5: Shear strength parameters of subballast and subgrade materials

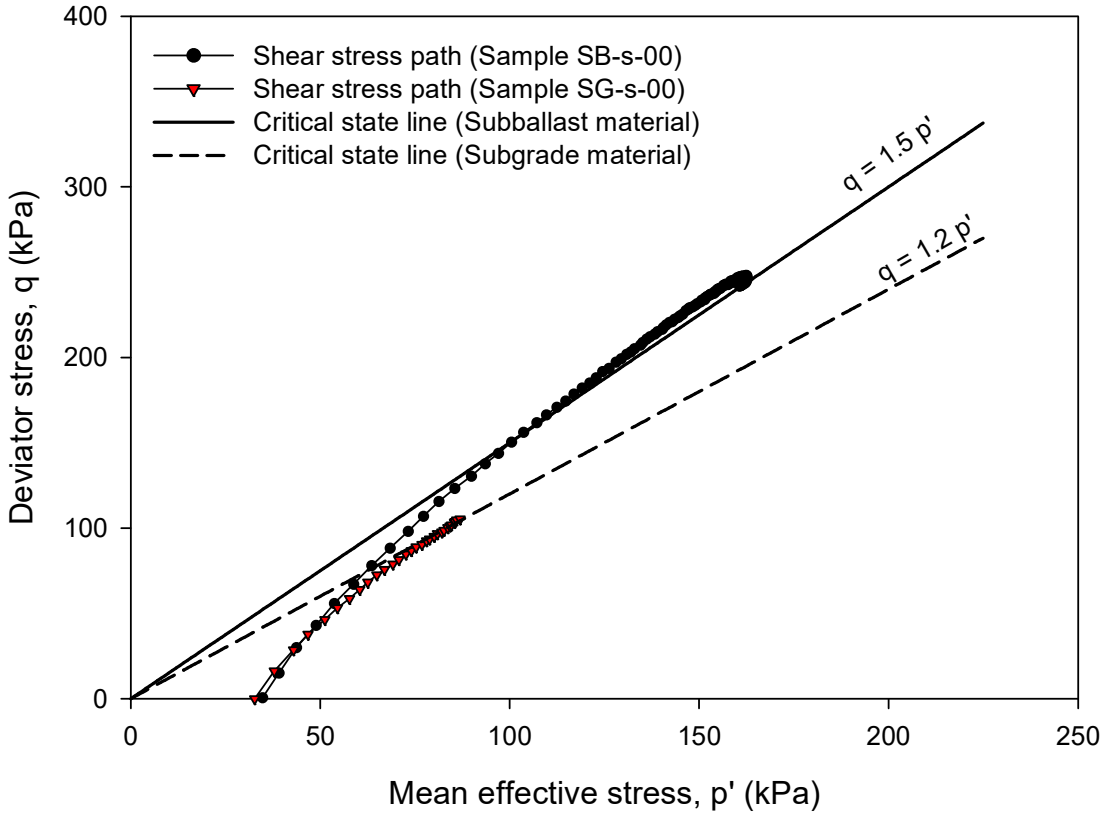

Figure 6-6: Stress paths of subballast and subgrade materials

6.3.2 SHEAR STRENGTH OF UNSATURATED SOILS BY NET STRESS ANALYSIS

The shear strength of the unsaturated soils was determined using the net stress principle as proposed by Fredlund and Morgenstern (1977). The failure criterion (or failure envelope) for the unsaturated soils was based on the critical state model as developed by Alonso et al. (1990) based on Equation (6-5).

$$q = M(s)\bar{p} + \mu(s) \tag{6-5}$$

Where:

q = deviator stress ($= \sigma_1 - \sigma_3$),

$\bar{p}$ = mean net stress ($= p - u_a$),

p = mean total stress ($= (\sigma_1 + 2\sigma_3)/3$),

M(s) = slope of the failure envelope for unsaturated soils,

$\mu(s)$ = intercept term,

σ_1 = total major principal stress,

σ_3 = total minor principal stress,

u_a = pore air pressure.

The equation of the failure envelope for the unsaturated soils in the net stress space, is formulated and obtained by determining the value of the slope of the failure envelope and the intercept term. The value of the slope of the failure envelope for unsaturated soils is assumed to be equal to the slope of the failure

envelope for saturated soils, such that, $M(s) = M$ as proposed by Alonso, et al. (1990). This proposal is also supported by Fredlund et al. (1978), where the slope of the failure envelope in the net stress space is equal to that in the effective stress space, as presented in Figure 6-7 and Figure 6-8. With the value of $M(s)$ known, the value of $\mu(s)$ is determined based on the deviator stress (q) and mean net stress $(\bar{p})$ at failure as represented by Equation (6-5).

In this study, it is assumed that the peak stress states are representative of failure based on the following reasons:

- In their research on the constitutive modelling of unsaturated soils, Wheeler and Sivakumar (1995) stated that it is possible that peak values of deviator stress can be representative of critical states (and subsequently failure) and the deviator stress post peak could be representative of the post-rupture values following the formation of a slip plane.
- In their study on the mechanical behaviour of unsaturated soils, Rahardjo et al. (2004) constructed Mohr circles of the failure envelope based on peak values of the deviator stress in the stress-strain curves.
- Whilst developing a railway foundation design model, Li and Selig (1998a; 1998b) highlighted that the allowable permanent strain of railway materials should be limited to 2%, which is where the peak deviator stress is expected to occur for most engineering soils.

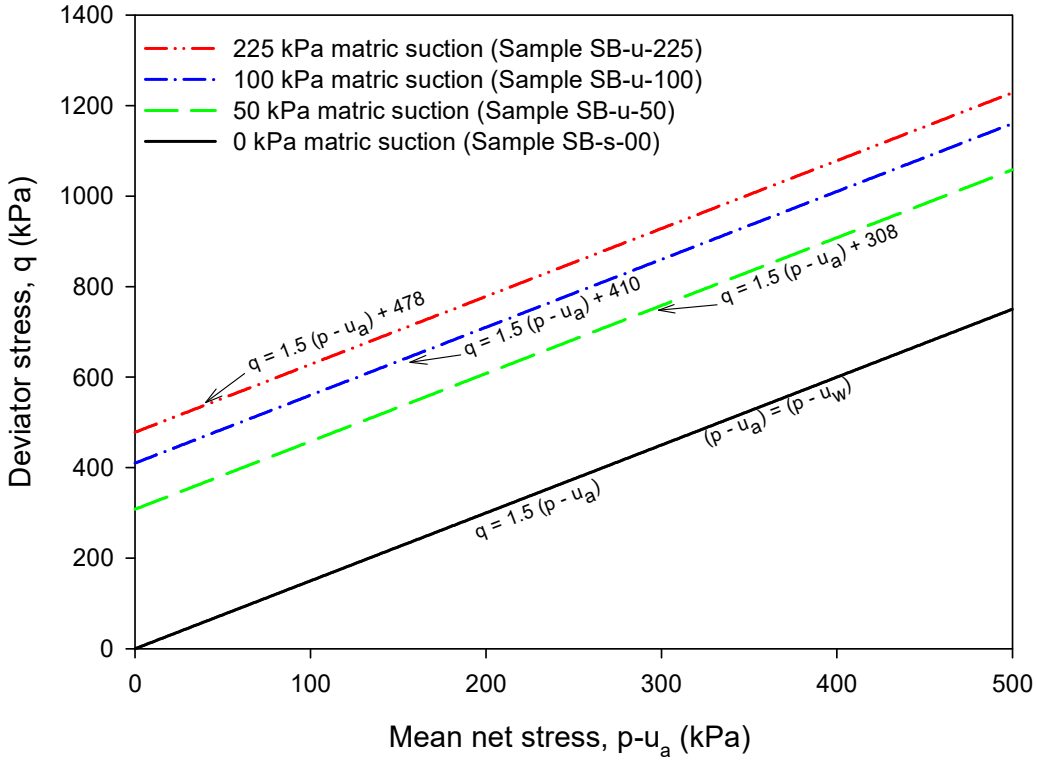

Figure 6-7: Failure envelopes of saturated and unsaturated subballast material

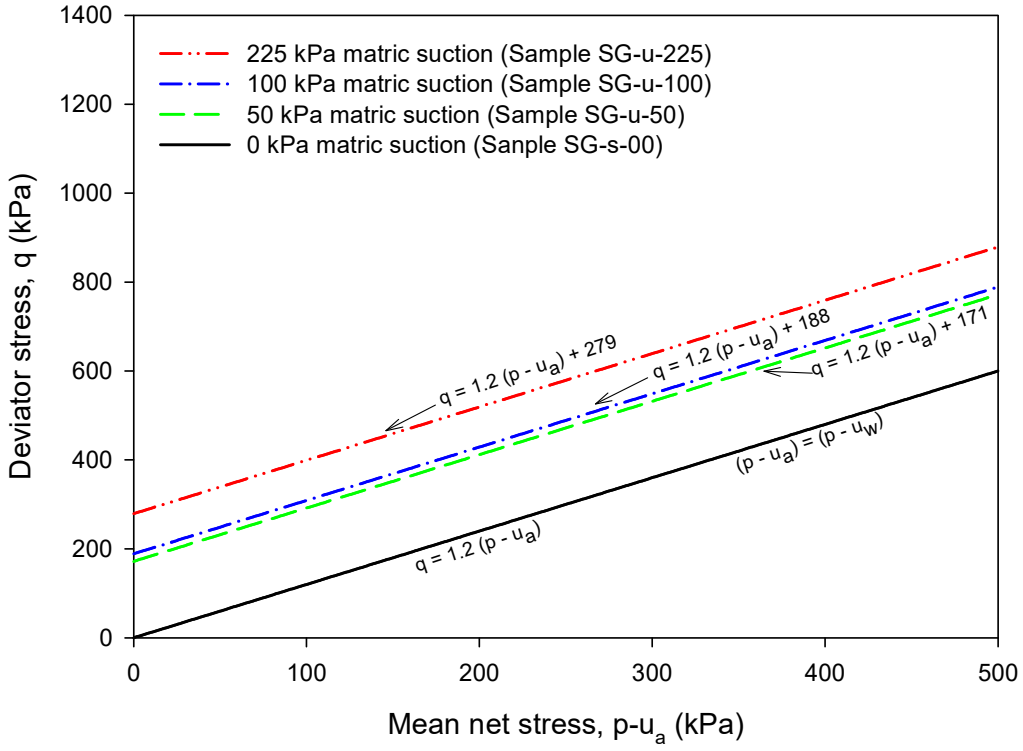

Figure 6-8: Failure envelope of saturated and unsaturated subgrade material

The values of the deviator stress and net mean stress at peak, where failure occurs, together with the values of the intercept term for matric suctions equal to 50, 100 and 225 kPa are presented in Table 6-

3. The equations of the failure envelopes are shown in Table 6-4. The failure envelopes of the subballast and subgrade materials for saturated and unsaturated soil conditions are shown in Figure 6-7 and Figure 6-8, which are used in the analyses of stress states in Section 6.4.1 and Section 6.5.1. As shown in Figure 6-7 and Figure 6-8, during saturated soil conditions, the value of the mean net stress $(p - u_a)$ is equal to the mean effective stress $(p - u_w)$, which is a direct result of the assumption that $M(s) = M$.

Table 6-3: Shear strength parameters of unsaturated test materials

Stress parameter	**Matric suction s (kPa)**	**Material**	
		Subballast	**Subgrade**
Deviator stress at failure, q (kPa)	50	353.4	208.0
	100	454.2	226.6
	225	526.9	316.2
Mean net stress at failure, $\bar{p}$ (kPa)	50	29.8	30.2
	100	29.5	31.5
	225	32.5	30.8
Intercept term, $\mu(s)$ (kPa)	50	308.7	171.8
	100	409.9	188.8
	225	478.1	279.2

Table 6-4: Equations of failure envelope of unsaturated material at various matric suctions

Material	**Matric suction (kPa)**	**Failure envelope equation (kPa)**
Subballast material	50	$q = 1.5\,\bar{p} + 308$
	100	$q = 1.5\,\bar{p} + 410$
	225	$q = 1.5\,\bar{p} + 478$
Subgrade material	50	$q = 1.2\,\bar{p} + 171$
	100	$q = 1.2\,\bar{p} + 188$
	225	$q = 1.2\,\bar{p} + 279$

The relationship between the matric suction and the intercept term of the failure envelopes (from Figure 6-7 and Figure 6-8) of the subballast and subgrade materials is shown in Figure 6-9. It is evident that the increase in the deviator stress of unsaturated soils is related to an increase in the intercept term. The intercept term can be interpreted as being similar to the cohesion term. The relationship between the matric suction and intercept term is logarithmic with a near perfect correlation associated with a coefficient of determination of 0.99 for the subballast material and 0.96 for the subgrade material. This implies that very low matric suctions (less than 50 kPa) are required to mobilise the intercept term in

the test materials. This logarithmic relationship is not unique and similar non-linear relationships between the matric suction and the intercept term or total cohesion[1] has been reported by Escario and Saez (1986) and Fredlund et al. (1987). The value of the graphs depicted in Figure 6-9 is that the increase of the shear strength as a result of unsaturated soil conditions is illustrated, which is one of the research questions of this study.

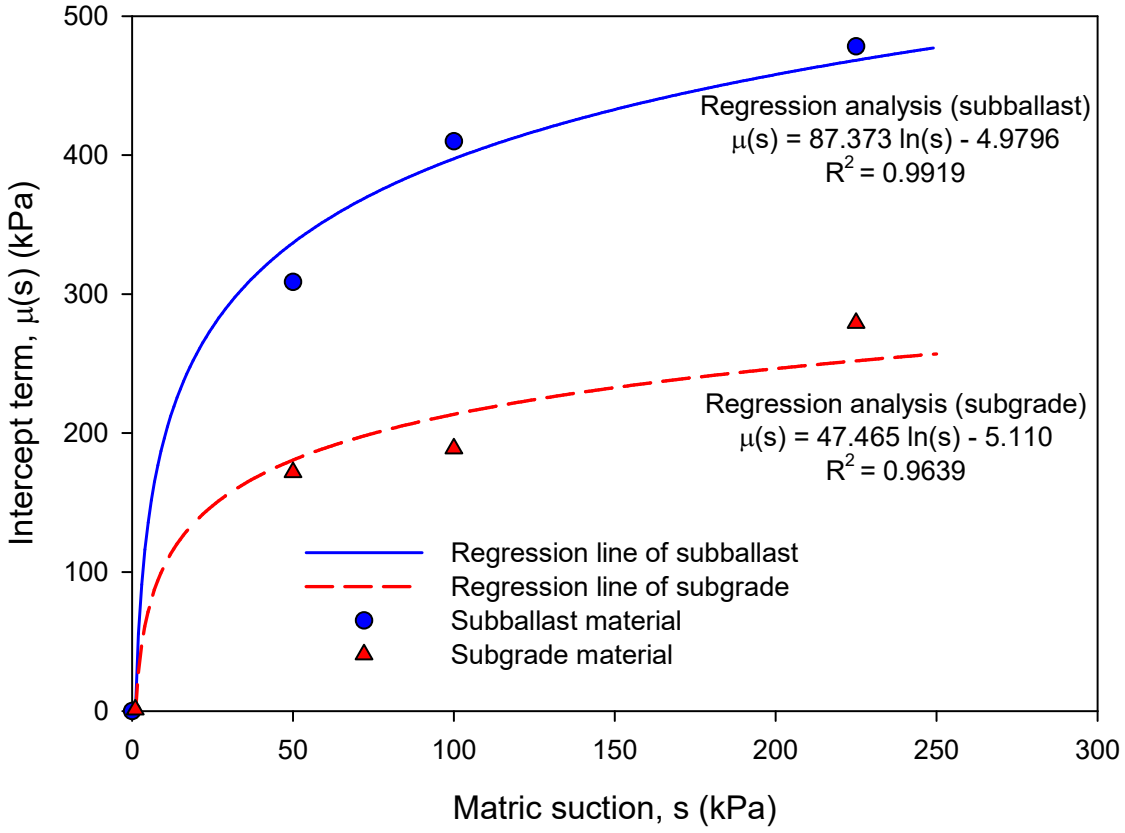

Figure 6-9: Relationship between matric suction and intercept term of failure envelope

6.4 THE EFFECTS OF INCREASED AXLE LOADING ON SATURATED SOILS DURING CYCLIC LOADING

The test results on the effect of increased axle loading on saturated railway foundation materials are presented in this section. The findings of the effect of increased axle loading are shown by investigating the trends and behaviour of the stress states, resilient modulus, strains and pore water pressure during cyclic loading at the various axle loadings.

[1] Total cohesion has been used in the extended Mohr-Coulomb failure envelope model by Fredlund et al. (1987)

6.4.1 STRESS STATES

The effect of increased axle loading on the stress state of saturated subballast and subgrade materials during cyclic loading is depicted in Figure 6-10 and Figure 6-11, respectively. Each point in the graphs represents the maximum deviator stress per load cycle with the corresponding mean effective stress. The critical state lines or failure envelopes determined in Section 6.3 are plotted in Figure 6-10 and Figure 6-11 for the subballast and subgrade materials, respectively. It is evident that for all axle loading cases and both materials, the initial stress states are in dilation, moving in the righthand direction, mainly due to the initially heavily overconsolidated state.

In the samples where the initial stress states are above the critical state line, the behaviour of the soil resulted in a *double-phase transition*, from dilation to contraction and then softening. The double-phase transition occurs in the subballast material at cyclic loading of 40 tonnes per axle and in the subgrade material at cyclic loading of 30, 32.5 and 40 tonnes per axle.

In the samples where the initial stress states plot on the critical state line, the behaviour of the soil resulted in a *single-phase transition*, from dilation to contraction. The single-phase transition occurs in the subballast material at cyclic loading of 30 and 32.5 tonnes per axle and in the subgrade material at cyclic loading of 26 and 30 tonnes per axle.

In the samples where initial and final stress states are below the critical state line, the behaviour of the soil resulted in a *no-phase transition* and remains in the initial state of dilation. The no-phase transition occurs in the subballast material at cyclic loading of 20 and 26 tonnes per axle and in the subgrade material at cyclic loading of 20 tonnes per axle.

Luong (1980a, 1980b) called the line where various phase transition in soil behaviour occurs the characteristic state ratio line. Wood (1990) argued that based on the soil-dilatancy theory, the characteristic state ratio line should be equivalent to the critical state line. The results presented in Figure 6-10 and Figure 6-11 are to some extent in line with the work by Wood (1990) and Luong (1980a, 1980b).

Further inspection of the stress states presented in Figure 6-10 and Figure 6-11, together with the permanent strains in Figure 5-14 in Chapter 5, indicates that samples with a double-phase transition in soil behaviour presented exponential permanent strains in the form of cyclic mobility. Samples with a single-phase transition in soil behaviour presented a combination of linear and exponential permanent strains. Lastly, samples with no-phase transition in soil behaviour presented linear permanent strains in the form of shakedown. It can therefore be said that increased axle loading on railway foundation

materials causes failure in materials which exhibit a double-phase transition in soil behaviour and such loading conditions on such materials should be avoided for prevention of excessive differential settlement during operation in a railway track. It is therefore reasonable to recommend that the use of foundation materials which exhibit a double-phase transition in soil behaviour should be avoided in a railway foundation. Lastly, the highest axle loading where a no-phase transition in soil behaviour occurs and the behaviour remains in dilation, should be taken as the maximum axle load.

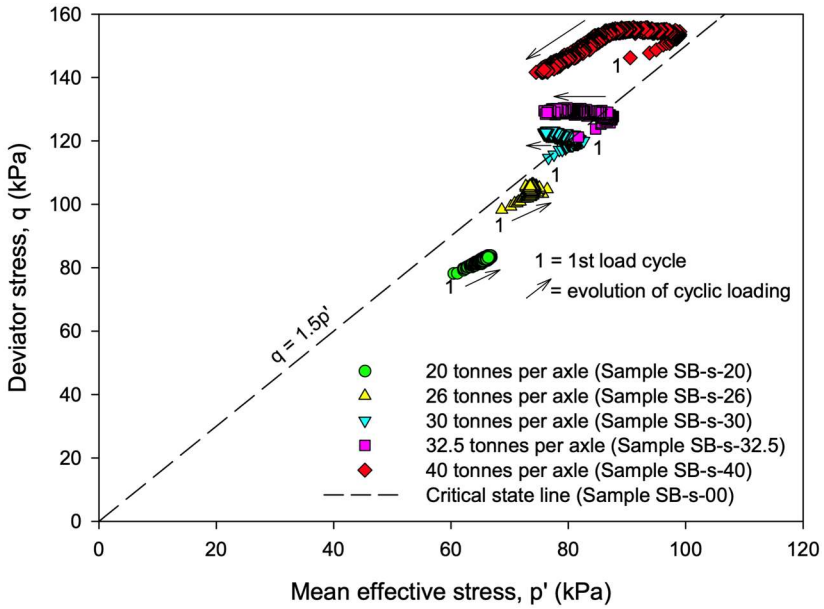

Figure 6-10: Effect of increased axle loading on the stress states of saturated subballast material

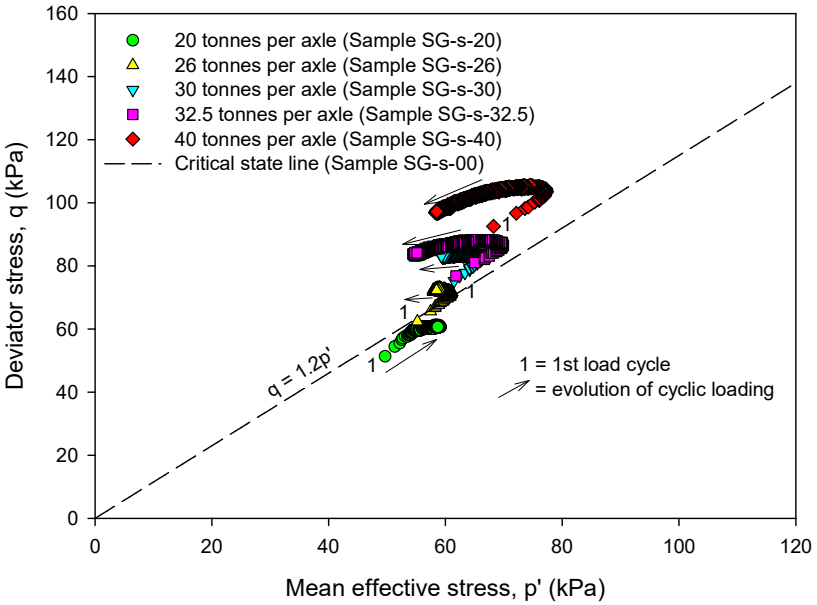

Figure 6-11: Effect of increased axle loading on the stress states of saturated subgrade material

6.4.2 RESILIENT MODULUS

The effect of increased axle loading on the resilient modulus of saturated subballast and subgrade materials is depicted in Figure 6-12. A consistent trend which is evident is that cyclic loading at increased axle loading resulted in a decreased resilient modulus for the subballast and subgrade materials. The resilient modulus during cyclic loading of 20 tonnes per axle is greater than that at 40 tonnes per axle, indicative of excessive deformations and deterioration of resilience.

Furthermore, increased axle loading resulted in a significant decrease in the resilient modulus as evident at cyclic loading of 40 tonnes per axle, where a turning point in the resilient modulus is present, which means the cyclic shear stress threshold is exceeded as stated by Mamou et al. (2017). Based on the trend in the resilient modulus depicted in Figure 6-12 and the behaviour of the stress states in Figure 6-10 and Figure 6-11, it can be said that increased axle loading beyond the shear strength can result in a rapid decrease in the resilient modulus which inevitably might lead to railway foundation failure.

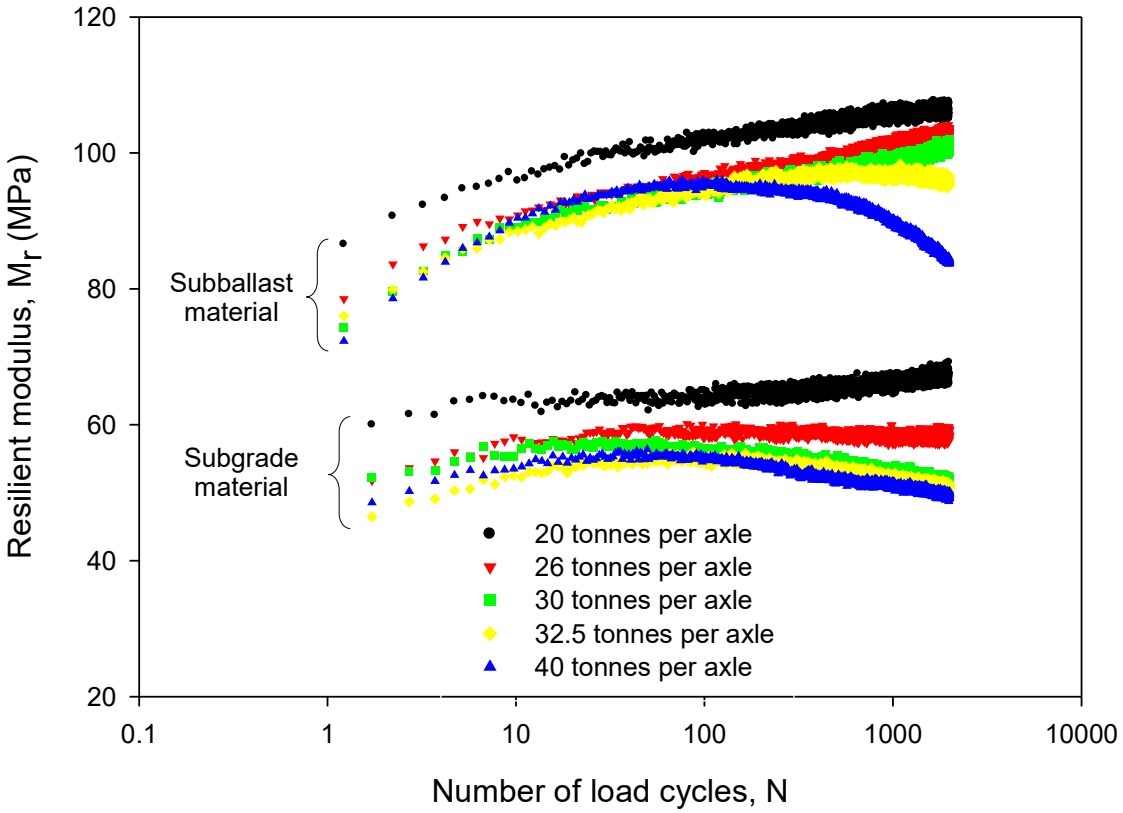

Figure 6-12: Effect of increased axle loading on resilient modulus of saturated subballast and subgrade materials

6.4.3 RESILIENT AND PERMANENT STRAINS

The effect of increased axle loading on the strains of saturated subballast and subgrade materials during cyclic loading is depicted in Figure 6-13 and Figure 6-14. The strains are inclusive of the resilient strain (or elastic strains) and the permanent strains (or plastic strains). It is evident that increased axle loading resulted in an increase in both the resilient and permanent strains. However, it is noticeable that a significant increase in the rate of the permanent strain resulted in a decrease in the rate of the resilient strain with increased axle loading. This trend is prominent in the subballast material from 32.5 to 40 tonnes and in the subgrade material from 30 to 32.5 tonnes per axle. The opposite is also true, that is, an increase in the rate of the resilient strain resulted in a decrease in the rate of the permanent strain, which is evident in the subgrade material between 30 and 32.5 tonnes per axle.

It can be concluded that increased axle loading in saturated railway material could result in increased permanent strains and reduced resilient strains. During plastic behaviour, the rate of the resilient strain is inversely related to the rate of the permanent strain. These results confirm the philosophy by Li and Selig (1996) that excessive cumulative permanent deformations in a railway foundation is indicative of failure which is associated with decreased resilient deformations. The same sentiments are maintained by Gräbe and Clayton (2014), that the response of a well-designed flexible pavement will be largely resilient with most of the deformations being recoverable.

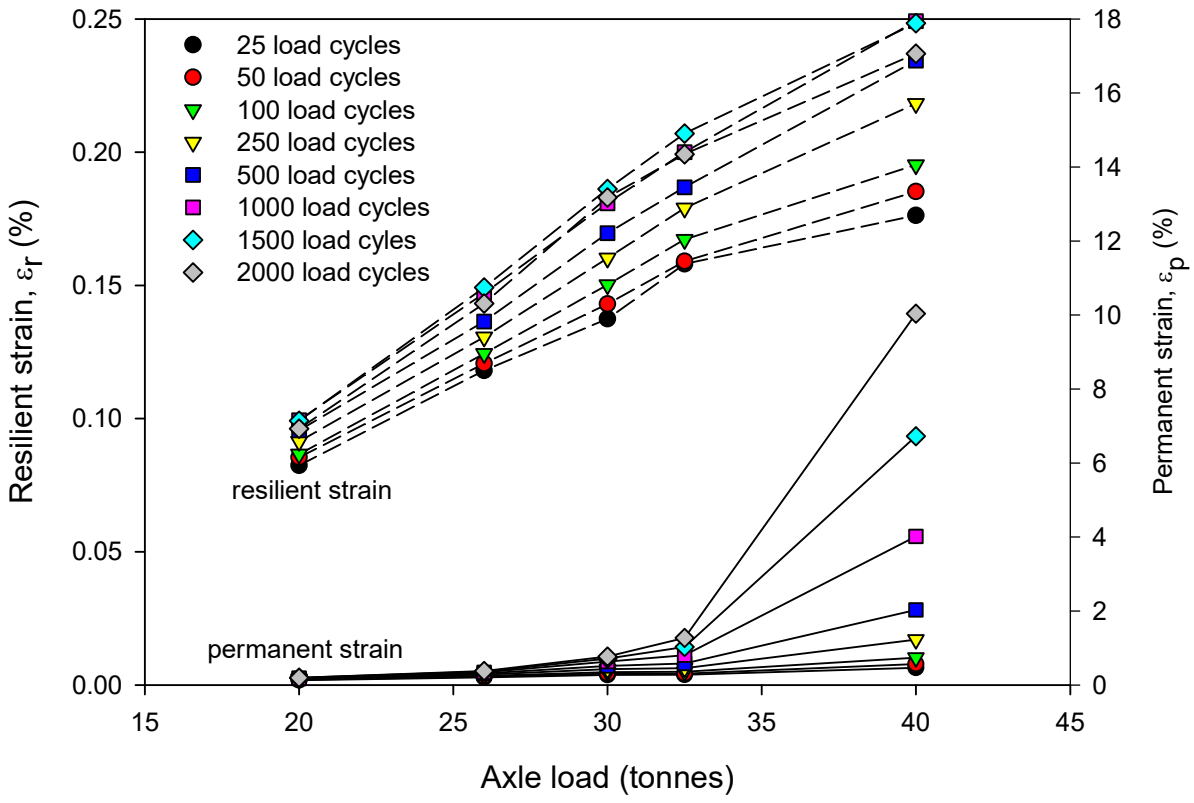

Figure 6-13: Effect of increased axle loading on strains of saturated subballast material

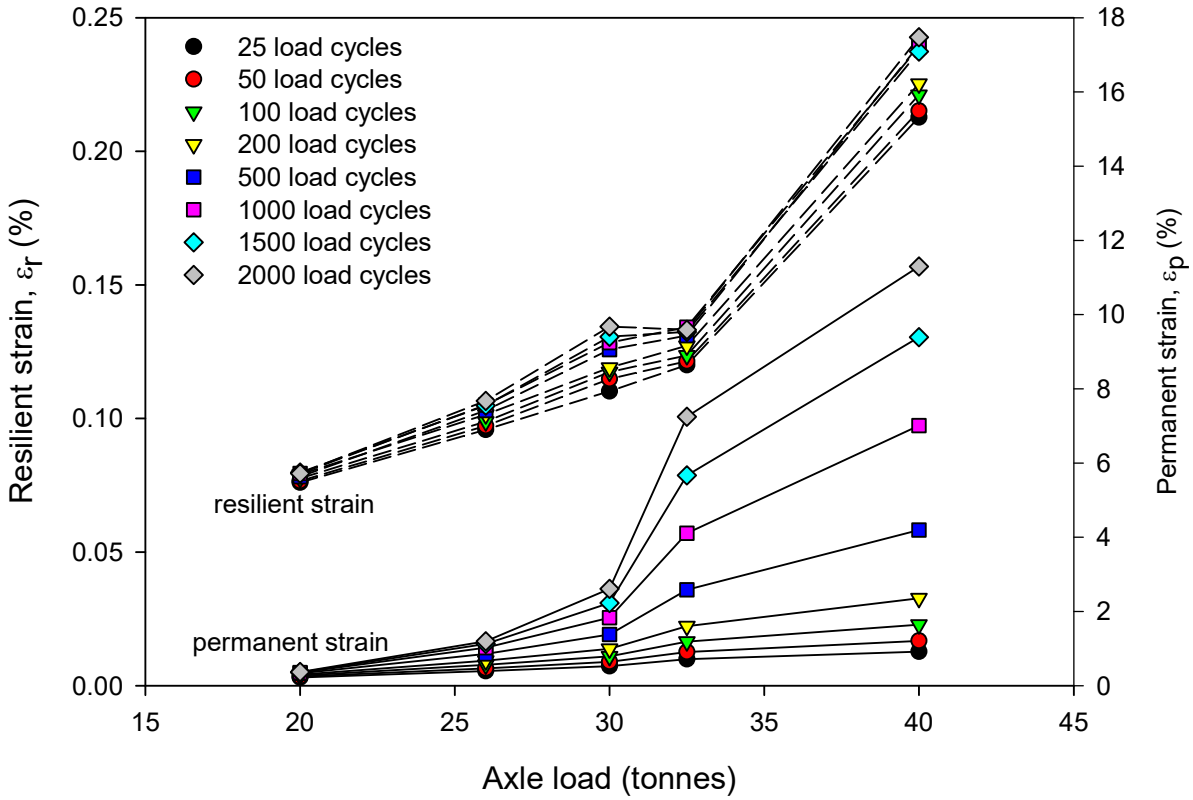

Figure 6-14: Effect of increased axle loading on strains of saturated subgrade material

6.4.4 PORE WATER PRESSURE

The effect of increased axle loading on the pore water pressure of saturated subballast and subgrade materials during cyclic loading is shown in Figure 6-15 and Figure 6-16. The pore water pressures are represented by the excess pore water pressure. The excess pore water pressure is the pore water pressure in the soil in excess of the static pore water pressure. The results give an indication of the increased axle loading and number of load cycles which will result in a phase-transition in behaviour, from negative to positive excess pore water pressure. The excess pore water pressure in the subballast and subgrade materials are negative up until 500 load cycles are reached and thereafter positive excess pore water pressure start to develop.

From Figure 6-15 and Figure 6-16 for 2000 load cycles, the excess pore water pressures in the subballast material are negative until an axle load of 32.5 tonnes per axle is reached while the excess pore water pressures in the subgrade material are negative until an axle load of 30 tonnes per axle is reached. In practical terms, a build-up of positive excess pore water pressures can be associated with the onset of failure. With that in mind, the results confirm that excess pore water pressure can be used to predict the phase transition from negative to positive excess pore water pressure which can be related to the phase

transition in behaviour as represented by the stress states, permanent and resilient strains and the resilient modulus.

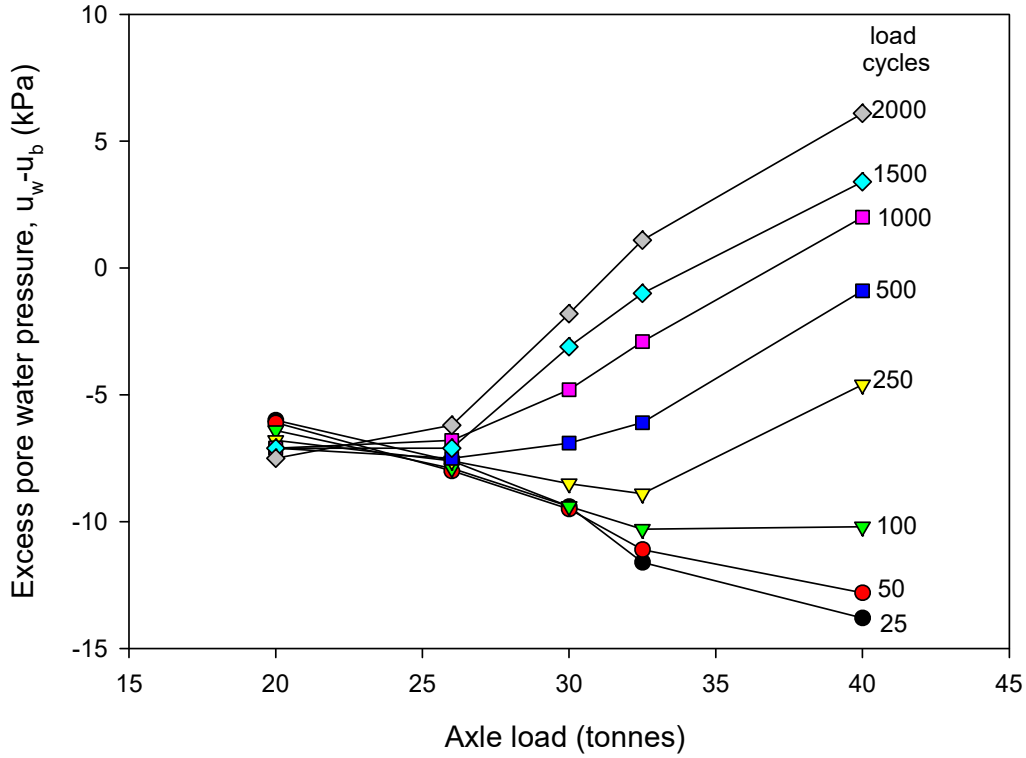

Figure 6-15: Effect of increased axle loading on pore water pressures of saturated subballast material

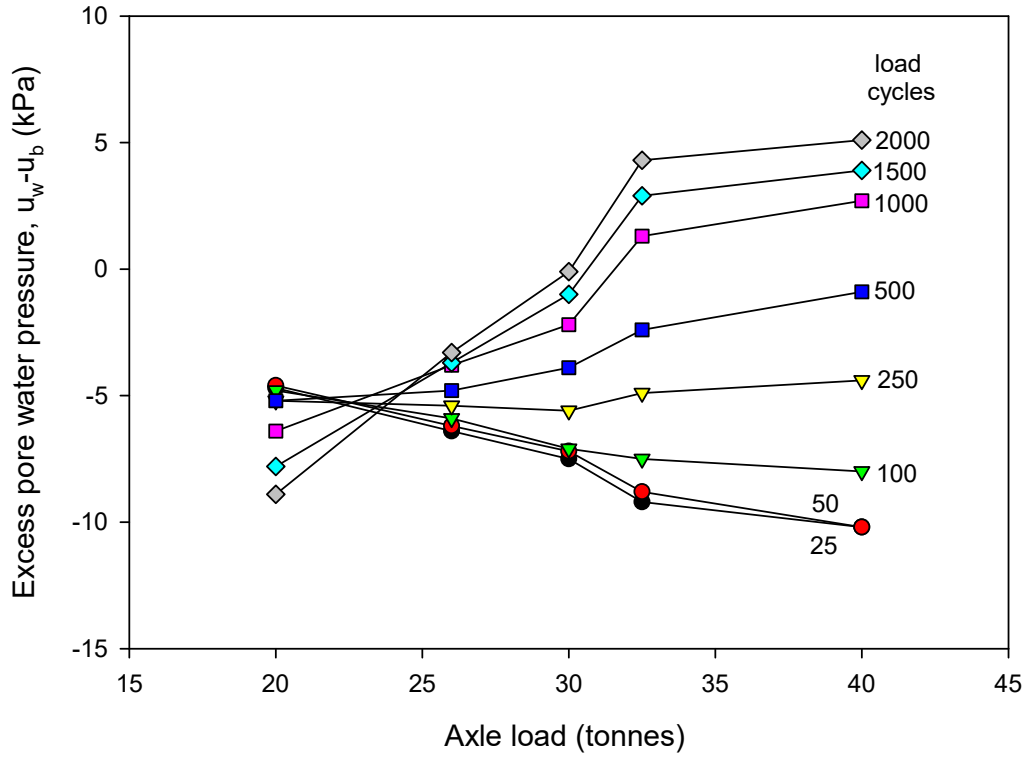

Figure 6-16: Effect of increased axle loading on pore water pressures of saturated subgrade material

6.5 THE EFFECTS OF INCREASED AXLE LOADING ON UNSATURATED SOILS DURING CYCLIC LOADING

The test results on the effect of increased axle loading on unsaturated railway foundation material are presented in this section. Similar to the saturated soil conditions, the findings are shown by investigating the trends and behaviour of the stress states, resilient modulus, strains and matric suction during cyclic loading.

6.5.1 STRESS STATES

The effect of increased axle loading on the stress state of unsaturated subballast and subgrade materials during cyclic loading is shown in Figure 6-17 and Figure 6-18, respectively. The stress states are expressed in terms of net stresses as previously discussed in Section 6.3. Each point in the graphs represents the maximum deviator stress per load cycle with the corresponding mean net stress. It should be noted that during constant water content conditions, the total mean stress (p) and the pore air pressure (p_a) remain constant, hence the overlapping of the stress state points in the graphs, as the mean net stress also remains constant. The failure envelopes plotted in the figures are determined based on the peak stress states, which are assumed to be representative of failure. Similar to saturated soil conditions, elastic behaviour is expected below the failure envelope and plastic behaviour is expected above or along the failure envelope.

It is evident that unsaturated samples with higher matric suction have a higher shear strength. The shear strength is developed by the upwards movement of the failure envelope away from the shear stresses induced by the increased axle loading. In all increased axle loading cases, the stress states in the soil are found to be well below the failure envelope line and the resultant strains are predominantly elastic. It is also evident that the increased shear strength induced by the unsaturated soil conditions and the initial matric suction of 50, 100 and 225 kPa, enable both the subballast and subgrade materials to withstand increased axle loading of up to 40 tonnes per axle, when loaded with a total of 2000 load cycles.

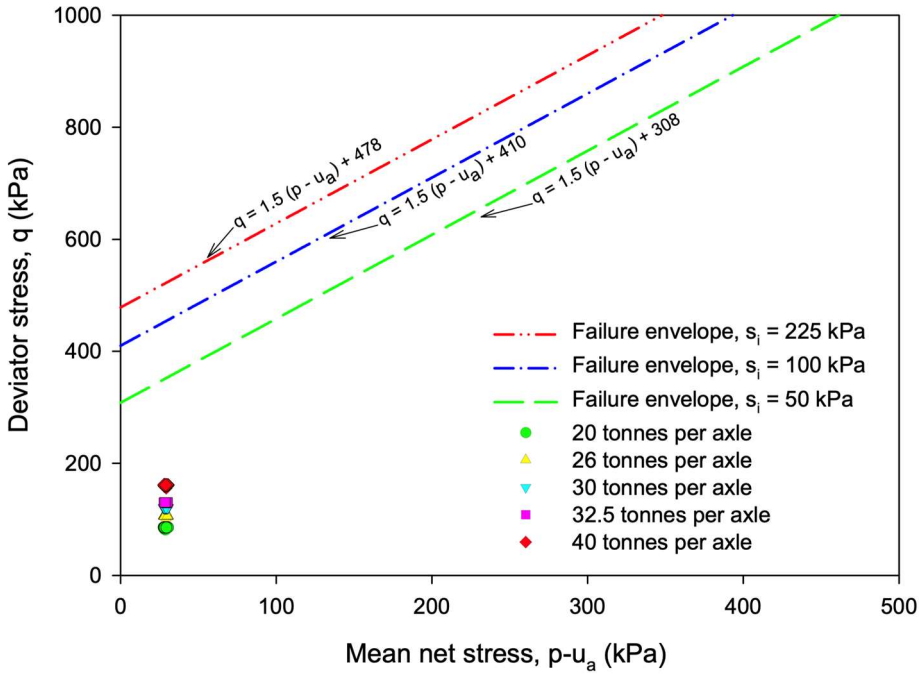

Figure 6-17: Effect of increased axle loading on stress states of unsaturated subballast material

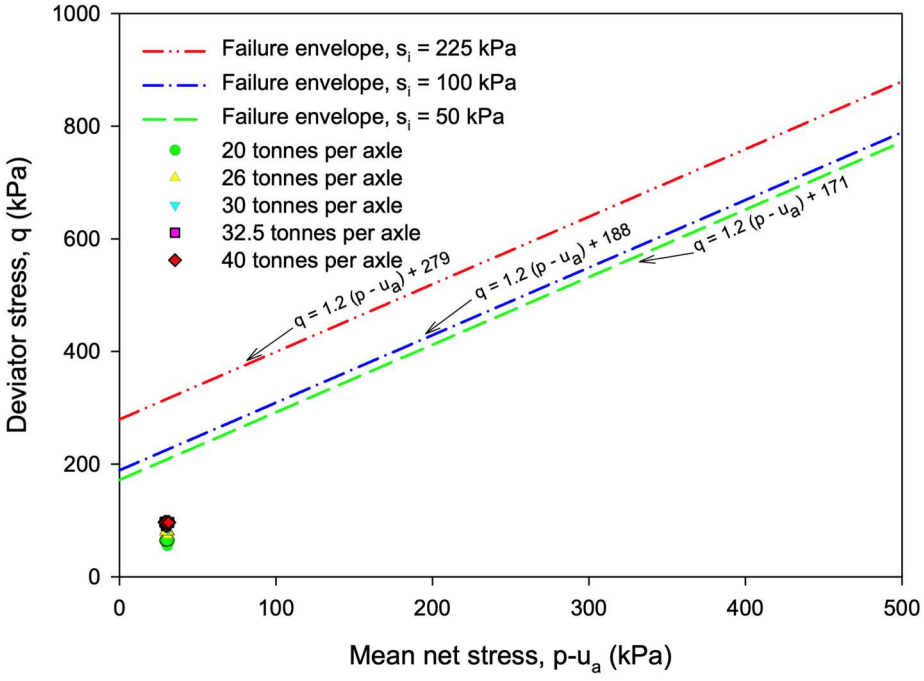

Figure 6-18: Effect of increased axle loading on stress states of unsaturated subgrade material

6.5.2 RESILIENT MODULUS

The relationship between the matric suction and resilient modulus is shown in Figure 6-19. It is shown for the subballast and subgrade materials with initial matric suction of 50, 100 and 225 kPa. The pore water pressure in the saturated materials is linked to the matric suction as negative excess pore water pressure and it is included as a reference point for comparison.

Based on the results depicted in Figure 6-19, a decrease in the matric suction is directly related to a decrease in the resilient modulus. However, the decrease in resilient modulus is more rapid during saturated soil conditions as compared to unsaturated soil conditions. The rate of the decrease is indicated by the arrows showing the direction of change of the resilient modulus relative to the matric suction. The direction of the arrows is near vertical for saturated soil conditions, indicative of a rapid decrease in the resilient modulus. Furthermore, a significant decrease in the resilient modulus of saturated materials is caused by a small decrease in the matric suction, when compared to the unsaturated materials. Based on these results, it can therefore be stated that a rapid rate of track deterioration should be expected during saturated soil conditions and a slower rate of track deterioration should be expected during unsaturated soil conditions. These results highlight the importance of adequate drainage in a railway foundation, as emphasised by Selig and Waters (1994) and Brown (1996).

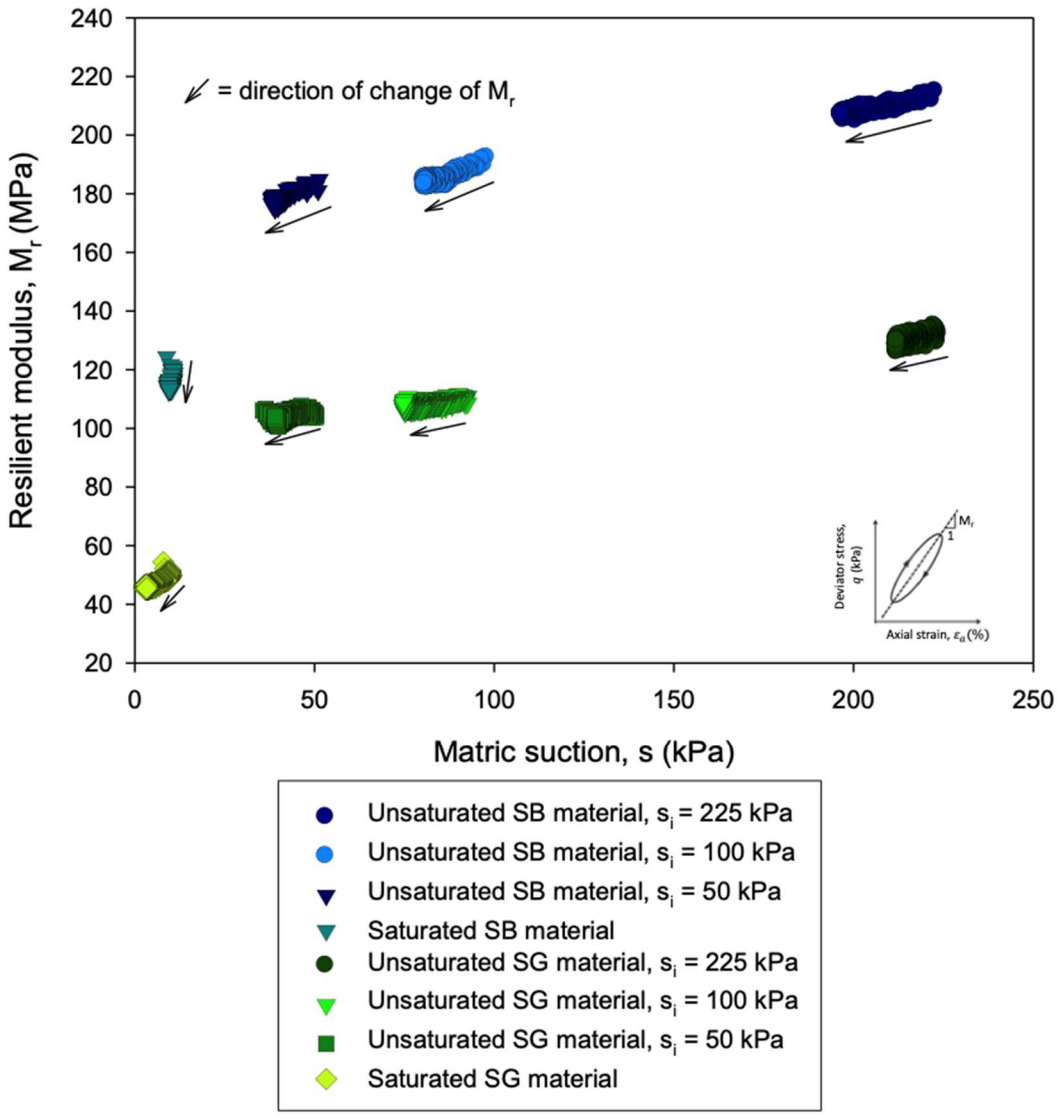

Figure 6-19: Relationship between matric suction and resilient modulus

6.5.3 RESILIENT AND PERMANENT STRAINS

The effect of increased axle loading on the resilient and permanent strains of unsaturated subballast and subgrade materials during cyclic loading is shown in Figure 6-20 and Figure 6-21. The figures captioned with (a) represent 25 load cycles and those captioned with (b) represent 2000 load cycles. The trend in the resilient and permanent strains of the unsaturated subballast and subgrade materials depicted in these figures is consistent for all three matric suction values. The resilient strains continue to increase with increased axle loading for all axle loading cases. However, the permanent strain initially decreases with increased axle loading. This is an interesting phenomenon which can be attributed to the unsaturated state of the soil matrix with the presence of pore air in the voids and the strain hardening properties. It is probable that during the initial cyclic loading at a low axle load of 20 tonnes per axle, the permanent strains are high due to the reorientation and settlement of the soil particles within the air pockets in the soil matrix. The decrease in the permanent strain with increased axle loading can be attributed to the strain hardening properties observed in the monotonic test results presented in Section 6.2. However, a further increase in the axle loading resulted in reaching the critical axle load of 32.5 tonnes per axle, where the permanent strains started to increase, albeit that the permanent strains are well below the 2 % allowable threshold.

This feature of soil behaviour is probably unique to unsaturated soils as the trend is present in all the matric suction cases. The strain hardening property of unsaturated soils has shown to be beneficial during cyclic loading at increased axle loading. However, for the test materials in this study, the benefit of the hardening properties is limited to the maximum stress level of 32.5 tonnes per axle, which Li et al. (2016) referred to as the critical level of repeated deviator stress. These results highlight the fact that similar to the ballast layer, consolidation after construction in the subballast and subgrade can also occur.

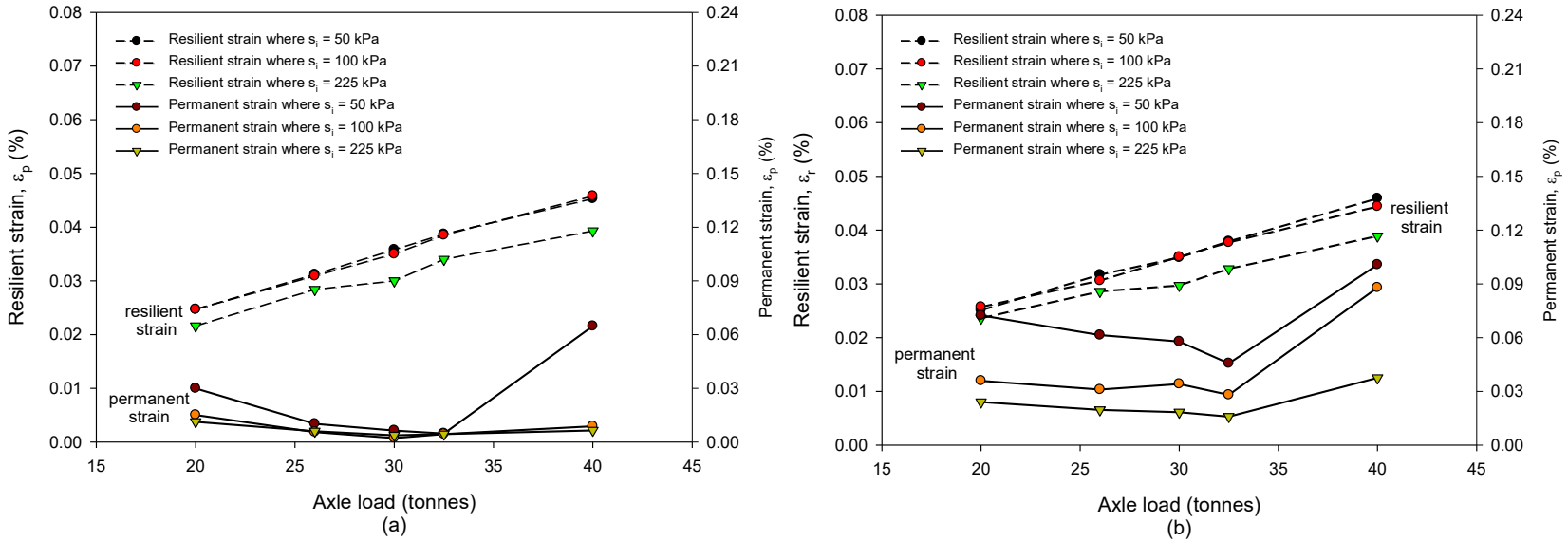

Figure 6-20: Effect of increased axle loading on strains of unsaturated subballast material after (a) 25 initial load cycles and (b) 2000 final load cycles

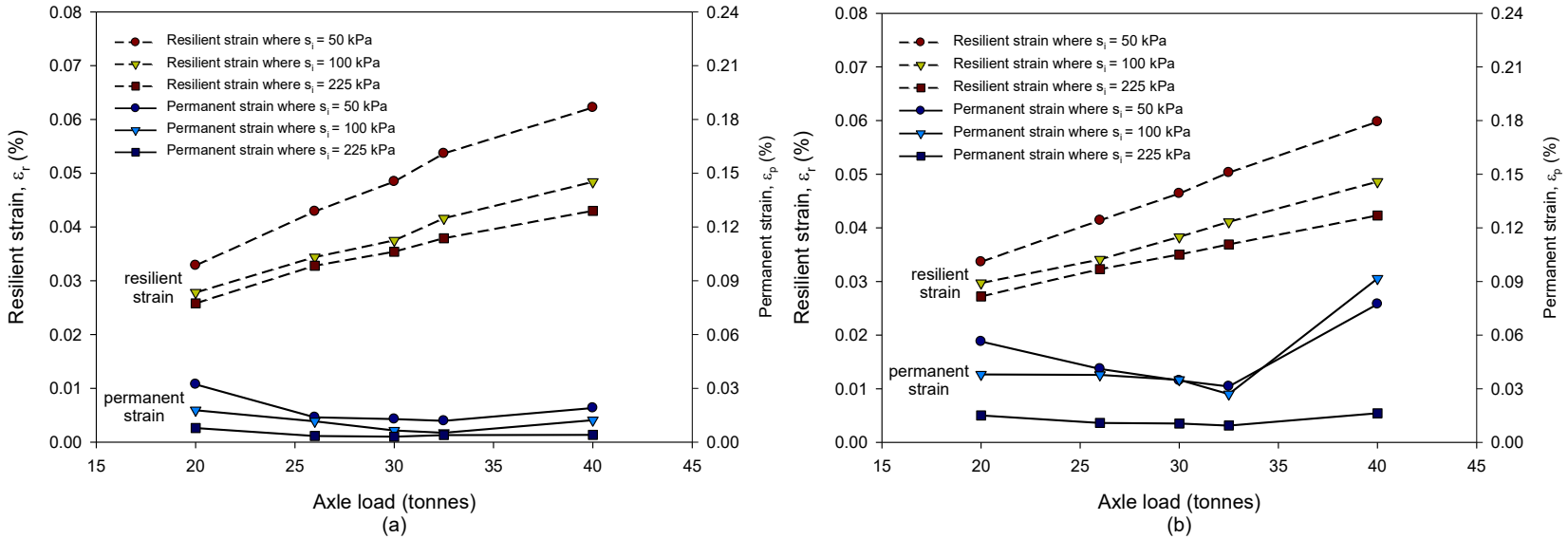

Figure 6-21: Effect of increased axle loading on strains of unsaturated subgrade material after (a) 25 initial load cycles and (b) 2000 final load cycles

6.5.4 MATRIC SUCTION

The effect of increased axle loading on the matric suction of unsaturated subballast and subgrade materials during cyclic loading is shown in Figure 6-22 and Figure 6-23, respectively from 25 and 2000 load cycles. The common trend is that the matric suction tends to decrease with increased axle loading. The decrease in the matric suction is higher in the subballast material due to the higher applied cyclic loading, both in terms of stress levels and number of loading cycles. It is probable that the decrease in the matric suction is caused mainly by the presence of the more compressible pore air and the increase in the pore water pressure.

The decrease of matric suction is higher when the materials are loaded with higher cyclic loading. The increase in matric suction, due to the development of negative pore water pressure is not present, even though the unsaturated materials are initially heavily overconsolidated, which is contrary to the behaviour of saturated materials. The test results highlight the fact that matric suction is not a fixed soil parameter, even under constant water content, but rather a dynamic soil parameter which can change according to the applied loading.

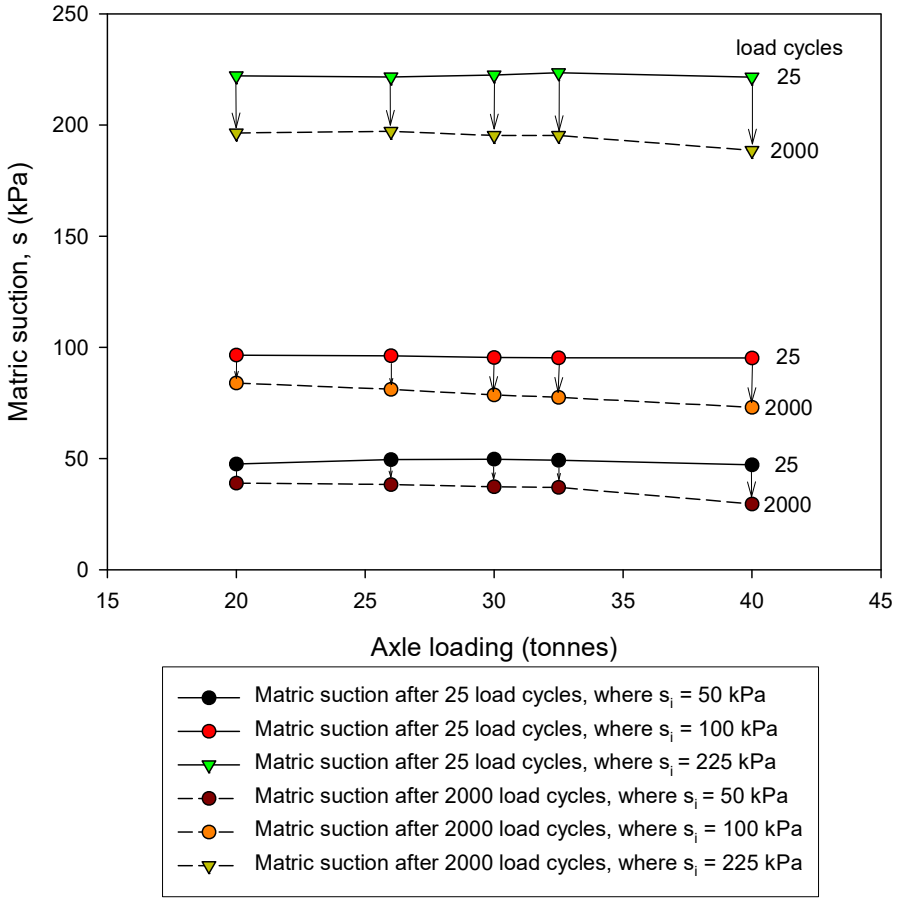

Figure 6-22: Effect of increased axle loading on matric suction of unsaturated subballast material

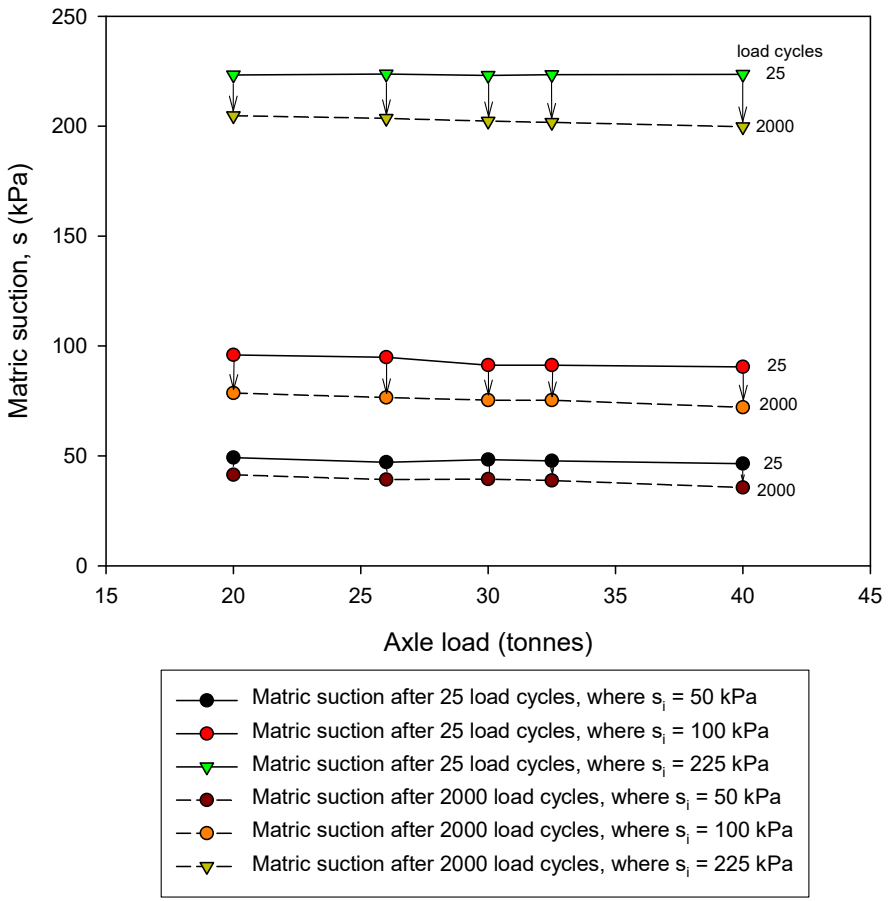

Figure 6-23: Effect of increased axle loading on matric suction of unsaturated subgrade material

6.6 THE SIGNIFICANCE OF THE RESEARCH

The significance of this research is that it highlights the engineering behaviour of saturated and unsaturated soils when subjected to monotonic and cyclic loading. Unsaturated soils can be expected to have higher shear strength relative to the same soil with saturated conditions as seen during monotonic loading. The increase in the shear strength is found to be mainly due to the strain hardening property induced by the unsaturated soil conditions, which resulted in the upward shift of the failure envelope in the net stress space. However, unsaturated soils can present load-collapse behaviour during shearing which may result in physical rupture and the formation of slip planes followed by excessive loss in shear strength.

The engineering behaviour of saturated and unsaturated soils during monotonic and cyclic loading was found to be different. The first difference is in the stress strain relationship and the pore water pressure response during monotonic loading. The second difference is in the stress state variables, which is effective stress for saturated soils and net stress for unsaturated soils. The third difference is in the shear strength, which is higher in unsaturated soils than in saturated soils. The fourth difference is in the resilient modulus, which deteriorates much faster in saturated soils than in unsaturated soils. The fifth difference is the permanent strains, which are directly related to increased axle loading in saturated soils and to some extent inversely related to increased loading in unsaturated soils.

The significance of this research is that unsaturated soil conditions are definitely beneficial for increased axle loading. Furthermore, it should be appreciated that the behaviour of unsaturated soils is different, slightly more complex and counterintuitive to saturated soils. With that in mind, a fundamental understanding of unsaturated soil behaviour will result in cost effective designs that harness the benefits of unsaturated soil conditions.

CHAPTER 7
CONCLUSIONS AND RECOMMENDATIONS

7.1 CONCLUSIONS

A good understanding of the engineering behaviour of railway foundation materials when subjected to increased axle loading is essential for the sustainability of the railway network and the economy of a country as a whole. The aim of this study is to investigate the effect of increased axle loading on saturated and unsaturated railway foundation materials for heavy haulage of freight, by so doing closing the lacuna in the knowledge around the topic. To meet this aim, a scientific research approach was undertaken, considering and addressing various issues identified as relevant within the scope of the study. This chapter is therefore dedicated to discussing the conclusions reached on each objective based on the findings.

7.1.1 EFFECT OF UNSATURATED SOIL CONDITIONS ON SOIL BEHAVIOUR

The effect of unsaturated soil conditions on the soil behaviour was investigated by analysing the results from the monotonic tests carried firstly on saturated samples and then on unsaturated samples with initial matric suction of 50, 100 and 225 kPa. Based on the test results, the following findings can be reported:

- Based on the stress strain relationship, unsaturated soil conditions increased the shear strength through strain hardening. However, the unsaturated samples presented a glaring peak deviator stresses followed by load-collapse associated with a rupture and the formation of shear bands, slip planes and multiple bifurcation.
- Unsaturated soil conditions changed the behavioural mechanism from linear-elastic-perfectly-plastic during saturated soil conditions to linear-elastic-strain-hardening during unsaturated soil conditions, with caused an upward movement of the failure envelope with increased matric suction in the net stress space.
- The relationship between the intercept term and matric suction was found to be logarithmic with the equation of the type $y = a \ln x + b$. The coefficient of determination was 0.991 and 0.963 for the subballast and subgrade materials. The implication is that the increase in shear strength due to unsaturated soil conditions is logarithmic and therefore low values of matric suction can mobilise higher values of the intercept term of the test materials.

7.1.2 EFFECT OF INCREASED AXLE LOADING ON SATURATED MATERIALS

The effect of increased axle loading was investigated by analysing the results from the cyclic test results. Cyclic loading equivalent to 20, 26, 30, 32.5 and 40 tonnes per axle were applied to saturated samples in a single stage manner under undrained conditions. Based on the results, the following findings and conclusions can be stated with regard to saturated railway foundation materials:

- In the effective stress space, increased axle loading causes the stress states in the soil to move from below the critical state line at low axle loading to above the critical state line at high axle loading. Stress states which plotted below the critical state line resulted in no-phase transition in soil behaviour. Stress states which plotted along the critical state line resulted in a single-phase transition in soil behaviour. Stress states which plotted above the critical state line resulted in a double-phase transition in soil behaviour.
- Resilient behaviour was found to be associated with a no-phase transition in soil behaviour, while failure was found to be associated with a double-phase transition in soil behaviour.
- Increased axle loading beyond the shear strength of the soil resulted in a decreased resilient modulus and plastic behaviour. During plastic behaviour, the rate of the permanent strain was found to be inversely related to the rate of the resilient strain.
- It is therefore concluded and recommended that the use of saturated railway foundation materials which undergo a double-phase transition in soil behaviour should be avoided and the highest axle loading which causes a no-phase transition in soil behaviour should be taken as the maximum axle load, which was found to be 20 and 26 tonnes per axle for saturated subballast and subgrade materials, respectively.

7.1.3 EFFECT OF INCREASED AXLE LOADING ON UNSATURATED MATERIALS

Cyclic loading equivalent to 20, 26, 30, 32.5 and 40 tonnes per axle were applied to unsaturated samples with initial matric suction of 50, 100 and 225 kPa in a multi stager manner under constant water content conditions. Based on the results, the following findings and conclusions can be stated with regard to unsaturated samples:

- The shear induced stress states in all the axle loading cases, matric suction cases and materials (subballast and subgrade) plotted well below the failure envelope and all the deformations were found to be predominately elastic or resilient.
- Unsaturated soil conditions caused an increase in the resilient modulus of test materials and the deterioration of the resilient modulus was found to be much slower during unsaturated soil conditions as compared to saturated soil conditions, which highlights the importance of adequate drainage in a railway track foundation.

- Furthermore, increased axle loading initially caused a decrease in the permanent strain of unsaturated materials until the critical axle loading of 32.5 tonnes per axle was reached, attributed to the strain hardening property found in unsaturated materials.
- It is therefore concluded that, as a result of the increased shear strength from the strain hardening property of unsaturated materials, an increased axle loading of 32.5 tonnes per axle can be safely sustained by both tested subballast and subgrade materials provided the matric suction in the soil is greater than 50 kPa.

7.1.4 FINAL REMARKS

In terms of increased axle loading, unsaturated soil conditions are beneficial to the shear strength of railway foundation materials as compared to saturated soil conditions. In terms of the permanent deformations, the benefits are limited to a critical level of repeated deviator stress. With regard to track foundation design, the consideration of saturated soil conditions only on the basis of worse-case scenario will likely lead to an overdesign or a conclusion that increased axle loading is impossible to implement. With that in mind, the inclusion of unsaturated soil conditions in track design will result in better and cost effective designs, given that sufficient historic data and information about the climatic conditions and moisture regime of the area is available.

7.2 RECOMMENDATIONS

The recommendations related to the study include further development of the cyclic triaxial apparatus and further research work on unsaturated soils.

7.2.1 FURTHER DEVELOPMENTS OF THE CYCLIC TRIAXIAL APPARATUS

In this study, the measurement of the change in volume of unsaturated samples was done using local instrumentations from LVDTs, which were found to be prone to inaccuracies probably due to effect of the double membrane slotted with aluminium foil in between. At high frequency testing, greater than 0.5 Hz, the use of bender elements, optical measurement technique or other forms of detached measurement technique are highly recommended for the measurement of radial and vertical deformation of the sample to increase the accuracy and precision of the volume change measurements.

7.2.2 FURTHER RESEARCH WORK ON UNSATURATED SOILS

The incorporation of the moisture content measured on site and stress-dependant soil water retention curve is also high recommended. The in-situ moisture content should be in line with the matric suction

at which test samples are tested in the laboratory. The determination of the stress-dependant soil water retention curve in the triaxial cell laboratory after isotropic consolidation will likely be a true reflection the field conditions after construction. Furthermore, field measurement of suctions can be used for verifications.

7.2.3 FURTHER RESEARCH WORK ON OTHER MATERIALS

This study was confined to two test materials, which were the subballast and subgrade materials and both classified as silty clay. It therefore means all the findings from the study are limited to the tested materials. Further research can include other materials such as sands and clays.

REFERENCES

Adams, B. A., Wulfsohn, D. & Fredlund D. G. (1996). Air volume change measurement in unsaturated soil testing using a digital pressure-volume controller. *Geotechnical Testing Journal,* Vol. 19, No 1, pp. 12-21.

Alonso, E. E., Gens, A. & Hight D.W. (1987). Special problem soils – general report. *Proceedings of the 9th European Conference on Soil Mechanics and Foundation Engineering,* Dublin, Ireland, 31 Aug – 3 Sept 1987, pp. 1087-1146.

Alonso, E. E., Gens, A. & Josa, A. (1990). A constitutive model for partially saturated soils. *Géotechnique*, Vol. 40, No. 3, pp. 405-430.

Alva-Hurtado, J. E. & Selig, E. T. (1982). Survey of laboratory devices for measuring soil volume change. *Geotechnical Testing Journal*, Vol. 4, No. 1, pp. 11-18.

Ahmadi-Naghadeh, R. & Toker, N. K. (2012). Volume change measurement in triaxial testing of unsaturated soils. *Proceedings of the 3rd International Conference on New Developments in Soil Mechanics and Geotechnical Engineering*, Nicosia, North Cyprus, Tukey, 28-30 June 2012, pp. 627-634.

Airó Farulla, C. & Ferrari, (2005). Controlled suction oedometric tests: analysis of some experiment aspects. *Proceedings of the International Symposium on Advanced Experimental Unsaturated Soil Mechanics*, Trento, Italy, 27-29 June 2005, pp. 43-48.

ASTM D5311/D5311/M - 13 (2013). *Standard test method for load control cyclic triaxial strength of soil. American Society of Testing and Materials*, West Conshohocken, Pennsylvania, United States of America.

Atkinson, J. H. & Bransby, P. L. (1978). *The mechanics of soils: an introduction to critical states soil mechanics*. 1st edition. McGraw-Hill Book Company, London, United Kingdom.

Bishop, A. W. & Henkel, D. J. (1957). *The measurement of soil properties in the triaxial test*. 1st edition. Edward Arnold Publishers, London, United Kingdom.

Bishop A. W. (1961a). Effective stress in soils, concrete and rocks, *Proceedings of the Conference on Pore Pressure and Suction in Soils*, 30-31 March 1960, London, United Kingdom, pp. 4-16.

Bishop, A. W. (1961b). The measurement of pore pressures in the triaxial. *Proceedings of the Conference on Pore Pressure and Suction in Soils*, London, United Kingdom, 30-31 March 1960, pp. 38-46.

Bishop, A. W. & Donald, I. B. (1961). The experimental study of partly saturated soils in the triaxial apparatus. *Proceedings of the 5th International Conference on Soil Mechanics and Foundation Engineering*, 17-22 July 1961, Paris, France, pp. 13- 21.

Black, D. K. & Lee, K. L. (1973). Saturating laboratory samples by back pressure. *American Society of Civil Engineering: Journal of the Soil Mechanics and Foundation Division*, Vol. 99, No. 1, pp. 75-93.

Blight, G. E. (2013). *Unsaturated soil mechanics in geotechnical practice.* 1st edition. Taylor & Francis Group, London, United Kingdom.

Briaud, J. (2013). *Geotechnical engineering: unsaturated and saturated soils*. 1st edition. John Wiley & Sons. New Jersey, United States of America.

Brown, S. F. (1996). Soil mechanics in pavement engineering. *Géotechnique*, Vol 46, No 3, pp. 383-426.

BS 1377 (1990). British Standard 1377. *Method for test for soils for civil engineering purposes.* British Standards Institution, London, United Kingdom.

Chui, C. F. & Ng. C. W. W. (2003). A state-dependant elasto plastic model for saturated and unsaturated soil. *Géotechnique*, No. 53, Vol. 9, pp. 809-829.

Clayton, C.R.I., Khatrush A.S., Bica A.V.D. & Siddique A. (1989). The use of Hall effect semiconductors in geotechnical instrumentation. *Geotechnical Testing Journal.* Vol. 12, No. 1, pp. 69-76.

Craig, R. F. (1983). *Soil mechanics.* 3rd edition, Van Nostrand Reinhold Co Ltd, United Kingdom.

Craig, R. F. (1997). *Soil mechanics.* 6th edition, Taylor & Francis Group, London, United Kingdom.

Craig, R. F. (2004). *Craig's soil mechanics*, 7th edition, Taylor & Francis Group, London, United Kingdom.

Delage, P. Romero, E. Tarantino, A. (2008). Recent developments in the techniques of controlling and measuring suction in unsaturated soils. *Proceedings of the 1st European Conference on Unsaturated Soils, Durham, United Kingdom,* 2-4 July 2008, pp. 33-52.

Department of Transport. (2017). National Rail Policy – Draft white paper. *Department of Transport,* South Africa.

Dunn, C.S. (1965). Development in the design of triaxial equipment for testing compacted soils. *Proceedings of the Symposium on the Economic Use of Soil Testing in Site Investigation*, Birmingham, Alabama, Vol 3, pp. 19-25.

Escario, V. & Saez, J. (1986). The shear strength of party saturated soils. *Gèotechnique*, Vol. 36, No. 3, pp. 453-456.

Fredlund, D. G. (2018). Role of the soil-water characteristic curve in unsaturated soil mechanics. *Proceedings of the 7th International Conference on Unsaturated Soils*, Hong Kong, 3-5 August 2018, pp. 1-28.

Fredlund, D. G., Morgenstern, N. R. & Widger, R. A. (1978). Shear strength of unsaturated soils. *Canadian Geotechnical Journal,* Vol. 15, No. 3, pp. 313-321.

Fredlund, D. G. (1979). Second Canadian geotechnical colloquium: Appropriate concepts and technology for unsaturated soils. *Canadian Geotechnical Journal,* Vol. 16, No. 1, pp. 121-139.

Fredlund, D. G. (1999). Appropriate concepts and technology for unsaturated soils. *The emergence of unsaturated soil mechanics.* Eds A. W. Clifton, G. W. Wilson & Barbour, S. L. National Research Council of Canada, Ottawa, Canada, pp. 111-126.

Fredlund, D. G. & Hasan, J. U. (1979). One-dimensional consolidation theory: unsaturated soils. *Canadian Geotechnical Journal,* Vol. 16, No. 3, pp. 521-531.

Fredlund, D. G. & Rahardjo, H. (1993). *Soil mechanics for unsaturated soils*. 1st edition. John Wiley & Sons, New Jersey, United States America.

Fredlund, D. G., Rahardjo, H. & Gan, J.K.M. (1987). Non-linearity of strength envelope for unsaturated soils. *Proceedings of the 6th Conference on Expansive Soils*, 1-4 December 1987, New Delhi, India, pp. 49-54.

Fredlund, D. G., Rahardjo, D. & Ng, T. (1993). Effect of pore-air and negative pore-water pressures on stability at the end-of-construction. *Proceedings of the International Conference on Dam Engineering*, 12-13 January 1993, Johor Bahru, Malaysia, pp. 43-51.

Fredlund, D. G., Rahardjo, H. & Fredlund, M. D. (2012). *Unsaturated soil mechanics in engineering practice*. 1st edition. John Wiley & Sons, New Jersey, United States America.

Fredlund, D. G. & Morgenstern, N. R. (1976). Constitutive relations for volume change in unsaturated soils. *Canadian Geotechnical Journal,* Vol. 13, No. 3, pp. 261-276.

Fredlund, D. G. & Morgenstern, N. R. (1977). Stress state variables for unsaturated soils. *American Society of Civil Engineers: Journal of Geotechnical Engineering Division*, Vol. 103, No. 5, pp. 447-466.

Fredlund, D. G., Morgenstern, N. R. & Widger, R. A. (1978). The shear strength of unsaturated soils. *Canadian Geotechnical Journal*, Vol. 15, No. 3, pp. 313-321.

Fung, Y. C. (1965). *Foundations of solid mechanics.* 1st edition. Prentice Hall, New Jersey, United States of America.

Futai, M. M. & Almeida, M. S. S. (2005). An experimental investigation of the mechanical behaviour of unsaturated gneiss residual soil. *Géotechnique*, Vol. 55, No. 3, pp. 201-213.

Gachet, P., Klubertanz, G. Vulliet, L. & Laloui, L. (2003). Interfacial behaviour of unsaturated soil with small-scale model and use of image processing techniques. *Geotechnical Testing Journal*, Vol. 26, No. 1, pp. 12-21.

Geiser, F, Laloui, L. & Vulliet, T. (2000). On the volume measurement in unsaturated triaxial tests. *Proceedings of the 1st Asian Conference in Unsaturated Soils,* Rotterdam, The Netherlands, 18-19 May 2000, pp. 669-674.

Gräbe, P. J. (2002). *Resilient and permanent deformation of railway foundation under principal stress rotation.* PhD thesis. University of Southampton, United Kingdom.

Gräbe, P. J. Freyer, R. V. & Furno, R. F. (2007). An intelligent condition monitoring system for the management of continuously welded rail. *Proceedings of the International Heavy Haul Association Conference: Specialist Technical Session*, Kiruna, Sweden, 11-13 June 2007, pp. 579-586.

Gräbe, P. J. & Clayton, C. R. I. (2009). Effects of principal stress rotation on permanent deformation in rail track foundations. *American Society of Civil Engineers: Journal of Geotechnical and Geoenvironmental Engineering*, Vol. 135, No. 4, pp. 555-565.

Gräbe, P. J. & Clayton, C. R. I. (2014). Effects of principal stress rotation on resilient behaviour in rail track foundation. *American Society of Civil Engineers: Journal of Geotechnical and Geoenvironmental Engineering,* Vol. 140, No. 2, pp. 1-10.

Halliday, D., Resnick, R. & Walker, J. (2005). Fundamentals of physics. 7th ed. John Wiley & Sons, Danvers, United Stated.

Harris, R. G. (1977). Economies of traffic density in the rail freight industry. *The Bell Journal of Economies,* Vol. 8, No. 2, pp. 556-564.

Hasan, J. U. & Fredlund, D. G. (1980). Pore pressure parameter for unsaturated soils. *Canadian Geotechnical Journal*, Vol. 17, No. 3, pp. 395-404.

Havenga, J. H. (2012). Rail renaissance based on strategic market segmentation principles. *South African Business Review,* Vol. 16, No.1, pp. 1-21.

Head, K. H. (1998). *Manual for soil laboratory testing – effective stress tests.* 2nd ed. John Wiley & Sons, West Sussex, United Kingdom.

Heyns, F. J. (2004). Geotechnical application in railway track design for track geotechnology. *Africon Training Academy,* Pretoria.

Hilf, J. W. (1948). Estimating construction pore pressure in rolled earth dams. *Proceedings of the 2nd International Conference on Soil Mechanics and Foundation Engineering.* Rotterdam, The Netherlands, 21-30 June 1948, pp. 234-240.

Ho, D. Y. F., Fredlund, D. G. & Rahardjo, H. (1992). Volume change indices during loading and unloading of an unsaturated soil. *Canadian Geotechnical Journal,* Vol. 29, pp. 195-207.

Houlsby, G. T. (1997). The work input to an unsaturated granular material. *Géotechnique*, Vol. 47, No. 1, pp. 193-196.

Hoyos L. R., Laikram, A. & Puppula, A. J. (2008). A novel suction-controlled true triaxial apparatus for unsaturated soils. *Proceedings of the 1st European Conference on Unsaturated Soils*. Durham, United Kingdom, 2-4 July 2008, pp. 83-88.

Hoyos, L. R., Laloui, L. & Vassallo, R. (2008). Mechanical testing of unsaturated soils. *Geotechnical and Geological Engineering*, Vol. 26, pp. 675-689.

Jennings, J. E. & Burland, J. B. (1962). Limitations to the use of effective stresses in partly saturated soil. *Géotechnique*, Vol. 12, No. 2, pp. 125-144.

Jones, G. A. (2008). Problem soils seminar. *Proceedings of Geotechnical Division of the South African Institution of Civil Engineering on problem soils in South Africa,* Midrand, South Africa, 3-4 November 2008, pp. 3-7.

Kimoto, S., Oka, F., Fukutani, J., Yubuki, T. & Nakashima, K. (2011). Monotonic and cyclic behaviour of unsaturated sandy soil under drained and fully undrained conditions. *Japanese Geotechnical Society: Soils and Foundations,* Vol. 51, No. 4, pp. 665-681.

Knappett, J. A. & Craig, R. F. (2014). *Craig's soil mechanics*, 8th edition. Spon Press, Oxon, United Kingdom.

Kuerbis, R. H. & Vaid, Y. P. (1988). Sand sample preparation - the slurry deposition method. *Japanese Society of Soil Mechanics and Foundation Engineering: Soils and Foundations*, Vol. 28, No. 4, pp 107-118

Ladd, R. S. (1978). Preparing test specimens using undercompaction. *Geotechnical Testing Journal*, Vol. 1, No. 1, pp. 16-23.

Laloui, L. Peron, H., Geiser, F. & Vulliet, L. (2006). Advances in volume measurement in unsaturated soil triaxial tests. *Japanese Society of Soil Mechanics and Foundation Engineering: Soils and Foundations*, Vol. 46, No. 3, pp. 341-349.

Lambe, T. W. (1967). Stress path method. *American Society of Civil Engineers: Journal of the Soil Mechanics and Foundations Division*, Vol. 93, No 6, pp. 309-331.

Lekarp, F., Isacsson, U. & Dawson, A. (2000). State of the art I: Resilient response of unbound aggregates. *American Society of Civil Engineers: Journal of Transportation Engineering*, Vol. 126, No. 1, pp. 66-75.

Li, D. (1994). *Railway track granular layer thickness design based on subgrade performance under repeated loading.* PhD dissertation, Department of Civil Engineering, University of Massachusetts, Amberts, MA.

Li, D, Hyslip, J., Sussmann, T. & Chrismer, S. (2016). *Track geotechnology*. 1st edition. Taylor & Francis Group, New York, United States of America.

Li, D. & Selig, E. T. (1994). Resilient modulus for fine-grained subgrade soils. *American Society of Civil Engineers: Journal of Geotechnical Engineering*, Vol. 120, No. 6, pp. 939-957.

Li, D. & Selig, E. T. (1996). Cumulative plastic deformation for fine-grained subgrade soils. *American Society of Civil Engineers: Journal of Geotechnical Engineering,* Vol. 122, No. 6, pp. 1006-1013.

Li, D. & Selig, E. T. (1998a). Method for railroad track foundation design I: development. *American Society of Civil Engineers: Journal of Geotechnical and Geoenvironmental Engineering*, Vol. 124, No. 4, pp. 316-322.

Li, D. and Selig, E. T. (1998b). Method for railroad track foundation design II: applications. *American Society of Civil Engineers: Journal of Geotechnical and Geoenvironmental Engineering*, Vol. 124, No. 4, pp. 323-329.

Lourens, J. P. & Maree, J.S. (1997). Rehabilitation design of high embankments and a coal line track formation. *Proceedings of the 6th International Heavy Haul Conference*, Cape Town, South Africa, 6-10 April 1997, Vol. 1, pp. 57-75.

Luong PM. Phénmoènes cycliques dans les sols pulvérulents (1980a). *Revue Française de Géotechnique*, Vol. 10, pp. 39-49.

Luong P. M. Stress-strain aspects of cohesionless soils under cyclic and transient loading. (1980b). *Proceedings of the International Symposium on Soils under Cyclic & Transient Loading*, 7-11 January, Rotterdam, The Netherlands, Balkema, pp. 315-24.

Lu, N. & Likos, W. J. (2004). *Unsaturated soil mechanics*. 1st edition. John Wiley & Sons, New Jersey, United States of America.

Maatouk, A., Leroueil, S. & La Rochelle, P. (1995), Yielding and critical state of a collapsible unsaturated silty soil. *Geotechnique*, Vol. 45, No. 3, pp. 465-477.

Mamou, A., Powrie, W., Priest, J. A. & Clayton, C. (2017). The effect of drainage on the behaviour of railway track foundation materials during cyclic loading. *Géotechnique*, Vol. 67, No. 10, pp. 845-854.

Matyas, E. L. & Radhakrishna, H. S. (1968). Volume change characteristics of partially saturated soils. *Géotechnique*, Vol. 18, pp. 432-448.

Mendes, J., Toll, D. G. & Evans, R. (2012). A double cell triaxial system for unsaturated soil testing. *Proceedings of the 2nd European Conference on Unsaturated Soils,* Napoli, Italy, 20-22 June 2012, pp. 5-10.

Michaels, A. S. (1956). Discussion on Paper by Rosenquist. *Proceedings of American Society of Civil Engineers*.

Miller, G. A., The, S. Y., Li, D. and Zaman, M. M. (2002). Cyclic shear strength of soft railroad subgrade. *Journal of Geotechnical and Geo-environmental Engineering,* Vol. 126, No. 2, pp. 139-147.

Mohr, O. (1882). Ueber die Darstellung des Spannungszustandes und des Deformationszustandeseines Körperelementes und über die Anwendung derselben in der Festigkeitslehre. Civilengenieur, No. 28, pp. 113-156.

Murray, E. J. & Sivakumar, V. (2010). *Unsaturated soils – a fundamental interpretation of soil behaviour.* 1st edition. John Wiley & Sons, West Sussex, United Kingdom.

Newman, R. R., Resor, R. R. & Zarembski, A. M. (1991). The effect of increased axle loads on maintenance of way and train operations at Burlington Northern railroads, *Proceedings of the Heavy Haul Workshop*, Vancouver, British Columbia, Canada, 9-12 June 1991, pp. 209-223.

Ng, C. W. W. & Menzies, N. (2007). *Advanced unsaturated soil mechanics and engineering*. 1st edition. Taylor & Francis, Abingdon, United Kingdom.

Ng, C. W. W., Zhan, L. T. & Cui, Y. J. (2002). A simple system for measuring overall volume change in unsaturated soils. *Canadian Geotechnical Journal,* Vol. 39, pp. 757-764.

ORE D 161. (1987). *The dynamic effects due to increasing axle loads from 20 to 22.5 tonnes and the estimated increase in track cost maintenance.* Report 4, Utrecht, The Netherland.

O'Reilly, M. P. & Brown, S. F. (1991). Cyclic loading in geotechnical engineering. *Cyclic loading of soils*. Eds M. P. O'Reilly & S. F. Brown. 1st edition. Blackie and Sons, London, United Kingdom, pp. 1-18.

Perez-Ruiz, D. D. (2009). *A refined true triaxial apparatus for testing unsaturated soils under suction-controlled stress paths*. PhD Thesis. University of Texas, United States of America

Pournaghiazar, M., Russel, A. R. & Khalili, N. (2013). The cone penetration test in unsaturated soils. Géotechnique, Vol. 63, No. 14, pp. 1209-1220.

Potts, D. M. & Zdravkovic, L. (1999). *Finite Element Analysis in Geotechnical Engineering: Volume I – Theory,* Telford Publishing, London, United Kingdom.

Potts, D. M. (2003). Numerical analysis: a virtual dream or practical reality. *Geotechnique*, Vol. 53, No. 6, pp. 535-573.

Powrie, W., Yang, L. A. & Clayton C. R. I. (2007). Stress changes in the ground below ballasted railway track during train passage. *Proceedings of the Institution of Mechanical Engineers, Part F: Rail and Rapid Transit.* Vol. 221, pp. 247-261.

Rahardjo, H., Heng, O. B. & Choon, L. E. (2004). Shear strength of a compacted residual soil from consolidated drained and constant water content triaxial tests. *Canadian Geotechnical Journal,* Vol. 41, pp. 421-436.

Romero, E., Facio, J.A., Lloret, A., Gens, A. & Alonso, E. E. (1997). A new suction and temperature controlled triaxial apparatus. *Proceedings of the 14th international conference on soil mechanics and foundation engineering*, Hambourg, Germany, 6-12 September 1997, pp. 185-188.

Roscoe, K. H., Schofield, M. A. & Wroth, M. A. (1958). On the yielding of soils. *Geotechnique*, Vol. 8, No. 1, pp. 1-18.

Rust, E. Heymann, G. & Jones, G. A. (2005). Collapse potential of partly saturated sandy soils from the east coast of Southern Africa. *Journal of the South African Institution of Civil Engineering*, Vol. 47, No. 1, pp. 8-14.

Rust, E., Heymann, G. & Jones, G. A. (2008). Collapsible soils: an overview. *Proceedings of Geotechnical Division of the South African Institution of Civil Engineering on problem soils in South Africa,* Midrand, South Africa, 3-4 November 2008, pp. 47-56.

SANS 3001: GR1. (2013). *Wet preparation and particle size analysis.* South African Bureau of Standards, Pretoria, South Africa.

SANS 3001: GR3. (2014). *Particle size analysis of material smaller that 2 mm (hydrometer method).* South African Bureau of Standards, Pretoria, South Africa.

SANS 3001: GR10 (2013). *Determination of the one-point liquid limit, plastic limit, plasticity index and linear shrinkage.* South African Bureau of Standards, Pretoria, South Africa.

Schofield and Wroth (1968). *Critical State Soil Mechanics.* McGraw-Hill, London.

Schuurman, E. (1966). The compressibility of an air/water mixture and a theoretical relation between the air and water pressures. *Géotechnique*, Vol. 16, No. 4, pp. 269-281.

Selig, E. T. & Chang, C. S. (1981). Soil failure modes in undrained cyclic loading. *Journal of Geotechnical Engineering Division: Proceedings of the American Society of Civil Engineer*s, Vol. 107, No GT5, pp. 539-551.

Selig, E. T. & Waters, J. M. (1994). *Track geotechnology and substructure management*. 1st edition. Thomas Telford Publications, London, United Kingdom.

Shahu, J. T. Yudhbir, & Kameswara Rao, N. S. V. (2000). A rational method for design of design of railroad track foundation. *Japanese Geotechnical Society,* Vol. 40, No. 6, pp. 1-10.

Shaw, F. J. (2006). *Railway track formation stiffnesses*, MSc Thesis. University of Pretoria, Pretoria, South Africa.

Sivakumar, V. (1993). *A critical state framework for unsaturated soils*. PhD Thesis, University of Sheffield, Sheffield, United Kingdom.

Sivakumar, R., Sivakumar, V., Blatz, J. & Vimalan, J. (2006). Twin-cell stress path apparatus for testing unsaturated soils. *Geotechnical Testing Journal,* Vol. 29, No. 2, pp. 175-179.

Skempton, A. W. (1954). The pore-pressure coefficients A and B. *Geotechnique*, Vol. 4, No. 4, pp. 143-147.

Skempton, A. W. (1961). Effective stress in soils, concrete and rocks, *Proceedings of the Conference on Pore Pressure and Suction in Soils,* London, United Kingdom, 30-31 March 1960, pp. 4-16.

Taylor, D. W. (1948). *Fundamentals of soil mechanics.* 1st edition. John Wiley & Sons Inc, New York, United States of America.

Terzaghi, K. (1921). Die physikalischen Grundlagen der technischgeologischen Gutachtens. *Osterreichischer Ingeniuerund Architekten-Verein, Zeitschrift*, Vol. 73, No. 36/37, pp. 237-241.

Terzaghi, K. (1923). Die berechnung der durchlassigkeitsziffer des tones aus dem verlauf der hydrodynamischen spannungser scheinungen, *Akademic der Wissenschaften in Wien, Sitzungsberichte, Mathematischnaturwissenschaftliche*, Vol. 132, No. 3/4, pp. 125-138.

Terzaghi, K. (1936). The shearing resistance of saturated soils. *Proceedings of the 1st Conference on Soil Mechanics*, Massachusetts, United States, 22-26 June 1936, Vol. 1, pp. 54-56.

Terzaghi, K. (1943). *Theoretical soil mechanics*. 1st edition. John Wiley & Sons, New York, United States of America.

Terzaghi, K., Peck, R. B. & Mesri, G. (1996). *Soil mechanics in Engineering Practice.* 3rd edition. John Wiley & Sons, New York, United States of America.

Toll, D. G. (1990). A framework for unsaturated soil behaviour. *Géotechnique,* Vol. 40, No. 1, pp. 31-44.

Toll, D. G. (2012). Tropical soils. *ICE Manual of Geotechnical Engineering: Volume 1.* 1st edition. Eds J. Burland, T. Chapman, H. Skinner & M. Brown. ICE Publishing, London, United Kingdom, pp. 341-335.

Toll, D. G. (2013). The behaviour of unsaturated soil. 1st edition. *Handbook of tropical residual soil engineering*. Eds B. G. K. Huant, D. G. Toll & A. Prasad. Taylor & Francis Group, London, United Kingdom, pp. 119-143.

Toll, D. & Ong, B. H. (2003). Critical state parameters for an unsaturated residual sandy soil. *Géotechnique*, Vol. 53, No 1, pp. 93-103.

Transnet Freight Rail. (2019). *Annual report.* Transnet Freight Rail, Parktown, Johannesburg, South Africa.

Vanapalli, S. K., Fredlund, D. G. & Pufahl, D. E. (1999). The influence of soil structure and stress history on the soil-water characteristics of a compacted till. *Géotechnique*, Vol. 49, No. 2, pp. 143-159.

Vaughan, P. R. (2003). Observations on the behaviour of clay fill containing occluded air bubbles. *Géotechnique*, Vol. 53, No. 2, pp. 265-272.

Wang, Q., Pufahl, D. E. & Fredlund, D. G. (2002). A study of critical state on an unsaturated silty soil. *Canadian Geotechnical Journal,* Vol. 39, pp. 213-218.

Weinert, H. H. (1980). *The natural road construction materials of Southern Africa*, 1st ed. H & R Academica, Pretoria, South Africa.

Wheeler, S. J. (1988). The undrained shear strength of soils containing large gas bubbles. *Géotechnique*, Vol. 28, No. 3, pp. 399-413.

Wheeler, S. J. & Sivakumar, V. (1995). An elasto-plastic state framework for unsaturated soil. *Géotechnique*, Vol. 40, No. 1, pp. 35-53.

Wood, D. M. (1982). *Soil mechanics-transient and cyclic loading.* 1st edition. John Wiley & Sons Ltd. Eds G. N. Pande & O.C. Zienkiewicz, pp. 513-582.

Wood, D. M. (1990). *Soil behaviour and critical state soil mechanics.* Cambridge University Press, United Kingdom.